Università
Ca'Foscari
Venezia

**Scuola Dottorale di Ateneo**
**Graduate School**

**Dottorato di ricerca**
**in Scienze Chimiche**
**Ciclo XXVII**
**Anno di discussione 2015**

# *Innovative and versatile heterogeneous catalysts for hydrogen production from renewable sources*

**SETTORE SCIENTIFICO DISCIPLINARE DI AFFERENZA: CHIM/04**
**Tesi di Dottorato di Valentina Nichele, matricola 816875**

| | |
|---|---|
| **Coordinatore del Dottorato** | **Tutore del Dottorando** |
| **Prof. Maurizio Selva** | **Prof.ssa Michela Signoretto** |

# Introduction

In the next years, the world will face a big challenge related to the energy crisis and the environmental problems. $CO_2$ emissions derive from the combustion of fossil fuels; human activities are the largest source of carbon dioxide. Raising atmospheric carbon dioxide levels cause an increase in globally averaged temperatures, the so-called "greenhouse effect", as well as negative effects on human health. It is clear that this way of energy production is no more sustainable. But how can we meet the ever growing world energy demand in a clean and sustainable way? Renewables can be the answer. Hydrogen (renewables-derived hydrogen in particular) is the ideal candidate for both energy and transport sectors. It is a high-density energy vector; it is clean and carbon-free and its sole combustion product is water.

Biomass derivatives such as ethanol and glycerol could be used as clean sources of hydrogen, since they are renewable, easy to store, handle and transport and have a high hydrogen content. The steam reforming of these oxygenated compounds is an attractive topic for researchers; the design of a highly active and selective catalyst is a key point for the fulfillment of this process on industrial scale.

# Objectives of the study

In this work several catalysts for the steam reforming of oxygenated compounds (ethanol or glycerol) derived from biomass were prepared. The main objective of this thesis was to study the effect of different parameters on the performance of Ni-based catalysts. The study focused in particular on: i) the physico-chemical properties of the support; ii) the metal-support interaction; iii) the reducibility and iv) the dispersion of the active phase.

The effect of each parameter was deeply analyzed and investigated through a proper modification of the synthesis procedure, for example through the doping of the support or the addition of a second active metal.

## Organization of the report

This thesis has 7 chapters. Chapter 1 presents the current world energy situation, underlining the global dependency on fossil fuels and reminding the need of a transition to renewable sources. Chapter 2 introduces the concept of *hydrogen economy* and describes the processes for a clean hydrogen production, highlighting the key role of heterogeneous catalysis. Chapter 3 describes the effect of the support ($TiO_2$, $ZrO_2$ and an ordered mesoporous $SiO_2$) on the performance of Ni catalysts in steam reforming reactions. Chapter 4 investigates the effect of the synthesis procedure on the properties of $Ni/TiO_2$ catalysts and then on their catalytic activity. Chapter 5 contains details on the optimization of the performance of $Ni/ZrO_2$ catalysts through the proper modification of the support. Chapter 6 shows the effects of the addition of a second metal (copper) to a $Ni/ZrO_2$ catalyst in terms of activity and selectivity. Chapter 7 summarizes the major results and presents the conclusions.

Chapters 3, 4, 5 and 6 and part of the data reported in Chapter 2 are already published in peer-reviewed journals.

# Table of contents

# Chapter 1. Energy rules the world

Energy is everywhere. Energy lights our cities and powers our vehicles, warms our homes and cooks our food. Energy is the basis for social development and economic growth. At present, energy demand is increasing and it has been estimated that global energy consumption will rise by 41% by 2035, with 95% of that growth coming from emerging economies[1]. Nowadays, energy demand is almost fully satisfied by fossil sources.

## 1.1 Current energy supply and use: an overview

Pre-industrial society depended primarily on biomass for its energy needs, but during the industrial revolution, when machinery began to replace manual labor, the demand for more powerful energy sources dramatically increased. It was at this point that fossil fuels, *i.e.* coal, oil and natural gas, replaced wood, water and wind.

From the beginning of industrialization up to nowadays, fossil sources have been the main source of energy. To this day, in an era of ever-increasing global energy demand, fossil fuels account for most (over 80%) of the world energy supply (Fig. 1.1)[2].

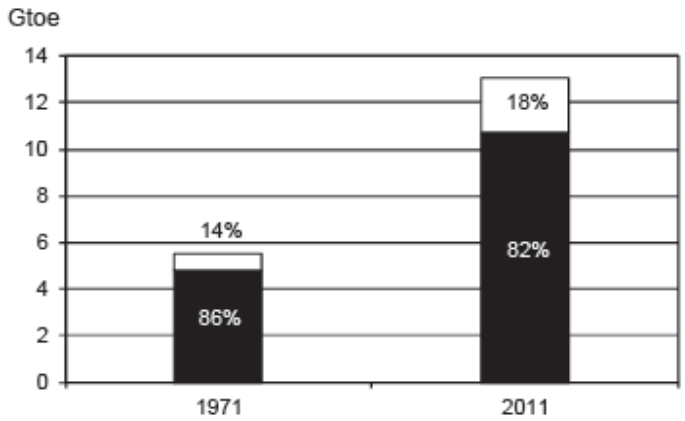


Fig. 1.1: World energy supply (■: fossil sources; □ non fossil sources)[2].

The US Energy Information Administration (EIA) credits fossil fuels for bringing about "*one of the most profound social transformations in history*". They dramatically changed

every aspect of human life and lifestyles, from health and life longevity to social improvements. In a certain sense, they made modern life possible.

Of course, the effects of the intensive exploitation of fossil sources were profound. Actually the major drawback of using fossil fuels is pollution, since burning fossil fuels generates carbon dioxide. Raising atmospheric carbon dioxide levels cause an increase in globally averaged temperatures (the so-called "greenhouse effect"), as well as negative effects on human health. Human activities are the largest source of carbon dioxide: since 1870, $CO_2$ emissions from fuel combustion have risen exponentially (Fig. 1.2)[2].

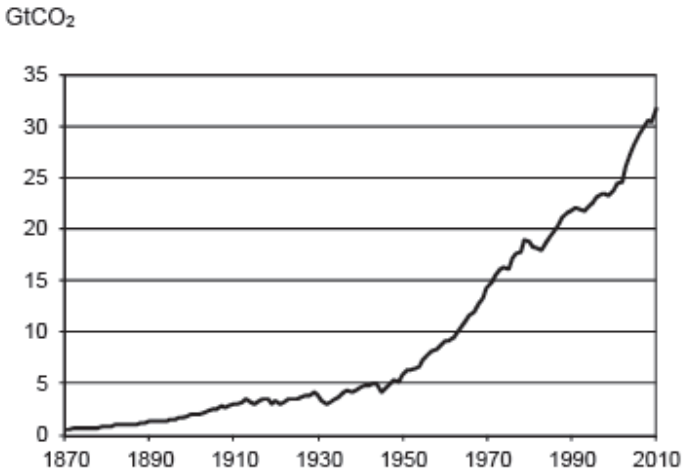


Fig. 1.2: Trend in $CO_2$ emissions from fossil fuel combustion[2].

Among the different human activities, two sectors produced nearly two-thirds of global $CO_2$ emissions in 2011: electricity and heat generation accounted for 42%, while transport accounted for 22%[2]. Moreover, according to current trends, $CO_2$ emissions are expected to increase by more than 80% until 2050[3].

A second concern is about fossil fuels depletion. Fossil fuels are considered non-renewable resources because they take millions of years to form so, although the discovery of new reserves and unconventional sources (heavy crude oil, oil sands, oil shale) and the development of new technologies to extract the fuels, they are being depleted much faster than they are being formed. This issue has also serious economical, political and social consequences.

It is quite evident that current trends in energy supply and use are unsustainable.

## 1.2 Renewables: the next energy revolution

One of the most important targets today is to find alternative energy sources which are highly available, cheap and non-polluting. Renewable sources can be the solution.

Renewable energy is defined as energy coming from resources which are replenished at a higher rate than they are consumed, such as sunlight, wind, geothermal heat and biomass. The use of renewable resources for energy production provides substantial benefits for both climate and human health (absence or drastic reduction of greenhouse gases emissions) and economy (inexhaustible energy supply and stable energy prices).

Global demand for renewable energy continued to rise in the recent years. Renewable energy supplied about 18% of global final energy consumption by the end of 2011 (see Fig. 1). Of this total, approximately 9.3% came from traditional biomass[4].

Biomass is biological material derived from living organisms. This definition includes a wide range of materials, such as wood, energy crops, agricultural residues and food waste. Using biomass can provide several benefits. In addition to the previously mentioned advantages related to the renewable and environmentally-friendly nature of biomass, other factors should also be considered[5]: i) biomass fuels have negligible sulfur content and do not contribute to sulfur dioxide emissions causing acid rain; ii) the combustion of biomass produces less ash than coal combustion; iii) the use of agricultural and forestry residues and solid wastes for energy production is an effective way to reduce the problem of waste disposal; iv) biomass is a domestic resource which is not subject to price fluctuations or to supply uncertainties. Moreover the use of biomass can reduce carbon dioxide emissions in the atmosphere. Biomass, which consists of carbon, hydrogen, oxygen and nitrogen, is usually considered to be a carbon neutral energy source, since the $CO_2$ released when the biomass is gasified is re-used by the growing plants through photosynthesis[6,7]. Nevertheless, the debate on biomass carbon neutrality is rather heated, since some studies claim that net carbon emissions from burning biomass are even higher than burning coal (see for example the *Biomass sustainability and carbon policy study*, also known as the *Manomet report*[8]).

As an energy source, biomass can be used either directly by combustion, producing heat or steam (then electricity), or indirectly after converting it to chemicals, such as biofuels. Moreover biomass and its derivatives have a great potential: they could be used for the massive production of hydrogen, the energy carrier of the future.

## References


[1] BP Energy Outlook 2035, January 2014.

[2] International Energy Agency, *$CO_2$ Emissions from Fuel Combustion: Highlights,* 2013 ed., IEA Publications, Paris, 2013.

[3] International Energy Agency, *Transport, energy and $CO_2$: Moving toward sustainability,* 2009 ed., IEA Publications, Paris, 2009.

[4] REN21, *Renewables 2013 Global Status Report,* REN21 Secretariat, Paris, 2013.

[5] R.C. Saxena, D.K. Adhikari, H.B. Goyal, Renewable Sustainable Energy Rev. 13 (2009) 167-178.

[6] Y. Kalinci, A. Hepbasli, I. Dincer, Int. J. Hydrogen Energy. 34 (2009) 8799-8817.

[7] H. Balat, E. Kirtay, Int. J. Hydrogen Energy. 35 (2010) 7416-7426.

[8] Manomet Center for Conservation Sciences, *Massachusetts Biomass Sustainability and Carbon Policy Study: Report to the Commonwealth of Massachusetts Department of Energy Resources*. T. Walker Ed., 2010. Contributors: P. Cardellichio, A. Colnes, J. Gunn, B. Kittler, R. Perschel, C. Recchia, D. Saah, T. Walker.

# Chapter 2. Hydrogen: clean energy for a clean future

In a world with a voracious appetite for energy, aiming at a future of renewable, inexpensive and non-polluting energy sources, hydrogen can play an important role.

Hydrogen is the ideal candidate to solve environmental problems. It is difficult to imagine a cleaner source of energy, since its only oxidation product is water. It can be used directly for generation of electricity in fuel cells. Moreover it is a good transportation fuel, with a rapid burning speed, a high effective octane number and much wider limits of flammability in air (4-75 v/v%) than methane (5.3-15 v/v%) and gasoline (1-7.6 v/v%)[1]. It has the highest utilization efficiency (although its very low density is also a drawback since pressurized on-board tanks are needed) and can be converted to useful energy forms through several processes[1,2].

Nevertheless, the hydrogen economy is not yet well developed: many challenges, technological and non-technical, must be overcome. Public acceptance of the introduction of a new energy carrier in everyday life have to be considered, together with appropriate safety and regulatory issues. Moreover the technological challenges related to hydrogen production, distribution and storage (at a competitive cost) must be solved.

In particular, the issue related to hydrogen production is one of the most challenging today. Although it is the most abundant element in the universe, hydrogen does not exist in high concentrations in elemental form on the earth: it must be produced from other compounds.

## 2.1 Current hydrogen production

Actually 47% of global hydrogen is produced from natural gas, 30% from oil, 19% from coal and the rest via water electrolysis[3]. Therefore approximately 96% of the hydrogen produced worldwide still derives from the conversion of fossil resources.

The *steam reforming of methane* is the most common method of producing hydrogen. Methane reacts with steam at high temperatures (700-1000 °C) in the presence of a Ni/α-$Al_2O_3$ catalyst to produce a mixture of hydrogen and carbon monoxide. The reaction (Eq. 1) is strongly endothermic; heat must be supplied for the reaction to proceed.

(1) $CH_4 + H_2O \rightleftharpoons CO + 3H_2$ $(\Delta H^0_{298} = +206 \text{ kJ mol}^{-1})$

In order to increase the selectivity to hydrogen and reduce the CO concentration, the steam reforming reaction is followed by the water-gas shift reaction (Eq. 2), where the carbon monoxide and steam are reacted. This reaction is carried out in two steps; the first (at high temperature, 350-500 °C) uses $Fe_3O_4/Cr_2O_3$ as catalyst, while the second (at low temperature, 200 °C) employs a $Cu/ZnO/Al_2O_3$ catalyst.

(2) $CO + H_2O \rightleftharpoons CO_2 + H_2$ $(\Delta H^0_{298} = -41 \text{ kJ mol}^{-1})$

*Partial oxidation of natural gas* is another common method to produce hydrogen. The hydrocarbons contained in natural gas (predominantly methane) reacts with oxygen in a substoichiometric amount, generating a hydrogen-rich syngas (Eq. 3).

(3) $CH_4 + 1/2\ O_2 \longrightarrow CO + 2H_2$ $(\Delta H^0_{298} = -36 \text{ kJ mol}^{-1})$

Also in this case, the water-gas shift reaction can increase hydrogen productivity. Partial oxidation can also serve as an initial step to provide heat for the steam reforming process (*autothermal reforming*).

Another possibility for hydrogen production is *coal gasification*, a thermo-chemical process in which heat and pressure break down coal into its chemical constituents. The resulting syngas is made up primarily of carbon monoxide and hydrogen.

These processes are based on mature and cost-effective technologies, but they all have a common negative feature: they are still based on fossil resources. Of course this is not a viable way to favor the hydrogen economy, since it does not decrease the dependence on fossil fuels (and the related problems). *Water electrolysis*, for example, is another well-known process for the production of hydrogen, but usually the electricity needed is produced from fossil fuels and the cost of hydrogen is even higher than it is if hydrogen is produced by steam reforming of methane.

The transition to a true renewable hydrogen era is based on the use of renewable sources and the development of environmentally friendly processes. The steam reforming of biomass derivatives could be the key for this transition.

## 2.2 Ethanol steam reforming (ESR)

Ethanol is one of the most important compound derived from biomass. It is produced by microbial fermentation of starch and sugar of a variety of feedstocks such as sugar cane, miscanthus, corn, grain, wheat, straw, cotton, sunflower, etc… and used mainly as an additive for gasoline. Ethanol is also very attractive for a clean hydrogen production because: i) it is renewable; ii) it has a high hydrogen content; iii) it is safe and non-toxic; iv) it is easy to store, handle and transport because of its low volatility[4,5]. Steam reforming, in particular, is a promising route to produce hydrogen from ethanol.

Stoichiometrically, the overall steam reforming reaction can be represented as reported in Eq. 4:

(4) $CH_3CH_2OH + 3H_2O \rightleftharpoons 6H_2 + 2CO_2$ $(\Delta H^0_{298} = +174 \text{ kJ mol}^{-1})$

which can be seen as the sum of the syngas production (Eq. 5) and the water-gas shift (WGS) of the intermediate CO (Eq. 6):

(5) $CH_3CH_2OH + H_2O \rightleftharpoons 2CO + 4H_2$ $(\Delta H^0_{298} = +255 \text{ kJ mol}^{-1})$

(6) $CO + H_2O \rightleftharpoons CO_2 + H_2$ $(\Delta H^0_{298} = -41 \text{ kJ/mol})$

However, ethanol steam reforming is a quite complex process since several reaction pathways can occur[6] (Fig. 2.1).

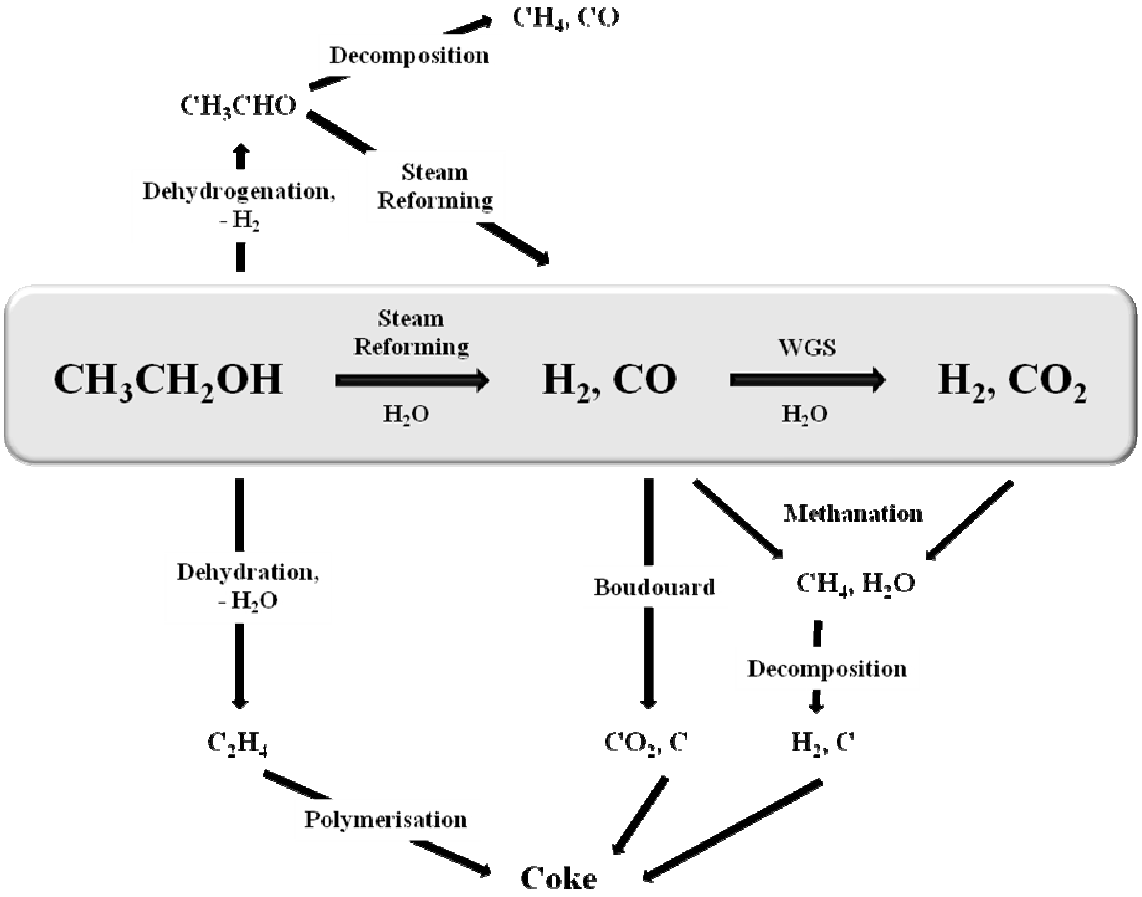


Fig. 2.1: Ethanol steam reforming is a complex network of reactions.

The thermodynamics of the process have been extensively studied[7-9] and the possible reactions are reported in the following (adapted from Ref.[10]).

(7) Ethanol dehydrogenation $CH_3CH_2OH \longrightarrow CH_3CHO + H_2$

(8) Acetaldehyde decomposition $CH_3CHO \longrightarrow CO + CH_4$

(9) Acetaldehyde steam reforming $CH_3CHO + H_2O \rightleftharpoons 2CO + 3H_2$

(10) Ethanol dehydration $CH_3CH_2OH \longrightarrow C_2H_4 + H_2O$

(11) Coke formation $C_2H_4 \rightarrow$ polymeric deposits (coke)

(12) Ethanol decomposition $CH_3CH_2OH \longrightarrow CH_4 + CO + H_2$

$2CH_3CH_2OH \longrightarrow C_3H_6O + CO + 3H_2$

$CH_3CH_2OH \longrightarrow 1/2\ CO_2 + 3/2\ CH_4$

(13) Methanation

$$CO + 3H_2 \rightleftharpoons CH_4 + H_2O$$

$$CO_2 + 4H_2 \rightleftharpoons CH_4 + 2H_2O$$

(14) Methane decomposition

$$CH_4 \rightleftharpoons C + 2H_2$$

(15) Boudouard reaction

$$2CO \rightleftharpoons CO_2 + C$$

Hydrogen production varies significantly with the different reaction pathways. A wide range of undesired byproducts, such as oxygenates compounds or hydrocarbons, as well as coke, can be generated, according to the experimental conditions[10,11]. High temperatures favor the endothermic reforming reaction which produces $H_2$ and CO (Eq. 5), while the WGS reaction (Eq. 6) is shifted to the left[12]. The reactants concentrations affect the products distribution too, since usually high water/ethanol molar ratios increase the hydrogen yield[13].

## 2.3 Glycerol steam reforming (GSR)

Biodiesel is another important biofuel derived from biomass. The term "biodiesel" refers to a vegetable oil- or animal fat-based diesel fuel consisting of long-chain alkyl esters. It is produced by transesterification with methanol of triglycerides obtained from a variety of natural crops (such as rapeseed, soybean, mustard, sunflower, palm oil). Biodiesel can be used, alone or blended with standard diesel fuel, in diesel engines with little or no modification needed. Glycerol is obtained as byproduct in biodiesel production, being approximately 10 wt% of the total[14]. It is commonly used in the manufacturing of drugs, as a sweetener and a preservative in foods and drinks and in a variety of cosmetics. However, global biodiesel production continued to increase in the last years, reaching 22.5 billion litres in 2012[15], and it is expected to increase even further. Therefore a glut of glycerol is expected. It is then essential to find useful applications for this by-product.

Waste glycerol could be efficiently employed for a clean hydrogen production. Like ethanol, glycerol is safe and non-toxic with a high hydrogen content[16].

The overall glycerol steam reforming reaction is reported in Eq. 16:

(16) $C_3H_8O_3 + 3H_2O \rightleftharpoons 3CO_2 + 7H_2$ $(\Delta H^0_{298} = +128 \text{ kJ mol}^{-1})$

which can be seen as the sum of an endothermic reaction, glycerol decomposition (Eq. 17), and the exothermic water-gas shift of the intermediate CO (Eq. 18):

(17) $C_3H_8O_3 \rightleftharpoons 3CO + 4H_2$ $(\Delta H^0_{298} = +250 \text{ kJ mol}^{-1})$

(18) $CO + H_2O \rightleftharpoons CO_2 + H_2$ $(\Delta H^0_{298} = -41 \text{ kJ mol}^{-1})$

However, as previously evidenced for ethanol steam reforming, also in this case a complex network of reactions can take place[17,18]. The most important are reported below.

(19) Methanation $CO + 3H_2 \rightleftharpoons CH_4 + H_2O$

$CO_2 + 4H_2 \rightleftharpoons CH_4 + 2H_2O$

(20) Methane decomposition $CH_4 \rightleftharpoons C + 2H_2$

(21) Boudouard reaction $2CO \rightleftharpoons CO_2 + C$

Nevertheless other side reactions, such as dehydration, dehydrogenation, cyclization and polymerization, can take place, thus leading to coke formation[19].

As for ESR, also in this case thermodynamic studies predict that the steam reforming reaction is favored at high temperature and high water/glycerol ratio, while the WGS is promoted at low temperature[20-22].

The analysis of the two processes should have evidenced that the choice of the proper reaction conditions is a critical point to be addressed. Nevertheless, the effectiveness of ethanol and glycerol steam reforming on the industrial scale relies also on another key component of a process: the catalyst.

## 2.4 Heterogeneous catalysis: the key to make the hydrogen dream come true

Catalysis played a crucial role in the success of the industry in the 20th century. Of course it will play an important role also in the development of new processes in the 21st century. Hydrogen production from renewable sources could be one of these processes.

A massive production of hydrogen from biomass is a challenge for catalysis. As shown in Sections 2.2 and 2.3, ethanol and glycerol steam reforming are characterized by a complex reaction network that includes dehydration, dehydrogenation, methanation, water-gas shift reaction, decomposition, Boudouard reaction and coke formation. Several undesired by-products such as methane, carbon monoxide, acetaldehyde, ethylene and coke can be generated depending on the catalyst. Such complex pathways make the design of an efficient and selective catalyst an essential step of the process. Moreover, the harsh conditions usually used in the steam reforming reactions require a robust and resistant catalyst.

The ideal catalyst should maximize the hydrogen production, as well as limit the side reactions. So far, the research focused mainly on heterogeneous supported metal catalysts. It is well known that both the active phase and the support play a key role in determining the productivity and selectivity of the reaction, because different catalysts induce different pathways for $H_2$ production[6,23,24]. An effective catalyst must break C–C, O–H and C–H bonds in the reactant and facilitate the water-gas shift reaction to remove adsorbed CO from the surface[25]. Noble metal catalysts have been extensively studied for their well-known high catalytic activity. Pt[16,26-30], Rh[31-35] and Ru[36-39] based catalysts are among the most investigated for both ethanol and glycerol steam reforming[10,40]. Supported Pt catalysts seem to be particularly active and selective to $H_2$ in the ESR at low temperature[41-43]. Liguras et al.[44] compared the catalytic performance of Rh, Ru, Pt and Pd catalysts in ESR at 600-850 °C with different metal loading (0-5 wt%). They found that, for low-loaded catalysts, Rh is much more active and selective towards hydrogen, while the catalytic performance of Ru is improved with increasing metal loading. Ru is getting more and more attention also for the GSR. Hirai et al.[45] made a systematic studies on Ru catalysts and showed that a $Ru/Y_2O_3$ catalyst was very active and stable against coke deactivation.

However, although noble metals exhibit a high catalytic activity, the research is focusing on less expensive and more available active phases.

## 2.5 Nickel catalysts for ethanol and glycerol steam reforming

Among non-noble metal catalysts, nickel is one of the most investigated for steam reforming reactions[46].

Nickel is commonly used in the industrial reforming processes[47] (see Section 2.1) and is particularly attractive also for the steam reforming of ethanol and glycerol because of its high activity and selectivity in breaking C–C, O–H and C–H bonds[48-50]. It catalyzes the water-gas shift reaction, thus removing adsorbed CO from the surface and the gas phase and improving the $H_2$ yield and purification[48,50]. Moreover it is far cheaper and more available than noble metals.

Other non-noble metals, such as cobalt and copper, have been considered to be used as active phases. Our studies[51,52] on the performance of Ni, Co and Cu catalysts supported on $TiO_2$, $ZrO_2$ and $SiO_2$ in the steam reforming of ethanol demonstrated that Ni is the most active metal regardless of the support, especially at low reaction temperatures[*].

Nevertheless, one of the most serious drawbacks of Ni-based catalysts is the deactivation due to sintering and coking[53-55]. Very dispersed Ni particles tend to agglomerate during high temperature operation and in the presence of water vapor[56-59]. The loss of exposed active phase influences activity and selectivity, since smaller Ni particles showed a lower selectivity to methane, one of the possible by-products. Moreover, sintering and coking phenomena are strictly interconnected, since it is well established that coking occurs more promptly over large Ni particles and aggregates than over very dispersed Ni crystallites[60-63]. The possibility to operate at low temperature may be advantageous to limit Ni sintering and also from the economical point of view, since a lower heat input would be required. Nevertheless, thermodynamic investigations on coke formation routes indicate that coke accumulation may be more severe at 500°C than at higher temperature[64,65].

---

[*] These data are reported in: 1. "*Silica and zirconia supported catalysts for the low-temperature ethanol steam reforming*", I. Rossetti, J. Lasso, V. Nichele, M. Signoretto, E. Finocchio, G. Ramis, A. Di Michele, Appl. Catal. B: Environ. 150-151 (2014) 257-267. Copyright © 2013 Elsevier B.V. All rights reserved.; 2. "*$TiO_2$-supported catalysts for the steam reforming of ethanol*", I. Rossetti, J. Lasso, E. Finocchio, G. Ramis, V. Nichele, M. Signoretto, A. Di Michele, Appl. Catal. A: General. 477 (2014) 42-53. Copyright © 2014 Elsevier B.V. All rights reserved.

A possible strategy to control coking phenomenon is to optimize the reaction conditions, for example working in excess of steam in order to inhibit coke deposition. Another possibility is to deal with the other component of a heterogeneous catalyst, *i.e*. the support. Because of its strategic role, the first part of the work was devoted to the investigation of the effect of the support on the performance of Ni catalysts in steam reforming reactions.

## References


[1] M. Balat, Int. J. Hydrogen Energy. 33 (2008) 4013-4029.

[2] T.N. Veziroğlu, S. Şahin, Energy Convers. Manage. 49 (2008) 1820-1831.

[3] G.J. Stiegel, M. Ramezan, Int. J. Coal Geol. 65 (2006) 173-190.

[4] M. Lindo, A.J. Vizcaíno, J.A. Calles, A. Carrero, Int. J. Hydrogen Energy. 35 (2010) 5895-5901.

[5] V. Palma, F. Castaldo, P. Ciambelli, G. Iaquaniello, *Sustainable hydrogen production by catalytic bio-ethanol steam reforming*, from "Greenhouse Gases - Capturing, Utilization and Reduction", G. Liu Ed., 2012, InTech.

[6] A. Haryanto, S. Fernando, N. Murali, S. Adhikari, Energy Fuels. 19 (2005) 2098-2106.

[7] A.N. Fatsikostas, X.E. Verykios, J. Catal. 225 (2004) 439-452.

[8] M. Benito, J.L. Sanz, R. Isabel, R. Padilla, R. Arjona, L. Daza, J. Power Sources. 151 (2005) 11-17.

[9] M. Benito, R. Padilla, A. Serrano-Lotina, L. Rodríguez, J.J. Brey, L. Daza, J. Power Sources. 192 (2009) 158-164.

[10] M. Ni, D. Y.C. Leung, M.K.H. Leung, Int. J. Hydrogen Energy. 32 (2007) 3238-3247.

[11] C.N. de Ávila, C.E. Hori, A.J. de Assis, Energy. 36 (2011) 4385-4395.

[12] R. Trane-Restrup, S. Dahl, A.D. Jensen, Int. J. Hydrogen Energy. 39 (2014) 7735-7746.

[13] L. Hernández, V. Kafarov, J. Power Sources. 192 (2009) 195-199.

[14] M.J. Haas, A.J. McAloon, W.C. Yee, T.A. Foglia, Bioresour. Technol. 97 (2006) 671-678.

[15] REN21, *Renewables 2013 Global Status Report,* REN21 Secretariat, Paris, 2013.

[16] F. Pompeo, G. Santori, N.N. Nichio, Int. J. Hydrogen Energy. 35 (2010) 8912-8920.

[17] D. Sutton, B. Kelleher, J.R.H. Ross, Fuel Process. Technol. 73 (2001) 155-173.

[18] M. Slinn, K. Kendall, C. Mallon, J. Andrews, Bioresour. Technol. 99 (2008) 5851-5858.

[19] A. Gallo, V. Dal Santo, C. Pirovano, La chimica e l'industria. (2011) 94-99.

[20] X. Wang, N. Wang, M. Li, S. Li, S. Wang, X. Ma, Int. J. Hydrogen Energy. 35 (2010) 10252-10256.

[21] M.L. Dieuzeide, N. Amadeo, Chem. Eng. Technol. 33 (2010) 89-96.

[22] C.C.R.S. Rossi, C.G. Alonso, O.A.C. Antunes, R. Guirardello, L. Cardozo-Filho, Int. J. Hydrogen Energy. 34 (2009) 323-332.

[23] J.A. Calles, A.Carrero, A.J. Vizcaíno, Microp. Mesop. Mater. 119 (2009) 200-207.

[24] S.M. de Lima, I.O. da Cruz,G. Jacobs, B.H. Davis, L.V. Mattos, F.B. Noronha, J. Catal. 257 (2008) 356-368.

[25] J.W. Shabaker, G.W. Huber, J.A. Dumesic, J. Catal. 222 (2004) 180-191.

[26] S. Ito, K. Tomishige, Catal. Commun. 12 (2010) 157-160.

[27] G. Jacobs, R.A. Keogh, B.H. Davis, J. Catal. 245 (2007) 326-337.

[28] S.M. de Lima, A.M. Silva, UM. Graham, G. Jacobs, B.H. Davis, L.V. Mattos, F.B. Noronha, Appl. Catal. A: General. 352 (2009) 95-113.

[29] P. Ciambelli, V. Palma, A. Ruggiero, Appl. Catal. B: Environ. 96 (2010) 18-27.

[30] F. Pompeo, G. Santori, N.N. Nichio, Catal. Today, 172 (2011) 183-188.

[31] C. Diagne, H. Idriss, A. Kiennemann, Catal. Commun. 3 (2002) 565-571.

[32] L. Coronel, J.F. Múnera, A.M. Tarditi, M.S. Moreno, L.M. Cornaglia, Appl. Catal. B: Environ. 160-161 (2014) 254-266.

[33] O.A. González Vargas, J.A. de los Reyes Heredia, J.A. Wang, L.F. Chen, A. Montesinos Castellanos, M.E. Llanos, Int. J. Hydrogen Energy. 38 (2013) 13914-13925.

[34] S. Cavallaro, V. Chiodo, S. Freni, N. Mondello, F. Frusteri, Appl. Catal. A: General. 249 (2003) 119-128.

[35] V. Chiodo, S. Freni, A. Galvagno, N. Mondello, F. Frusteri, Appl. Catal. A: General. 381 (2010) 1-7.

[36] P. Lu, T. Chen, J. Chern, Catal. Today. 174 (2011) 17-24.

[37] S. Tosti, A. Basile, F. Borgognoni, V. Capaldo, S. Cordiner, S. Di Cave, F. Gallucci, C. Rizzello, A. Santucci, E. Traversa, J. Membr. Sci. 308 (2008) 250-257.

[38] A. Gallo, C. Pirovano, P. Ferrini, M. Marelli, R. Psaro, S. Santangelo, G. Faggio, V. Dal Santo, Appl. Catal. B: Environ. 121-122 (2012) 40-49.

[39] J. Kim, D. Lee, Int. J. Hydrogen Energy. 38 (2013) 11853-11862.

[40] P.D. Vaidya, A.E. Rodrigues, Chem. Eng. Technol. 32 (2009) 1463-1469.

[41] A.C. Basagiannis, P. Panagiotopoulou, X.E. Verykios, Top Catal. 51 (2008) 2-12.

[42] J. Raskó, M. Dömök, K. Baán, A Erdohelyi, Appl. Catal. A: General. 299 (2006) 202-211.

[43] P. Panagiotopoulou, X.E. Verykios, Int. J. Hydrogen Energy. 37 (2012) 16333-16345.

[44] D.K. Liguras, D.I. Kondarides, X.E. Verykios, Appl. Catal. B: Environ. 43 (2003) 345-354.

[45] T. Hirai, N. Ikenaga, T. Miyake, T. Suzuki, Energy Fuels. 19 (2005) 1761-1762.

[46] J. Llorca, V. Cortés Corberán, N.J. Divins, R. Olivera Fraile, E. Taboada, in: L.M. Gandia, G. Arzamendi, P.M. Dieguez Eds. Renewable Hydrogen Technologies, 2013, pp. 135-169.

[47] C.K. Cheng, S.Y. Foo, A.A. Adesina, Catal. Today. 178 (2011) 25-33.

[48] A. Iriondo, V.L. Barrio, J.F. Cambra, P.L. Arias, M.B. Guemez, M.C. Sanchez-Sanchez, R.M. Navarro, J.L.G. Fierro, Int. J. Hydrogen Energy. 35 (2010) 11622-11633.

[49] A.J. Vizcaíno, A. Carrero, J.A. Calles, Int. J. Hydrogen Energy. 32 (2007) 1450-1461.

[50] C.D. Dave, K.K. Pant, Renew. Energy. 36 (2011) 3195-3202.

[51] I. Rossetti, J. Lasso, V. Nichele, M. Signoretto, E. Finocchio, G. Ramis, A. Di Michele, Appl. Catal. B: Environ. 150-151 (2014) 257-267.

[52] I. Rossetti, J. Lasso, E. Finocchio, G. Ramis, V. Nichele, M. Signoretto, A. Di Michele, Appl. Catal. A: General. 477 (2014) 42-53.

[53] Z. Zhang, X.E. Verykios, Appl. Catal. A: General. 138 (1996) 109-133.

[54] A.S.A. Al-Fatish, A.A. Ibrahim, A.H. Fakeeha, M.A. Soliman, M.R.H. Siddiqui, A.E. Abasaeed, Appl. Catal. A: General. 364 (2009) 150-155.

[55] Z. Li, X. Hu, L. Zhang, S. Liu, G. Lu, Appl. Catal. A: General. 417-418 (2012) 281-289.

[56] S.Q. Chen, Y. Liu, Int. J. Hydrogen Energy. 34 (2009) 4735-4746.

[57] F. Frusteri, S. Freni, V. Chiodo, L. Spadaro, G. Bonura, S. Cavallaro, J. Power Sources. 132 (2004) 139-144.

[58] S. Freni, S. Cavallaro, N. Mondello, L. Spadaro, F. Frusteri, J. Power Sources. 108 (2002) 53-57.

[59] M. Ni, D. Leung, M. Leung, Int. J. Hydrogen Energy. 32 (2007) 3238-3247.

[60] G. Centi, S. Perathoner, Catal. Today 148 (2009) 191-205.

[61] V.M. Gonzalez-DelaCruz, J.P. Holgado, R. Pereníguez, A. Caballero, J. Catal. 257 (2008) 307-314.

[62] K.O. Christensen, D. Chen, R. Lødeng, A. Holmen, Appl. Catal. A: General. 314 (2006) 9-22.

[63] D. Chen, K.O. Christensen, E. Ochoa-Fernandez, Z. Yu, B. Tøtdal, N. Latorre, A. Monzòn, A. Holmen, J. Catal. 229 (2005) 82-96.

[64] L.J.I. Coleman, W. Epling, R.R. Hudgins, E. Croiset, Appl. Catal. A: General. 363 (2009) 52-63.

[65] A. Lima da Silva, C. de Fraga Malfatti, I.L. Müller, Int. J. Hydrogen Energy. 34 (2009) 4321-4330.

# Chapter 3. Effect of the support on the performance of Ni catalysts in glycerol steam reforming*

## 3.1 Introduction

As reported in Section 2.5, nickel is a promising active phase for heterogeneous catalysts in steam reforming reactions. Nevertheless, it is well known that also the nature of the support affects the performance of a catalyst[1-3]. The support should possess a good chemical and mechanical resistance and a high surface area, in order to favour the dispersion of the active phase[4,5]. The interactions of the support with the metal are also important to stabilize the active phase and control sintering phenomena[6-8]. Finally, the support can strongly affect the selectivity of the catalyst, since the different pathways are determined not only by the nature of the active phase, but also by the nature of the support, for example its acidity and redox properties[2,9,10].

In this part of the work, the effect of the support on the performance of Ni-based catalysts, in terms of both activity and selectivity in the steam reforming of glycerol, is investigated. Three materials were chosen, *i.e.* $TiO_2$, $ZrO_2$ and an ordered mesoporous $SiO_2$ (SBA-15), for their different acidic and redox properties. Moreover, each material has some peculiar features. Titania was chosen for its well-known ability to interact with metals[11,12]. Zirconia has high thermal stability and steam adsorption ability[13,14]. Finally, SBA-15 was selected because the active phase can be better dispersed than on conventional silica because of its high surface area[4,15]. The selected nickel content was 10 wt% in all the samples. Nickel is usually used in higher amounts than noble metals, both in commercial SR catalysts[5,16] and in the literature[1,17], but the economical convenience is still guaranteed because of the very low cost of Ni compounds with respect to noble metals.

---

* The results reported in this chapter are published as: "*Glycerol steam reforming for hydrogen production: Design of Ni supported catalysts*", V. Nichele, M. Signoretto, F. Menegazzo, A. Gallo, V. Dal Santo, G. Cruciani, G. Cerrato, Appl. Catal. B: Environ. 111-112 (2012) 225-232. 

## 3.2 Experimental

### 3.2.1 Catalysts preparation

#### *3.2.1.1 Supports synthesis*

$TiO_2$ was prepared by a conventional precipitation method[18]. 20 g of $TiOSO_4$ $xH_2SO_4$ $xH_2O$ (*Aldrich, synthesis grade*) were dissolved in 300 mL of distilled water at room temperature, then NaOH (*Carlo Erba*, 9 M) was added dropwise until the system reached a pH of 5.5. The precipitate was aged at 60 °C for 20 hours, then repeatedly washed with distilled water and finally dried overnight at 110 °C.

SBA-15 was synthesized as previously reported[19], in the presence of Pluronic 123 (P123, *Aldrich*) as structure directing agent. 8 g of Pluronic 123 were dissolved in an aqueous solution of HCl (*Sigma Aldrich*) at 45 °C, then the silica precursor (TEOS, *Aldrich, purity 98%*) was added dropwise. The system was aged at the same temperature for 20 hours, then at 100°C for 48 hours in a hermetically sealed vessel. The solid was extensively washed with distilled water and dried at room temperature for several days, then calcined in flowing air (50 mL/min STP) at 500 °C for 6 hours.

$ZrO_2$ was prepared by a conventional precipitation method[20]. A solution of 26 g of $ZrOCl_2$*8 $H_2O$ (*Fluka, purity ≥99%*) in 100 mL of distilled water was added with a peristaltic pump under vigorous stirring to an ammonia solution. During the precipitation, the pH value was kept constant at 10.0 by the continuous addition of a 33% ammonia solution (*Riedel-de Haën*). After the complete addition of the salt solution, the hydroxide suspension was aged for 20 h at 90 °C, then filtered and washed with warm distilled water until it was free from chloride ions ($AgNO_3$ test) and dried overnight at 110 °C.

#### *3.2.1.2 Introduction of the active phase*

The active phase was added to each support by incipient wetness impregnation with an aqueous solution of the metallic precursor ($Ni(NO_3)_2$*$6H_2O$, *Sigma – Aldrich, purity ≥98.5%*), in the proper concentration in order to obtain the desired Ni loading (10 wt%). It was chosen to use this technique to achieve a high dispersion of the active phase, which is essential in order to obtain active and selective catalysts. Moreover it should be underlined

that this synthesis method is reproducible, easy and cheap. The catalyst was dried overnight at 110 °C and then calcined in flowing air (50 mL/min STP) at 500 °C for 4 hours. Samples are identified as TNi (Ni/$TiO_2$), SNi (Ni/SBA-15) and ZNi (Ni/$ZrO_2$).
This synthesis procedure allows a deeper control on the final properties of the samples with respect to other techniques. The flame pyrolysis method was also used to prepare some samples for comparison[21,22], but we decided to use the synthesis procedure here reported because it is highly versatile. Since we were interested in understanding which are the most important features of a SR catalyst, we needed a synthesis method that could be easily modulated in order to achieve them. The one here reported was the most suitable for this purpose.

### 3.2.2 Catalysts characterization

The temperature programmed reduction (TPR) measurements were carried out by placing the catalyst in a quartz reactor and heating in a 5% $H_2$/Ar mixed gas stream flowing at 40 mL/min at a heating rate of 10 °C/min from 25 to 600 °C. $H_2$ consumption was monitored with a TCD detector.
Before the other characterization measurements, the samples were reduced in $H_2$ flow for 1 h at 500 °C and 700 °C ($N_2$ physisorption) or only at 500 °C (XRD and HR-TEM).
Specific surface area and pores size distribution were evaluated through $N_2$ adsorption-desorption isotherms at 77 K (MICROMERITICS, ASAP 2000 Analyser). Surface area was calculated on the basis of the BET equation[23], whereas the pores size distribution was determined by the BJH method, applied to the $N_2$ desorption branch of the isotherm[24]. Prior to the analyses the samples were dried overnight at 110 °C and then outgassed in vacuum at 110 °C for 2 hours.
X-ray powder diffraction (XRD) analyses were carried out in the lab of Prof. Giuseppe Cruciani in the University of Ferrara. XRD patterns were measured by a Bruker D8 Advance diffractometer equipped with a Si(Li) solid state detector (SOL-X) and a sealed tube providing Cu Kα radiation. The quantitative phase analysis and crystal size determination of the support and metal phases in the samples were obtained by the Rietveld refinement method as implemented in the Bruker TOPAS program.

(High-Resolution) Transmission electron microscopy (HR-TEM) analyses were carried out in the lab of Dr. Giuseppina Cerrato in the University of Turin. HR-TEM images were obtained by using a JEOL JEM 3010UHR (300 kV) TEM fitted with a single crystal $LaB_6$ filament and an Oxford INCA Energy TEM 200 energy dispersive X-ray (EDX) detector. All samples were dry deposited on Cu "holey" carbon grids (200 mesh).

### 3.2.3 Catalytic tests

The GSR catalytic tests were carried out in the lab of Dr. Vladimiro Dal Santo in the CNR-ISTM of Milan. The activity of Ni catalysts in glycerol steam reforming was evaluated in a fixed-bed quartz reactor (diameter 12 mm) operating at atmospheric pressure and at different temperatures (500 and 650 °C) for 20 h. Catalytic tests were carried out in a home-made equipment. 200 mg of catalyst sieved to 35-45 mesh were loaded in the reactor and reduced *in situ* at 500 °C (if the reaction was performed at 500 °C) or 700 °C (if the reaction was performed at 650 °C) under hydrogen flow for 1 h prior to the reaction. Then a glycerol (10 wt%)/water solution was fed (0.060 mL/min) by means of a diaphragm metering pump (*Stepdos, KNF*) and helium was used as carrier gas (30 mL/min); a pressure controller was placed before the inlet gas to prevent overpressure phenomena. Vaporization of the solution took place before the catalytic bed in a unit filled with quartz beads at 250 °C. The analysis of the gaseous products was carried out by a gaschromatograph (*Agilent 6890N*) equipped with two columns connected in series (MS and Poraplot Q) with thermal conductivity and flame ionization detectors (TCD-FID), properly calibrated for the detection of $CH_4$, CO, $CO_2$, $H_2$; condensables were removed through a refrigerated coil. The steam reforming of glycerol leads to the formation of $H_2$ and $CO_2$ according to the reaction $C_3H_8O_3 + 3\ H_2O \rightarrow 7\ H_2 + 3\ CO_2$. The performance of the catalysts is presented in terms of $H_2$ yield, C conversion and CO, $CH_4$ and $CO_2$ selectivity, calculated from Eq.s 1-3:

$$\%H_2\ yield = \frac{H_2\ mol\ produced}{(mol\ glycerol\ in\ the\ feed) * 7} * 100 \qquad \text{Eq. 1}$$

$$\%C\ conversion = \frac{(CO_2 + CO + CH_4)\ mol\ produced}{3 * (mol\ glycerol\ in\ the\ feed)} * 100 \qquad \text{Eq. 2}$$

Eq.3 $$\%Selectivity\ of\ i\ = \frac{i\ mol}{(\sum i\ species)mol\ \ produced} * 100 \quad (i: CO, CO_2, CH_4)$$

## 3.3 Results and discussion

Before discussing the experimental results, it can be useful to remind how hydrogen production through glycerol steam reforming takes place.

Eq. 4 $C_3H_8O_3 + 3H_2O \rightleftharpoons 7H_2 + 3CO_2$

Eq. 5 $C_3H_8O_3 \rightleftharpoons 4H_2 + 3CO$

Eq. 6 $CO + H_2O \rightleftharpoons H_2 + CO_2$

Eq. 4 represents the overall steam reforming reaction, an endothermic transformation favoured at low pressure which is due to the contribution of two reactions, namely glycerol decomposition (Eq. 5) and water gas shift (WGS, Eq. 6). The reaction pathway is quite complex and many other reactions can take place, in particular CO and $CO_2$ hydrogenation, which leads to the formation of methane, and side reactions, such as dehydration, dehydrogenation, cyclization and polymerization, that can lead to coke deposition[25, 26].

The activity of the catalysts in the steam reforming of glycerol performed at 500 °C and at 650 °C is reported in Fig. 3.1; activity is presented in terms of glycerol conversion and hydrogen yield. In Fig. 3.2 the selectivity to CO and $CO_2$ is shown.

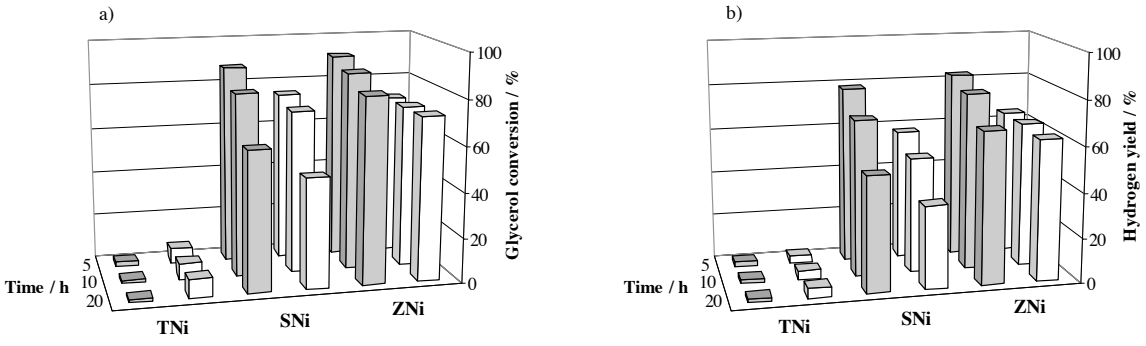


Fig. 3.1: Catalytic performance of the catalysts in glycerol steam reforming at two different temperatures: ■ 500 °C; □ 650 °C. a) Glycerol conversion; b) Hydrogen yield.

Fig. 3.1 shows that TNi exhibits negligible catalytic activity at both temperatures: after 20 h-on-stream, glycerol conversion is lower than 10% and hydrogen yield does not reach 5%. This catalyst has a high selectivity to CO, which is the main carbon product. $CO_2$ production greatly differs according to the reaction temperature (see Fig. 3.2 (b)): it is very low at 650 °C, while it is prominent at 500 °C. Moreover, when the reaction is performed at 650 °C, a little amount (~10%) of $CH_4$ is also present. In the generally accepted mechanism of metal catalysed glycerol steam reforming, the rate determining step is C–C cleavage, which leads to adsorbed CO. Carbon monoxide must be removed from the catalyst surface by the water-gas shift reaction because high surface coverage by CO decreases the catalytic activity[27]. The results obtained for TNi show that this catalyst has a very low activity in C–C bond cleavage, even at the highest temperature, and that the contribution of the water-gas shift reaction is even smaller.

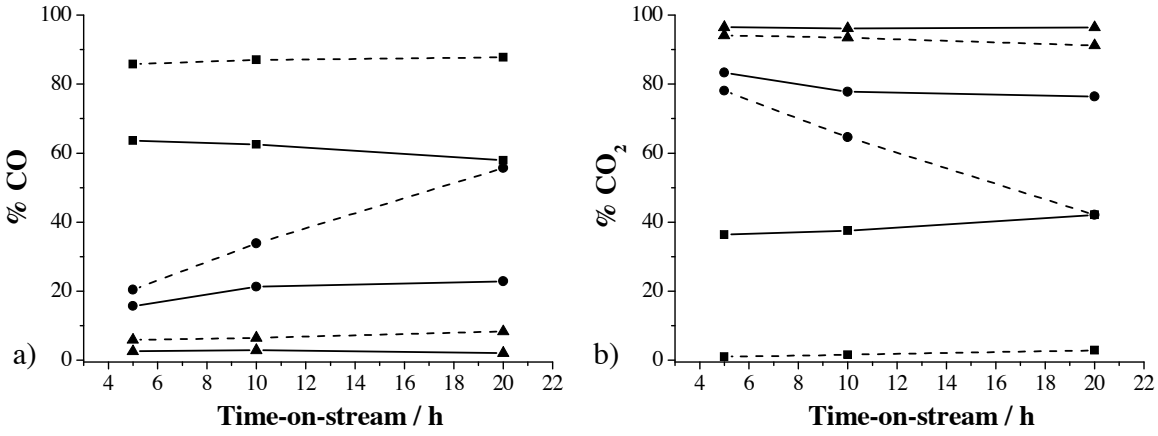


Fig. 3.2: CO (a) and $CO_2$ (b) selectivity for TNi (■), SNi (●) and ZNi (▲) at 500 °C (solid line) and at 650 °C (dash line).

The SNi sample shows the same behaviour at both temperatures (Fig. 3.1): it has a high initial activity, but it undergoes a deactivation process which decreases the glycerol conversion. At 500 °C, after 20 h-on-stream, a glycerol conversion of 62% and a hydrogen yield of 51% were obtained. CO formation is quite stable in the course of time. At 650 °C glycerol conversion and hydrogen yield are much lower (49% and 37% respectively), while CO production is significant and increases with time.

The ZNi sample achieved the best performance (Fig. 3.1); the most relevant difference related to the reaction temperature is that a little deactivation is detected at 500 °C, while a

stable glycerol conversion of ~72% and a hydrogen yield of 65% are obtained at 650 °C. In both cases the main carbon product is $CO_2$: this evidences the important contribution of the water-gas shift reaction that consumes CO and increases $H_2$ production even further.

The origin of the differences in the catalytic behaviour of the samples can be discussed on the basis of the characterization measurements we carried out.

First of all we carried out TPR measurements (Fig. 3.3), in order to identify the different NiO species on the surface of the supports and their reduction temperature.

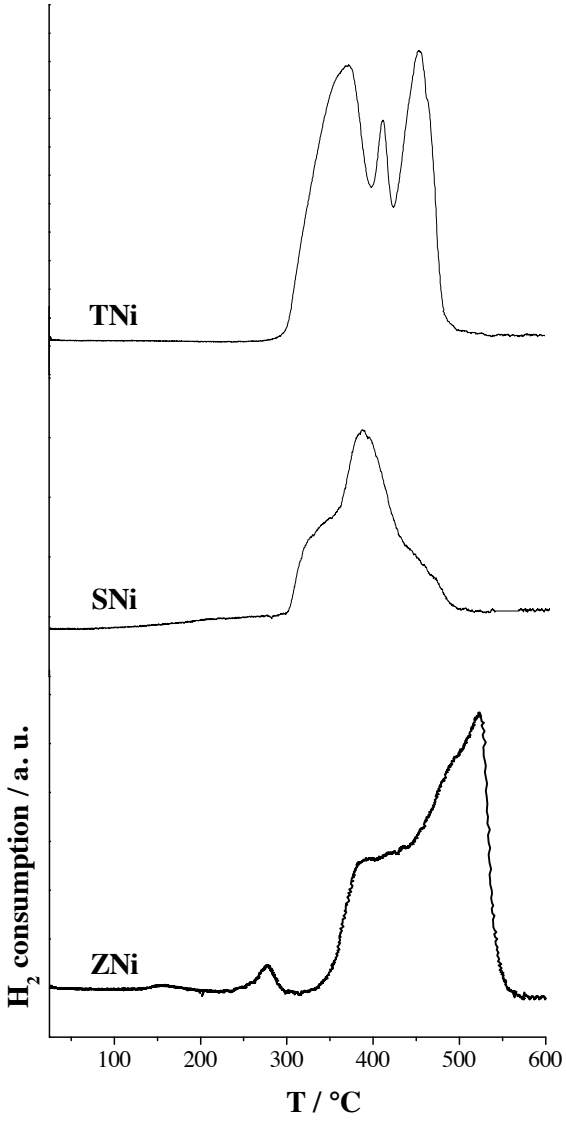


Fig. 3.3: TPR profiles of the catalysts.

It is possible to note that three different NiO species are present on the samples. The TPR pattern of the TNi sample shows a broad reduction region, in the range 290-500 °C; three

different peaks at 370 °C, 410 °C and 450 °C can be detected. The TPR profile of SNi is quite broad too: a well-defined peak with its maximum at 390 °C, a shoulder between 300 and 360 °C and another one between 420 and 500 °C are present. Lastly ZNi TPR reveals three peaks at 280 °C, 380 °C and 520 °C.

The peak located at the lowest temperature is ascribable to non-interacting metal oxide particles, more easily reduced (unsupported NiO has a reduction temperature of about 280 °C[28]). The other two peaks can be assigned to NiO particles weakly (peak at a lower temperature) or strongly (peak at a higher temperature) interacting with the support[29-33]. It can be noted that the position of the peaks differs according to the nature of the support.

All the catalysts are completely reduced within 550 °C and strong interactions between Ni and the support exist in all the samples. A relevant percentage of non-interacting Ni particles is present on the $TiO_2$ sample.

One of the most important parameters in the design of heterogeneous catalysts is the specific surface area: in fact, it is well known that a high surface area greatly improves the dispersion of the active phase[34,35]. The specific surface area (Fig. 3.4) was evaluated after reduction of the samples at 500 °C and at 700 °C, thus reproducing the reduction treatment performed before the catalytic tests.

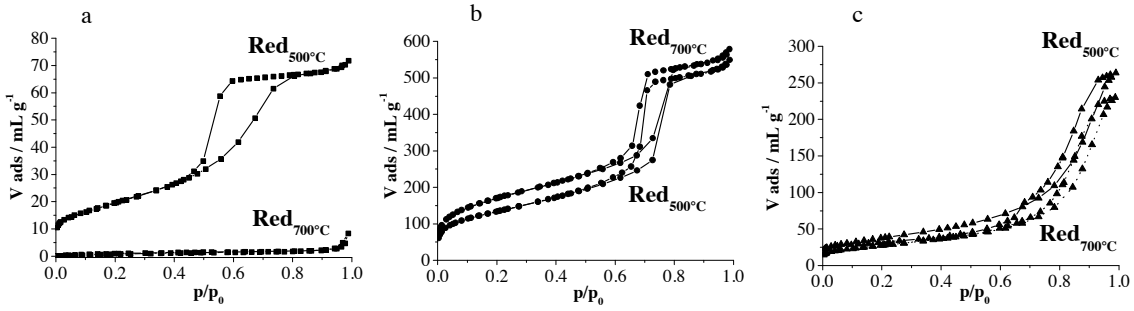


Fig. 3.4: $N_2$ adsorption/desorption isotherms of TNi (a), SNi (b) and ZNi (c) after reduction of the samples.

Concerning SBA-15 and $ZrO_2$ samples, it is quite evident that the reduction temperature does not affect the structure of the materials, which has been preserved in both cases. According to IUPAC classification[36], SNi (Fig. 3.4 (b)) shows a IV-type isotherm with a H1-type hysteresis, which is typical of this support, a mesoporous material with a high surface area of about 600 $m^2/g$ and a sharp pores size distribution with a maximum at 6

nm, whereas ZNi (Fig. 3.4 (c)) exhibits a IV-type isotherm containing a H3-type hysteresis, typical of materials that don't possess a well-defined mesoporous structure, and a surface area of approximately 100 $m^2/g$.

The behaviour of the $TiO_2$ sample is completely different. It can be noted that the TNi (Fig. 3.4 (a)), after reduction at 500 °C, shows a IV-type isotherm, which is typical of mesoporous materials characterized by a quite high surface area and an unimodal pores size distribution; the high temperature (700 °C) reduction treatment, on the contrary, caused the collapse of the porous structure of the oxide and the decrease of the specific surface area from 70 $m^2/g$ to 4 $m^2/g$.

Physisorption measurements seem to suggest a plausible explanation of the negligible activity of TNi in the reaction performed at 650 °C, whereas an exhaustive study of the other samples is still necessary.

X-ray diffraction measurements were carried out on the reduced samples (Fig. 3.5).

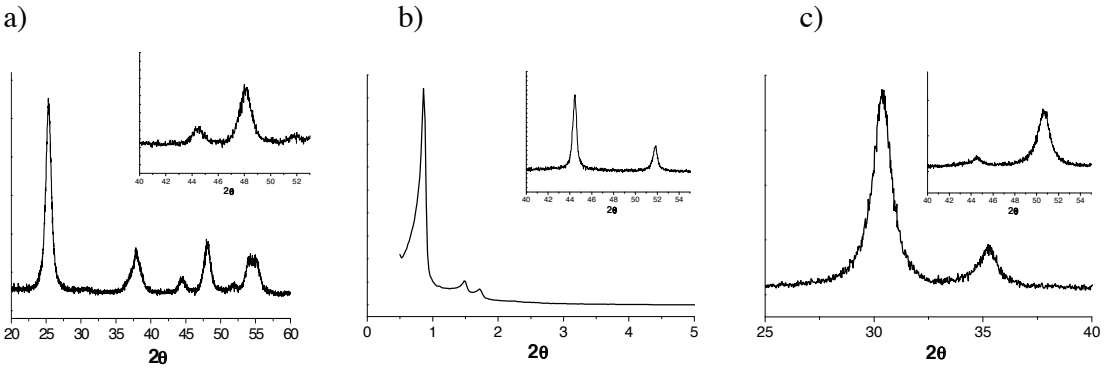


Fig. 3.5: XRD profiles of reduced TNi (a), SNi (b) and ZNi (c); Ni peaks at 2θ~44.5° and 2θ~51.8° (insets).

The high 2θ angle region of the XRD profile for reduced TNi (Fig. 3.5 (a)) shows that anatase is the main phase of the sample (~10% is brookite). The two peaks at 2θ ~44.5° and 51.8° reveal the occurrence of metallic nickel but its content, calculated by detailed Rietveld quantitative phase analysis, is much lower than the effective Ni concentration (about 3 wt%). The low Ni concentration can be related to another unexpected result: in the XRD pattern of uncalcined TNi (Fig. 3.6) only nanocrystalline anatase was found, whereas NiO (peak at 2θ ~43.4°) is totally absent. This result led us to believe that all nickel has been incorporated in the anatase lattice, thus making Ni unavailable to the reaction. This

interpretation is in agreement with previous reports in which sol-gel prepared Ni-doped $TiO_2$ nanoparticles or films heated in air at 450 °C or 500 °C did not show any Ni phase not only for Ni ion concentration up to 2 mol% in the 0-2 mol% doping range[37] or up to 8 mol% in a doping range 0-10 mol%[38] but even when Ni was as high as 10 mol%[39]. In all these cases the diffraction peaks of doped anatase do not show any detectable shift compared to the undoped sample. Based on this consideration and the closer similarity of $Ni^{3+}$ ionic radii (60 pm) to $Ti^{4+}$ ions (60.5 pm), compared to $Ni^{2+}$ (69 pm), it is likely that Ni ions are incorporated in the higher oxidation state according to a mechanism of 2 $Ni^{3+}$ coupled to an oxygen vacancy as previously documented[40].

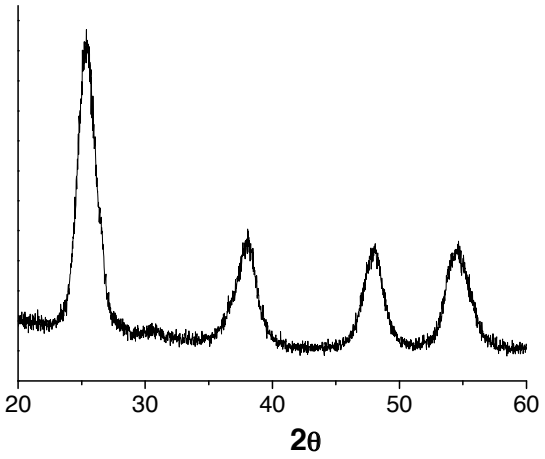


Fig. 3.6: XRD profile of unreduced TNi.

So we suppose that the reason for the low activity of TNi is that the little fraction of metallic nickel available is not sufficient to catalyse the steam reforming reaction. This is due to Ni incorporation in the support and to its lower availability to be reduced in $H_2$ flow. Ni incorporation in the anatase lattice was probably caused by the preparation method we adopted, in which the active phase was added to an uncalcined support.

For what concerns reduced SNi, the low angle XRD pattern of SBA-15 (Fig. 3.5 (b)) is characterised by the presence of a prominent peak located at 2θ~0.8° and of another weak peak at 2θ~1.8°: they can be ascribed to the (100) and (110) diffractions, respectively, associated with the 2-D p6 mm hexagonal symmetry. The peaks at 2θ ~44.5° and 51.8° correspond to metallic Ni. Finally, in the XRD profile of the reduced $ZrO_2$ sample (Fig. 3.5 (c)) only a tetragonal phase is observed and, also in this case, the presence of metallic Ni (peaks at 2θ ~44.5° and 51.8°).

We then carried out the transmission electron microscopy (HR-TEM) investigation on both fresh and exhausted catalysts in order to follow the evolution and/or transformation of the samples under the reaction conditions, thus explaining their catalytic performances.

Fig. 3.7 (a) shows that the support of reduced TNi before the reaction is made up of a highly crystalline titanium dioxide, as confirmed by the high incidence of fringes patterns, generated by the presence of crystalline planes exhibiting low hkl indexes. In particular, the inspection in detail of the spacing (d = 0.357 nm) among the interference fringes indicates that the most preferentially exposed planes belong to the (101) $TiO_2$ anatase polymorph. Moreover, the dispersion of Ni particles on titania is very high: an average nanoparticles dimension of about 0.5 nm has been estimated (see the 10x blown-up section of Fig. 3.7 (a)).

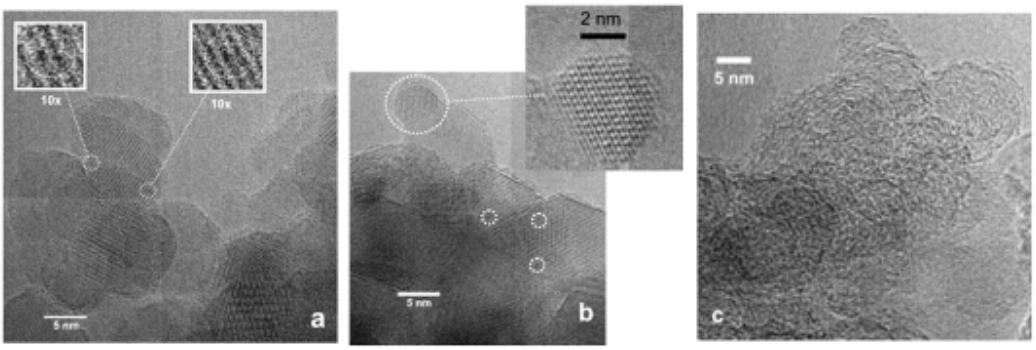


Fig. 3.7: TEM images of TNi: fresh TNi (a), TNi after SR at 500 °C (b), TNi after SR at 650 °C (c).

EDS (Energy Dispersive X-ray Spectroscopy) measurements demonstrated the presence of Ni (spectra not reported for the sake of brevity). These results are in agreement with XRD data and confirm the presence of Ni species on the surface but, apparently, in a too low concentration.

Moreover, TEM measurements relative to the corresponding exhausted sample (SR at 500 °C; see Fig. 3.7 (b)) reveal that, in these reaction conditions, the $TiO_2$ support remains almost unchanged, whereas Ni species are present both as individual metallic particles and also in a partial oxidised form. In fact, the detailed inspection of the fringe patterns indicates that the particles are here and there made up of NiO ($d_{hkl}$ = 0.208 nm) and the most exposed crystal planes belong to the (200) face of NiO (ICDD-PDF file n. 47-1049): see the inset of Fig. 3.7 (b).

Ni oxidation is one of the most common deactivation phenomena of Ni-based catalysts[41]. Nickel can be oxidized by gaseous oxygen, but even by steam at low temperature, as reported by Liberatori et al.[42], and Ni in the oxide form is inactive in steam reforming reactions. A possible explanation of this phenomenon could be the low interactions between the metal and the support, as suggested by TPR measurements, which cannot stabilise the metal phase. It has been demonstrated that Ni activity can be increased through the addition of small amounts of noble metals, which can stabilise the Ni sites in the reduced state[43]. Another possibility is to strengthen the interactions of Ni with the support (SMSI) by increasing the calcination temperature. It is well known that at high temperatures NiO and $TiO_2$ interdiffuse leading to the formation of an ilmenite type structure ($NiTiO_3$)[44]; Zhang et al. established that nickel in $NiTiO_3$ is still reducible to $Ni^0$ (although at higher temperatures than NiO) and active in the partial oxidation of methane[45]. The small amount of metallic Ni available, together with its oxidation in the SR conditions, is then likely to be the reason why, though its high dispersion, TNi is almost entirely inactive in glycerol steam reforming. Some metal particles (of almost unchanged dimensions: see the white circled portions in Fig. 3.7 (b)) can be still detected on the support: they are probably responsible for the very low conversion obtained with this sample (see Fig. 3.1).

Concerning the exhausted catalyst at 650 °C, TEM micrographs (Fig. 3.7 (c)) show that the support is now very hardly observable, as it turns out to be almost totally covered by a thin and amorphous overlayer (coating). Moreover, the collapse of the surface area of the support (revealed also by $N_2$ physisorption analysis; see Fig. 3.4 (a)) caused the sintering of the active phase (Ni particles diameter, determined by the Rietveld refinement method, of about 50 nm).

As for SNi, TEM images (reported in Fig. 3.8) of the fresh sample show that in the support it is possible to observe a highly ordered structure with a hexagonal array of cylindrical pores, thus corroborating both physisorption and XRD data. It is quite difficult to detect Ni nanoparticles, although Ni presence has been ascertained by EDS (see the spectrum reported in section 3.8 (a)). This result seems to suggest that Ni nanoparticles are located mainly within the pores of the support; this hypothesis is further supported by the decrease (about 20%) of the specific surface area of pure SBA-15 after the introduction of the metal phase.

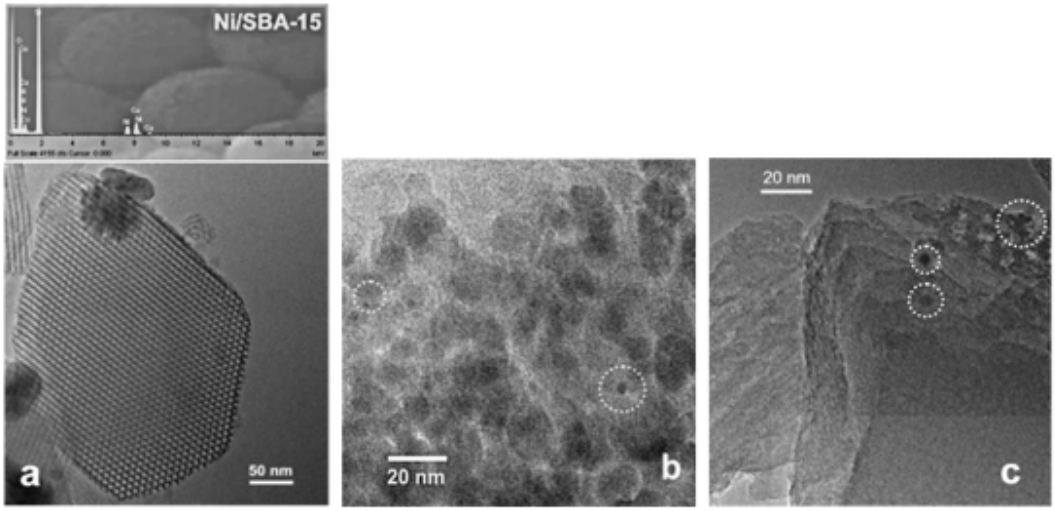


Fig. 3.8: TEM images of SNi: fresh SNi (a), SNi after SR at 500 °C (b), SNi after SR at 650 °C (c).

The morphological features reported in Fig. 3.8 (b) and 3.8 (c) indicate the possible reason of the fast deactivation that occurs for this sample in glycerol steam reforming at both temperatures, as the SBA-15 mesostructure is gradually destroyed. This is probably due to the poor mechanical and hydrothermal stability of this material: its strength in water steam at high temperatures is known to be too low. The decrease in the catalytic activity can be then ascribed to the collapse of the pore walls, which renders the Ni nanoparticles, located inside the matrix, inaccessible to reagent molecules; the residual observed activity is due to Ni particles exposed on the surface. Many efforts have been spent in order to increase the hydrothermal stability of mesoporous silicas, such as addition of inorganic salts during the synthesis or incorporation of metal oxides, as well as the increase of calcination temperature[46]. Once again, the key role of the support in stabilising the metal phase has been evidenced.

As for the third catalytic system, Fig. 3.9 (a) reports a TEM image relative to fresh ZNi, which achieved the best performance in terms of both $H_2$ yield and stability. As far as the support is concerned, the detailed analysis of the fringe patterns indicates the presence of the tetragonal polymorph of $ZrO_2$ ($d_{hkl}$ = 0.296 nm; (111) face; ICDD PDF file n. 79-1763) with an average dimension of the particles of the support of 5-8 nm. Moreover, as for TNi, the dispersion of Ni particles on the support is very high and a nanoparticles dimension of about 0.5 nm has been estimated; once again, EDS measurements (not reported for the sake of brevity) ensured that Ni is present.

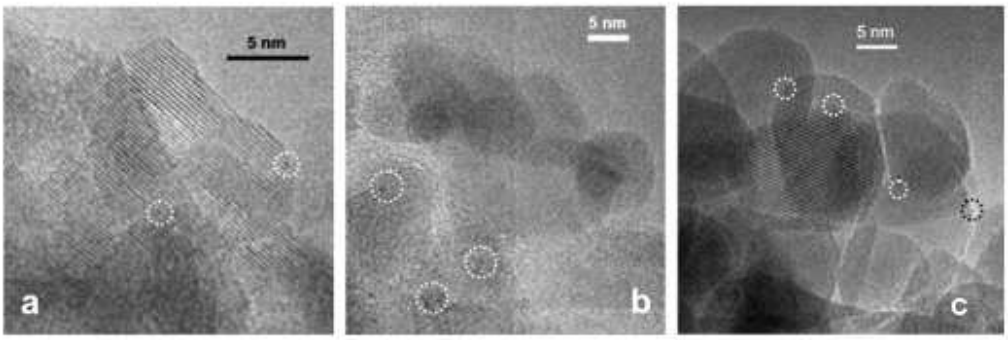


Fig. 3.9: TEM images of ZNi: fresh ZNi (a), ZNi after SR at 500 °C (b), ZNi after SR at 650 °C (c).

Fig. 3.9 (b) and 3.9 (c) clearly explain the reason of the excellent catalytic performance maintained by this material: the structure of the zirconia support is fully preserved even after 20 h in the SR conditions, as well as the dispersion of the active phase (Ni nanoparticles dimension remained unchanged).

It has been demonstrated that zirconia improves both thermal stability and oxygen storage capacity, which favours carbon gasification[47]: this study confirms the high capability of zirconia to stabilize the active phase, and this is probably due to the strong interactions between Ni and zirconia, as also highlighted by TPR measurements too (see Fig. 3.3). Moreover, zirconia is known to possess the ability to first adsorb and then dissociate water, thus enhancing the adsorption of steam on its surface and activating the gasification of hydrocarbons in the SR reactions[48] and the water-gas shift[49].

However, TEM of ZNi tested at 500 °C evidenced the presence of coke, that could be the cause of the slight deactivation of this sample. Coke deposition could be related to the presence of acid sites on the surface of the support, which can catalyze the side reactions responsible for coke formation. Zirconia indeed is known to be a solid acid: both acidic OH groups and Lewis acid sites (coordinatively unsaturated, *cus*, $Zr^{4+}$ ions) can be detected on the surface, depending on the synthesis conditions[50-52]. Probably the addition of oxides of alkaline earth metals (*i.e.* CaO, MgO, BaO), which are strong Lewis bases, could decrease the acidity of the support[53-55].

## 3.4 Conclusions

The preliminary results reported in this chapter demonstrated the suitability of Ni-based catalysts to be used in the steam reforming of biomass derivatives, due to Ni activity in breaking C–C bonds and also in promoting the water-gas shift reaction. In particular, the results highlighted the key role of the support in designing the catalytic performance and demonstrated that several factors should be considered.

First of all, the mechanical and thermal stability is an essential feature of the support. The poor mechanical and hydrothermal resistance of the SBA-15 support caused the progressive deactivation of the catalyst, since the collapse of the pore walls made the Ni nanoparticles, located inside the matrix, inaccessible to reagent molecules.

A second key factor to be considered is the ability of the support to make the active phase available for the reaction, *i.e.* through a high dispersion on the surface. The titania-supported catalyst was almost completely inactive because of the tendency of titania, probably intensified by the synthesis procedure we adopted, to incorporate Ni ions into the anatase lattice. After treatment under $H_2$ flow only a fraction on Ni was effectively reduced to metallic particles.

Strong metal-support interactions are also essential. The weak interactions between titania and metallic Ni did not prevent the oxidation (*i.e.* inactivation) of the active phase in the SR conditions.

Finally, the acidic properties of the support cannot be neglected. The zirconia support possesses all the necessary features, such as high surface area, high stability in the reaction conditions and strong interactions with the metal phase, to guarantee a high catalytic performance. Nevertheless, its acidic features were probably responsible for coke formation, thus causing a slight deactivation of the catalyst.

In conclusion, these preliminary results demonstrated that several properties simultaneously affect the catalytic performance. In the next chapters the effect of both synthesis parameters and chemical modifications on these properties will be investigated.

# References


[1] A.J. Vizcaíno, A. Carrero, J.A. Calles, Int. J. Hydrogen Energy. 32 (2007) 1450-1461.

[2] M.H. Youn, J.G. Seo, H. Lee, Y. Bang, J.S. Chung, I.K. Song, Appl. Catal. B: Environ. 98 (2010) 57-64.

[3] U. Oemar, K. Hidajat, S. Kawi, Appl. Catal. A: General. 402 (2011) 176-187.

[4] M. Lindo, A.J. Vizcaíno, J.A. Calles, A. Carrero, Int. J. Hydrogen Energy. 35 (2010) 5895-5901.

[5] A. Iriondo, V.L. Barrio, J.F. Cambra, P.L. Arias, M.B. Guemez, M.C. Sanchez-Sanchez, R.M. Navarro, J.L.G. Fierro, Int. J. Hydrogen Energy. 35 (2010) 11622-11633.

[6] C. Zhang, S. Li, G. Wu, J. Gong, Catal. Today. 233 (2014) 53-60.

[7] S. Li, C. Zhang, Z. Huang, G. Wu, J. Gong, Chem. Commun. 49 (2013) 4226-4228.

[8] F. Mariño, G. Baronetti, M. Jobbagy, M. Laborde, Appl. Catal. A: General. 238 (2003) 41-54.

[9] A. Denis, W. Grzegorczyk, W. Gac, A. Machocky, Catal. Today. 137 (2008) 453-459.

[10] G. Wen, Y. Xu, H. Ma, Z. Xu, Z. Tian, Int. J. Hydrogen Energy. 33 (2008) 6657-6666.

[11] S. Adhikari, S. D. Fernando, A. Haryanto, Renewable Energy. 33 (2008) 1097-1100.

[12] S.J. Tauster, S.C. Fung, R.L. Garden, J. Am. Chem. Soc. 100 (1978) 170-175.

[13] M. Rezaei, S.M. Alavi, S. Sahebdelfar, Z.F. Yan, Mater. Lett. 61 (2007) 2628-2631.

[14] M.H. Youn, J.G. Seo, S. Park, J.C. Jung, D.R. Park, I.K. Song, Int. J. Hydrogen Energy. 33 (2008) 7457-7463.

[15] J.A. Calles, A.J. Vizcaíno, A. Carrero, Microporous Mesoporous Mater. 119 (2009) 200-207.

[16] M.A. El-Bousiffi, D.J. Gunn, Int. J. Heat Mass Transfer. 50 (2007) 723-733.

[17] F. Frusteri, S. Freni, V. Chiodo, L. Spadaro, G. Bonura, S. Cavallaro, J. Power Sources. 132 (2004) 139-144.

[18] V. Trevisan, M. Signoretto, F. Pinna, G. Cruciani, G. Cerrato, Chem. Today. 30 (2012) 25-28.

[19] E. Ghedini, M. Signoretto, F. Pinna, G. Cruciani, Catal. Lett. 125 (2008) 359-370.

[20] F. Zane, S. Melada , M. Signoretto, F. Pinna, Appl. Catal. A: General. 299 (2006) 137-144.

[21] I. Rossetti, C. Biffi, C. L. Bianchi, V. Nichele, M. Signoretto, F. Menegazzo, E. Finocchio, G. Ramis, A. Di Michele, Appl. Catal. B: Environ. 117-118 (2012) 384-396.

[22] I. Rossetti, A. Gallo, V. Dal Santo, C. L. Bianchi, V. Nichele, M. Signoretto, E. Finocchio, G. Ramis, A. Di Michele, ChemCatChem. 5 (2013) 294-306.

[23] S. Brunauer, P.H. Emmett, E. Teller, J. Am. Chem. Soc. 60 (1938) 309-319.

[24] E.P. Barrett, L.G. Joyner, P.P. Halenda, J. Am. Chem. Soc. 73 (1951) 373-380.

[25] C.K. Cheng, S.Y. Foo, A.A. Adesina, Ind. Eng. Chem. Res. 49 (2010) 10804–10817.

[26] V. Chiodo, S. Freni, A. Galvagno, N. Mondello, F. Frusteri, Appl. Catal. A: General. 381 (2010) 1–7.

[27] G.W. Huber, J.W. Shabaker, S.T. Evans, J.A. Dumesic, Appl. Catal. B: Environ. 62 (2006) 226-235.

[28] L. Zhang, J. Lin, Y. Chen, J. Chem. Soc., Faraday Trans. 88 (1992) 2075-2078.

[29] Y. Q. Song, D. H. He , B. Q. Xu, Appl. Catal. A: General. 337 (2008) 19-28.

[30] V. García, J. J. Fernández, W. Ruíz, F. Mondragón, A. Moreno, Catal. Commun. 11 (2009) 240-246.

[31] M.J. Lazaro, Y. Echegoyen, C. Alegre, I. Suelves, R. Moliner, J.M. Palacios, Int. J. Hydrogen Energy. 33 (2008) 3320-3329.

[32] B. Huang, X. Li, S. Ji, B. Lang, F. Habimana, C. Li, J. Nat. Gas Chem. 17 (2008) 225-231.

[33] S. Ren, P. Zhang, H. Shui, Z. Lei, Z. Wang, S. Kang, Catal. Commun. 12 (2010) 132-136.

[34] F. Pinna, Catal. Today. 41 (1998) 129-137.

[35] A. Taguchi, F. Schüth, Microporous Mesoporous Mater. 77 (2005) 1-45.

[36] IUPAC Recommendations, Pure Appl. Chem. 57 (1985) 603-619.

[37] D. Zhang, J. Sol-Gel Sci. Technol. 58 (2011) 312-318.

[38] P. Guo, L. Guo, in: Detlef Stolten, Thomas Grube (Eds.), 18th World Hydrogen Energy Conference 2010 - WHEC 2010 - Parallel Sessions Book 3: Hydrogen Production Technologies - Part 2, Proceedings of the WHEC, May 16.-21. 2010, Essen - Schriften des Forschungszentrums Jülich / Energy & Environment, Vol. 78-3 -Institute of Energy Research - Fuel Cells (IEF-3) - Forschungszentrum Jülich GmbH, Zentralbibliothek, Verlag, 2010.

[39] S.D. Sharma, D. Singh, K.K. Saini, C. Kant, V. Sharma, S.C. Jain, C.P. Sharma, Appl. Catal. A: General. 314 (2006) 40-46.

[40] J. Chen, G-H. Lu, H. Cao, T. Wang, Y. Xu, Appl. Phys. Lett. 93 (2008) 172504-172506.

[41] K. Takehira, T. Ohi, T. Miyata, M. Shiraga, T. Sano, Topics in Catal. 42-43 (2007) 471-474.

[42] J.W.C. Liberatori, R.U. Ribeiro, D. Zanchet, F.B. Noronha, J.M.C. Bueno, Appl. Catal. A: General. 327 (2007) 197-204.

[43] L.P.R. Profeti, E.A. Ticianelli, E.M. Assaf, Int. J. Hydrogen Energy. 34 (2009) 5049-5060.

[44] P.K. de Bokx, R.L.C. Bonne, J.W. Geus, Appl. Catal. 30 (1987) 33-46.

[45] Y. Zhang, Z. Li, X. Wen, Y. Liu, Chem. Engin. J. 121 (2006) 115-123.

[46] E.B. Celer, M. Kruk, Y. Zuzek, M. Jaroniec, J. Mater. Chem. 16 (2006) 2824-2833.

[47] I.N. Buffoni, F. Pompeo, G.F. Santori, N.N. Nichio, Catal. Commun. 10 (2009) 1656-1660.

[48] M.H. Youn, J.G. Seo, H. Lee, Y. Bang, J.S. Chung, I.K. Song, Appl. Catal. B: Environ. 98 (2010) 57-64.

[49] K.G. Azzam, I.V. Babich, K. Seshan, L. Lefferts, J. Catal. 251 (2007) 153-162.

[50] C Morterra, G Cerrato, M. Signoretto, Catal. Lett. 41 (1996) 101-109.

[51] C. Morterra, G. Cerrato, V. Bolis, S. Di Ciero, M. Signoretto, J. Chem. Soc., Faraday Trans. 93(6) (1997) 1179-1184.

[52] C. Morterra, G. Cerrato, S. Di Ciero, Appl. Surf. Sci. 126 (1998) 107-128.

[53] J.A. Calles, A. Carrero, A.J. Vizcaíno, Micropor. Mesopor. Mater. 119 (2009) 200.207.

[54] Z. Hou, O. Yokota, T. Tanaka, T. Yashima, Appl. Catal. A: General. 253 (2003) 381-387.

[55] J. da S. Lisboa, D.C.R.M. Santos, F.B. Passos, F.B. Noronha, Catal. Today. 101 (2005) 15-21.

# Chapter 4. Effect of the synthesis procedure on the performance of $Ni/TiO_2$ catalysts in ethanol steam reforming*

## 4.1 Introduction

In Chapter 3 the crucial role of the support was highlighted. Titania was chosen as support for the preparation of one of our catalysts for its well-known ability to interact with metals[1]. The so-called strong metal-support interaction (SMSI) effect, firstly introduced by Tauster et al.[2] and observed for group VIII metals over reducible support materials, deeply affects the properties of a catalyst[3-6]. The synergism between the support and the metal is fundamental in order to stabilize the active phase and decrease the rate of coke formation[7,8]. However, in the case of our $Ni/TiO_2$ catalyst, the TPR analysis revealed a relevant percentage of non-interacting Ni particles, which did not prevent the oxidation (*i.e.* inactivation) of the active phase in the SR conditions. Moreover, Ni incorporation in the anatase lattice led to a negligible activity of the catalyst[9]. We concluded that these phenomena (weak metal-support interaction and Ni incorporation in the lattice) could be due to the preparation method, in which the active phase was added to an uncalcined support.

In this chapter, the effect of the synthesis parameters (i. Ni addition on $Ti(OH)_4$ or $TiO_2$; ii. calcination temperature) on the properties of the catalyst, and then on its activity, is investigated. In this case ESR was chosen as test reaction and the results compared with those of GSR reported in Chapter 3. ESR was carried out at relatively low temperature, *i.e.* 500 °C, in order to limit the energy input to the process.

---

* The results reported in this chapter are published as: "*Hydrogen production by ethanol steam reforming: Effect of the synthesis parameters on the activity of $Ni/TiO_2$ catalysts*", V. Nichele, M. Signoretto, F. Menegazzo, I. Rossetti, G. Cruciani, Int. J. Hydrogen Energy. 39 (2014) 4252-4258. 

## 4.2 Experimental Section

### 4.2.1 Catalysts preparation

$Ti(OH)_4$ was prepared by a conventional precipitation method[9,10], as reported in Chapter 3. Part of the titanium hydroxide was calcined at 500 or 800 °C. The active phase was added to the support through the incipient wetness impregnation technique using $Ni(NO_3)_2*6H_2O$ (*Sigma – Aldrich, purity ≥98.5%*), in the proper concentration in order to obtain a 10 wt% Ni loading.

Four different samples were synthesized. Two samples were prepared by adding Ni on the $Ti(OH)_4$ support ($T_H$) and calcining at 500 °C ($T_HNi500$[**]) or 800 °C ($T_HNi800$) for 4 hours. The two other samples were prepared by adding Ni on the $TiO_2$ support ($T_{Ox}$) and calcining at 500 °C ($T_{Ox}Ni500$) or 800 °C ($T_{Ox}Ni800$) for 4 hours.

### 4.2.2 Catalysts characterization

Specific surface area and pores size distribution were evaluated through $N_2$ adsorption-desorption isotherms at -196 °C (MICROMERITICS, ASAP 2000 Analyser). Surface area was calculated on the basis of the BET equation[11], whereas the pores size distribution was determined by the BJH method, applied to the $N_2$ desorption branch of the isotherm[12]. Prior to the analyses the samples were reduced in $H_2$ flow for 1 h at 500 °C ($T_HNi500$ and $T_{Ox}Ni500$) or 800 °C ($T_HNi800$ and $T_{Ox}Ni800$), dried overnight at 110 °C and then outgassed in vacuum at 110 °C for 2 hours. For the samples with low surface area a lab-made equipment for single point analysis has been used[13].

Temperature programmed reduction (TPR) measurements were carried out by placing the catalyst in a quartz reactor and heating in a 5% $H_2$/Ar mixed gas stream flowing at 40 mL/min at a heating rate of 10 °C/min from 25 to 800 °C. $H_2$ consumption was monitored with a TCD detector.

X-ray powder diffraction (XRD) analyses were carried out in the lab of Prof. Giuseppe Cruciani in the University of Ferrara. XRD patterns were measured by a Bruker D8 Advance diffractometer equipped with a Si(Li) solid state detector (SOL-X) and a sealed

[**] $T_HNi500$ was prepared in the same way of TNi, as described in Chapter 3.

tube providing Cu Kα radiation. The quantitative phase analysis and crystal size determination of the support and metal phases in the samples were obtained by the Rietveld refinement method as implemented in the Bruker TOPAS program. Also in this case, the samples were reduced in $H_2$ flow for 1 h at 500 °C ($T_H$Ni500 and $T_{Ox}$Ni500) or 800 °C ($T_H$Ni800 and $T_{Ox}$Ni800) before the analysis.

### 4.2.3 Catalytic tests

The ESR catalytic tests were carried out in the lab of Dr. Ilenia Rossetti in the University of Milan.

Activity tests were performed by means of a micropilot plant constituted by an Incoloy 800 continuous downflow reactor (*i.d.* 0.9 cm, length 40 cm), heated by an electric oven. The reactor temperature was controlled by an Eurotherm 3204 TIC. The catalysts were pressed, ground and sieved into 0.15-0.25 mm particles and *ca.* 0.5 g were loaded into the reactor after dilution 1:3 (vol/vol) with SiC of the same particle size. The void part of the reactor over and below the catalyst bed has been filled with quarts beads (0.5-1 mm size). Catalyst activation was accomplished by feeding 50 $cm^3$/min of a 20 vol% $H_2/N_2$ gas mixture, while heating by 10 °C/min up to 500 °C ($T_H$Ni500 and $T_{Ox}$Ni500) or 800 °C ($T_H$Ni800 and $T_{Ox}$Ni800), then kept for 1 h. During activity testing 0.017 $cm^3$/min of a 3:1 (mol/mol) $H_2O$:$CH_3CH_2OH$ liquid mixture were fed to the reactor by means of a Hitachi, mod. L7100, HPLC pump, added with 56 $cm^3$/min of $N_2$, used as internal standard, and 174 $cm^3$/min of He. Such dilution of the feed stream was calibrated so to keep the reactants mixture in the vapour phase even at zero conversion at the reactor outlet. No liquid phase was ever detected at reactor outlet. The activity tests were carried out at atmospheric pressure, GHSV = 2500 $h^{-1}$ (referred to the ethanol + water gaseous mixture) at 500 °C. The analysis of the out-flowing gas was carried out by a gaschromatograph (Agilent, mod. 7980) equipped with two columns connected in series (MS and Poraplot Q) with a thermal conductivity detector (TCD), properly calibrated for the detection of ethanol, acetaldehyde, acetic acid, water, ethylene, CO, $CO_2$, $H_2$. Material balance on C-containing products was checked to quantify coke deposition. Repeated analyses of the effluent gas were carried out every hour and the whole duration of every test at each temperature was *ca.* 8 h. The raw

data, expressed as mol/min of each species outflowing from the reactor, have been elaborated as follows.

**Products distribution**[14]: $Y_i$ = mol i / Σ(mol i)

**C balance:** 100 - (((mol $CH_3CH_2OH$ *2)$_{in}$ – Σ (mol $C_i$ * $\chi_i$)$_{out}$) / (mol $CH_3CH_2OH$ * 2)$_{in}$ )*100

**Conversion:** $X_i$ = (mol i $_{in}$ - mol i $_{out}$) / mol i $_{in}$ i= $H_2O$, $CH_3CH_2OH$

**Selectivity:** $S_i$ = (mol i / $\nu_i$) / (mol ethanol $_{in}$ - mol ethanol $_{out}$)

**$H_2$ productivity:** mol $H_2$ out / min $kg_{cat}$

where *i* = products detected, dry basis; $\chi_i$ = number of C atoms in the *i*-th molecule; $\nu_i$ = stoichiometric coefficient of species *i* in the ESR reaction.

## 4.3 Results and discussion

As reported in Section 2.2, ESR is an endothermic reaction that leads to the formation of $H_2$ and $CO_2$ according to the stoichiometric reaction, Eq. 1:

Eq.1 $$CH_3CH_2OH + 3H_2O \rightleftharpoons 6H_2 + 2CO_2$$

including the water-gas shift of the intermediate CO, which further increases the hydrogen yield (Eq. 2):

Eq. 2 $$CO + H_2O \rightleftharpoons CO_2 + H_2$$

However the overall process is quite complex and several side reactions can take place, such as ethanol dehydrogenation, dehydration and decomposition, leading to the formation of acetaldehyde, ethylene and methane respectively. These by-products compete for hydrogen atoms, thus lowering the overall $H_2$ yield[15,16].

In Chapter 3 it was shown that a $Ni/TiO_2$ catalyst prepared by impregnating the uncalcined support was almost completely inactive in glycerol steam reforming[9]. We supposed that all nickel was incorporated in the anatase lattice. This hypothesis is in agreement with

previous reports[17]. Two different substitution mechanisms have been suggested to explain the incorporation of $Ni^{2+}$ in anatase: occupation of nickel ions in octahedral interstitial positions charge-compensated by $Ti^{4+}$ vacancies or substitution of $Ti^{4+}$ with $Ni^{2+}$ balanced by oxygen vacancies. However, it is more likely that Ni is incorporated as $Ni^{3+}$, because of the closer similarity of $Ni^{3+}$ ionic radii (60 pm) to $Ti^{4+}$ ions (60.5 pm), compared to $Ni^{2+}$ (69 pm)[18]. The work reported in this chapter is aimed to further verify the effect of the synthesis procedure on the properties of $Ni/TiO_2$ catalysts.

### 4.3.1 Samples calcined at 500 °C

The samples calcined at 500 °C were characterized by $N_2$ physisorption measurements (Fig. 4.1).

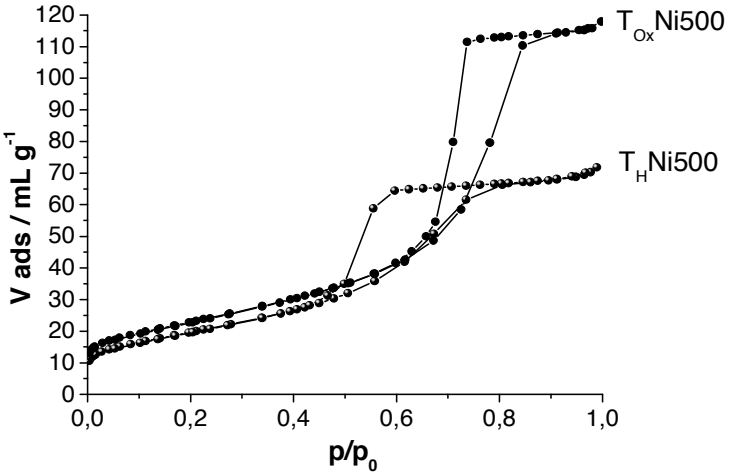


Fig. 4.1: Physisorption isotherms of $T_H$Ni500 and $T_{Ox}$Ni500.

It can be noted that both $T_H$Ni500 and $T_{Ox}$Ni500 exhibit a IV-type isotherm and a H2-type hysteresis loop. However, the shape of both the isotherms and the hysteresis loops are quite different. In $T_H$Ni500 the hysteresis loop starts at a lower value of $p/p_o$ if compared with $T_{Ox}$Ni500, which suggests a smaller average pores diameter (4 nm and 7 nm respectively). The increase of average pore size is consistent with the double calcination step. The larger hysteresis loop in $T_H$Ni500 denotes a larger pores size distribution. Both catalysts are characterized by a rather high surface area (71 and 82 $m^2/g$ respectively).

Fig. 4.2 shows the TPR profiles of samples $T_H$Ni500 and $T_{Ox}$Ni500.

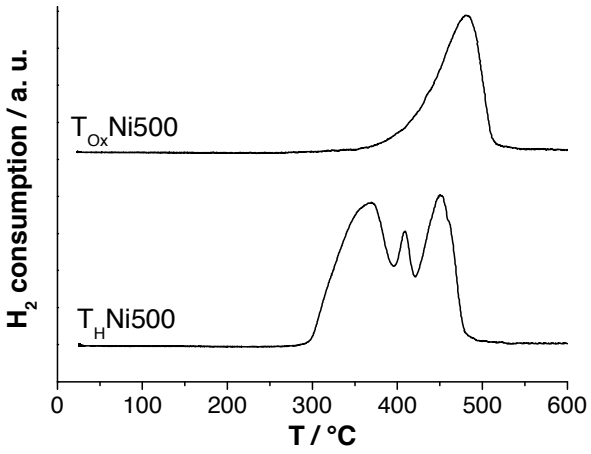


Fig. 4.2: TPR profiles of $T_H$Ni500 and $T_{Ox}$Ni500.

The most evident difference between $T_H$Ni500 and $T_{Ox}$Ni500 is the number of NiO species found on the support. As already seen in Chapter 3[9], the TPR pattern of $T_H$Ni500 shows three peaks, centred at 370 °C, 410 °C and 450 °C, ascribable to as many NiO species more or less strongly interacting with the titania support[19]. On $T_{Ox}$Ni500 only one peak centred at 480 °C, ascribable to NiO species strongly interacting with the support, can be detected. These results seem to suggest a kind of heterogeneity of NiO species on sample $T_H$Ni500. On the contrary $T_{Ox}$Ni500 exhibits a single NiO species with strong interactions with the support.

X-ray diffraction measurements on both unreduced and reduced catalysts were also carried out. Fig. 4.3(a) compares the XRD profiles of $T_H$Ni500 and $T_{Ox}$Ni500 before the reduction.

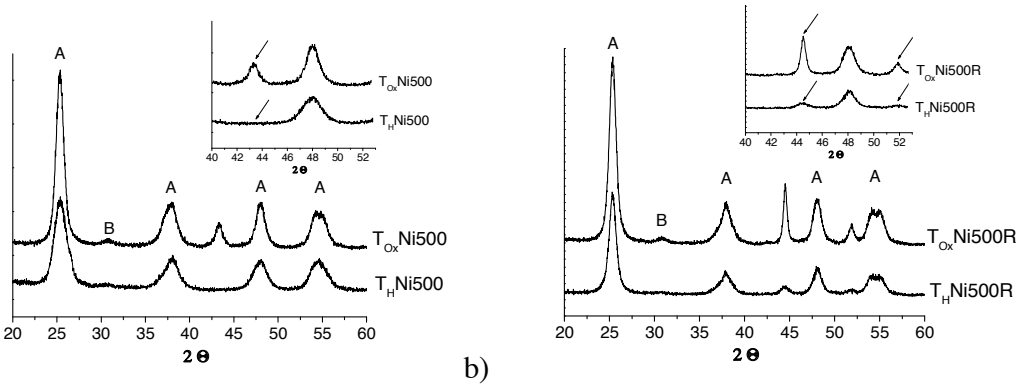


a) b)

Fig. 4.3: XRD profiles of: a) unreduced $T_H$Ni500 and $T_{Ox}$Ni500 (inset: NiO peak at 2θ ≈ 43.4°); b) reduced (R) $T_H$Ni500R and $T_{Ox}$Ni500R (inset: Ni peaks at 2θ ≈ 44.5° and 2θ ≈ 51.8°). A = Anatase; B = Brookite.

In both samples the main phase of the support is nanocrystalline anatase (A), with a small percentage of brookite (B). On the contrary, with regard to the metal phase, a basic difference can be detected: the occurrence of NiO is clearly detected (inset of Fig. 4.3(a) with peak at $2\theta \approx 43.4°$) only in sample $T_{Ox}$Ni500. As reported in Chapter 3[9], the absence of NiO diffraction peak in $T_H$Ni500 can be explained by nickel incorporation into the anatase lattice. Its presence in the XRD pattern of $T_{Ox}$Ni500 suggests the strong influence of the synthesis procedure: the calcination of the support before Ni addition seems to prevent the incorporation of the Ni phase in the support. It is plausible that this difference strongly affects nickel reducibility. In fact, XRD analyses of the reduced (R) catalysts (reported in Fig. 4.3(b)) show that the diffraction peaks of metallic nickel are clearly observable only for $T_{Ox}$Ni500R, whereas for $T_H$Ni500R they can be hardly evidenced. Moreover, the Ni contents obtained by Rietveld quantitative phase analysis, although affected by a large potential uncertainty, appear almost complete in $T_{Ox}$Ni500R (about 8%) and much smaller in $T_H$Ni500R (about 3%). These results suggest that Ni reduction is inhibited by its incorporation in the anatase lattice, which can be avoided by the choice of the proper synthesis procedure.

$T_H$Ni500 and $T_{Ox}$Ni500 were tested in ethanol steam reforming at 500 °C (Tab. 4.1).

| | **$T_H$Ni500** | **$T_{Ox}$Ni500** | **$T_H$Ni800** | **$T_{Ox}$Ni800** |
|---|---|---|---|---|
| *Ethanol conversion (%)* | 33 ± 6 | 80 ± 20 | 99 ± 1 | 86 ± 2 |
| *$H_2$ productivity (mol/min*$kg_{cat}$)* | - | 0.21 ± 0.05 | 0.84 ± 0.02 | 0.44 ± 0.06 |
| *C balance (%)* | 74 ± 7 | 70 ± 10 | 77 ± 1 | 66 ± 4 |
| *$CO/CO_2$* | - | 2.5 ± 0.9 | 1.3 ± 0.1 | 1.1 ± 0.2 |
| *$CH_3CHO$ selectivity (%)* | 82 ± 7 | 19 ± 6 | 0.24 ± 0.01 | 5.9 ± 0.5 |
| *$CH_4$ selectivity (%)* | - | 6 ± 2 | 7.1 ± 0.3 | 13.1 ± 0.8 |

Tab. 4.1: Catalytic activity data in ethanol steam reforming. Average values over 4-8 h-on-stream. Maximum $H_2$ productivity theoretically achievable = 1.83 mol/min*$kg_{cat}$.

Operating at the lowest possible temperature is advantageous to limit the heat input to the reaction and thus fuel consumption. Nevertheless, at 500 °C many active phases fail in completely convert ethanol or, even at full reactant conversion, lead to unsatisfactory carbon balance. Indeed, catalyst coking is more sensitive around this temperature.

Therefore, a challenging goal would be to find out active and sufficiently stable catalysts for ESR at this temperature.

Ethanol conversion at this temperature was incomplete and almost undetectable $H_2$ amount was achieved with $T_H$Ni500, as already observed in GSR in Chapter 3. As explained in Section 2.3, both ESR and GSR are characterized by a complex network of reactions and require a highly selective catalyst. Of course the two reactions cannot be considered "interchangeable", since the reagents have quite different properties, thus leading to different selectivity to the possible by-products. Nevertheless, the effective utilization of biomass as a hydrogen source depends critically on the discovery of versatile catalysts, that can be used indifferently in both processes with high performance. We wanted to verify if our catalysts were sufficiently versatile to be used in both GSR and ESR.

$T_H$Ni500 was only active for ethanol dehydrogenation to acetaldehyde and also led to extensive coke deposition as suggested by the poor C balance. The latter value should be compared with that of a blank test reported in Ref. 20, which closed to 91% at the same testing temperature. The low C balance can be probably related to a strong sintering of the active phase (Ni particles of 40 nm were detected by XRD after the reaction).

By contrast, $T_{Ox}$Ni500 exhibited higher ethanol conversion, though $H_2$ productivity remained limited due to a high amount of by-products unreformed (acetaldehyde and methane). Also in this case the poor carbon balance suggested some coke deposition and a poor stability was observed during testing, as evidenced by the very high standard deviation on almost every parameter reported in Table 4.1. In particular, the C balance was initially ca. 60%, increasing up to *ca*. 80% after 5 h-on-stream, when ethanol conversion started decreasing from 100% to *ca*. 50%.

The present catalytic data indicate a remarkable increase in activity for the $T_{Ox}$Ni500 catalyst with respect to $T_H$Ni500. This difference can be ascribed to the availability of the active phase in $T_{Ox}$Ni500, whereas in $T_H$Ni500 Ni incorporation in the anatase lattice depressed the catalytic activity. Nevertheless, the catalytic performance is not optimal yet, as $T_{Ox}$Ni500 exhibits a low carbon balance, which suggests some coke deposition that deactivates the most active Ni sites, leading to lower ethanol conversion and a poor hydrogen productivity. Coking can be related to the contribution of the Lewis acidity of the support[21]. Moreover, coking is thought to occur more promptly over bigger Ni sites[22-25] and, as a matter of fact, a certain sintering of the active phase was detected by XRD

analysis of spent $T_{Ox}$Ni500. The Rietveld refinement analysis revealed that Ni particle size increased from 14 to 21 nm.

In conclusion these preliminary results show that, for the samples calcined at 500 °C, the calcination of the support is essential to prevent Ni incorporation in the anatase lattice, thus making the catalyst active in steam reforming reactions. Nevertheless, the catalyst still shows a certain instability, with sintering even at such low temperature, and coking, which is likely to be ascribed to the low temperature thermal treatment.

### 4.3.2 Samples calcined at 800 °C

In order to verify the effect of calcination temperature on the physico-chemical properties of the catalysts, a series of characterization measurements was carried out onto the catalysts calcined at 800°C.

Physisorption analyses revealed that both $T_H$Ni800 and $T_{Ox}$Ni800 suffered the collapse of the porous structure of the support, thus obtaining a non-porous material. This effect can be ascribed to the strong thermal treatment that the samples experienced. A single point BET measurement was carried out and a specific surface area of *ca*. 4 and 2 $m^2/g$, respectively, was obtained.

Fig. 4.4 compares the XRD patterns of $T_H$Ni800 and $T_{Ox}$Ni800 before the reduction treatment.

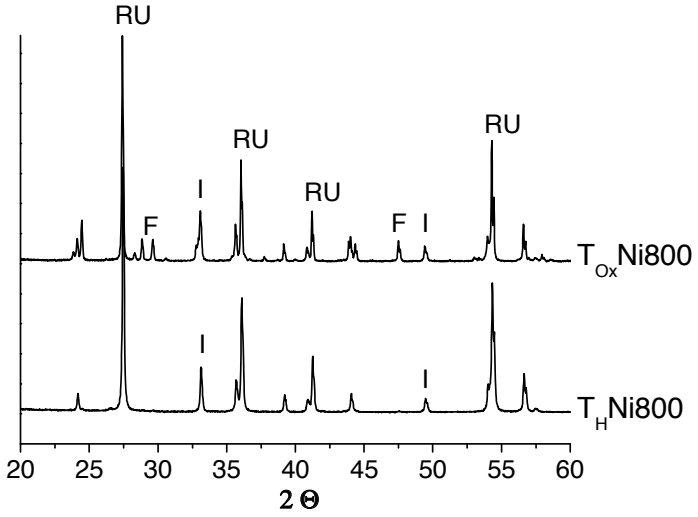


Fig. 4.4: XRD profiles of unreduced $T_H$Ni800 and $T_{Ox}$Ni800 (RU = Rutile; I = Ilmenite; F = Freudenbergite).

The collapse of the specific surface area values is supported by the presence of very sharp diffraction peaks, in good agreement with the above physisorption data. It is evident that the titania support is present mainly in the rutile (RU) phase in both samples, because of the high calcination temperature. As for the Ni phase, the XRD patterns clearly indicate the presence of different Ni species depending on the synthesis procedure. In $T_H$Ni800, Ni is present mainly as $NiTiO_3$. This ilmenite-type structure (I) formed as a consequence of the reaction between NiO and $TiO_2$ during the calcination at high temperature, as also previously reported[19,26,27]. On the contrary, in the case of $T_{Ox}$Ni800, Ni is present both as $NiTiO_3$ (I) and as a Ni-freudenbergite phase (F).

These results are confirmed by the TPR measurements, reported in Fig. 4.5.

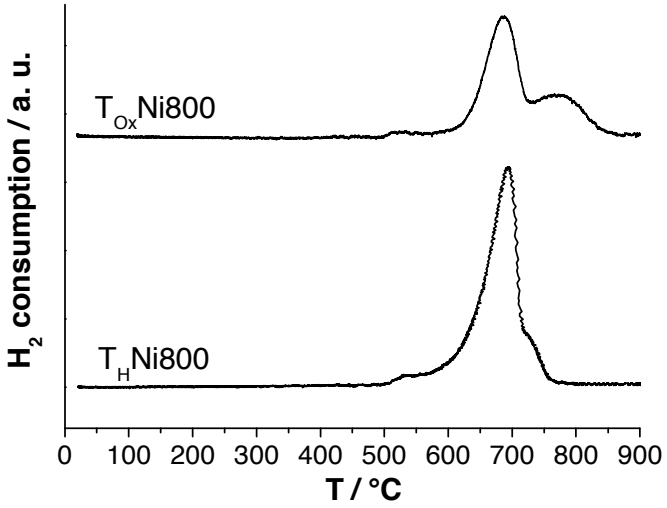


Fig. 4.5: TPR profiles of $T_H$Ni800 and $T_{Ox}$Ni800.

The TPR profile of $T_H$Ni800 exhibits only one peak at about 690 °C, due to the reduction of $NiTiO_3$, whereas in $T_{Ox}$Ni800 two peaks can be detected, ascribable to the reduction of $NiTiO_3$ (690 °C) and Ni-freudenbergite (785 °C). As a general comment, it can be noted that the TPR patterns of the samples calcined at 800 °C show a shift of the reduction peaks towards much higher temperatures with respect to the catalysts calcined at 500 °C. Harder reducibility of samples calcined at 800°C can be ascribed to the presence of a mixed oxide. Moreover, it is well known that the interaction between metal and support increases with calcination temperature[27]. Nevertheless the nature of these interactions changes according to the synthesis procedure and leads to the formation of various Ni-species characterized by a different reducibility. In fact, in the XRD analysis of reduced (R) $T_H$Ni800R (Fig. 4.6)

the ilmenite diffraction peaks disappeared, with the parallel appearance of those of metallic nickel, revealing the complete reduction of $NiTiO_3$ to $Ni^0$. On the contrary, on $T_{Ox}$Ni800R only a fraction of the Ni-species was reduced to $Ni^0$, as part of Ni is still present as Ni-freudenbergite.

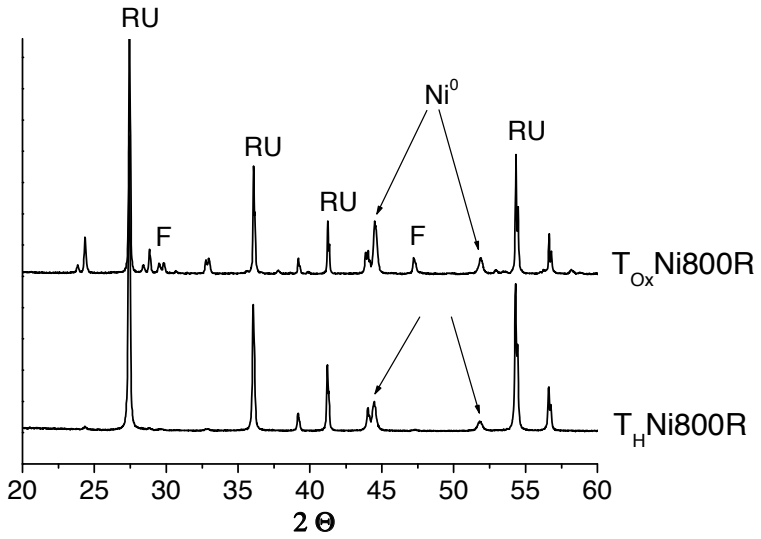


Fig. 4.6: XRD profiles of reduced (R) $T_H$Ni800R and $T_{Ox}$Ni800R (RU = Rutile; F = Freudenbergite).

As previously observed for the samples calcined at 500 °C, the interaction of the Ni-species with the titania support and their reducibility to metallic nickel seem to be strongly affected by the synthesis procedure. The catalytic performance is affected as well (see Table 4.1). In fact, $T_H$Ni800 was the most active catalyst of this series, with an almost complete ethanol conversion, whereas $T_{Ox}$Ni800 had a lower and decreasing conversion of the alcohol. These results seem to be related, also in this case, to the availability of metallic nickel, which depends on the reducibility of the different Ni-species. Nickel in $NiTiO_3$ is completely reduced to $Ni^0$, as also reported by Zhang et al.[28]. This is the reason why $T_H$Ni800 is active in ESR, with total conversion of the reagent. On the contrary, the presence of Ni-freudenbergite hinders Ni reduction, thus depressing the catalytic activity of $T_{Ox}$Ni800.

With regard to hydrogen, $T_H$Ni800 hydrogen productivity was twice as large as the $T_{Ox}$Ni800 one. The higher catalytic activity of the $T_H$Ni800 sample with respect to the $T_{Ox}$Ni800 one was also demonstrated in terms of lower selectivity to by-products, indicating reforming activity also for methane and acetaldehyde at such low temperature.

The induction period before reaching optimal and stable operation may be ascribed to the harsh reducibility of the mixed oxide formed, so that a longer period under reducing atmosphere may help exploiting the best performance.

Also the carbon balance for $T_H$Ni800 was higher and stable with respect to $T_{Ox}$Ni800, although still not optimal. Both samples are characterized by Ni particles with quite big dimensions (27 nm in $T_H$Ni800, 41 nm in $T_{Ox}$Ni800, determined by Rietveld refinement analysis). This can be the reason for the low values of C balance and our results seem to confirm that the higher the Ni particles size, the lower the C balance (the C balance for $T_H$Ni800, that possesses smaller Ni particles than $T_{Ox}$Ni800, is a little higher). Nevertheless it should be underlined that, even if not optimal, the carbon balance is very stable with time-on-stream, especially for $T_H$Ni800, and this is because nickel sintering did not take place. Ye et al.[29] found that $Ni^0$ reduced from $NiTiO_3$ was highly dispersed and that the agglomeration and sintering of the nickel particles was inhibited. Our XRD results confirmed that Ni particle size remained constant also after the reaction. This result can be attributed to the SMSI effect, due to the strong interaction between Ni and titania, and to the phase transformation of the support from anatase to rutile as a consequence of the calcination temperature, which hinders a significant Ni incorporation in the titania lattice. Although an early study suggested that nickel oxide solubility would be enhanced upon anatase-to-rutile conversion[30], no definite results are available on this issue. In fact the oxygen vacancy defects which charge-compensate the incorporation of $Ni^{2+}$ or $Ni^{3+}$ ions into the anatase lattice are likely to be removed by annealing at high temperature and transformation to rutile, leading to expulsion of Ni from rutile lattice. Recently Raj at al.[5] found that a Ni/rutile catalyst is more active in selective hydrogenation of acetophenone than Ni/anatase because of higher concentration of Ni on the surface and SMSI.

The availability of metallic Ni sites, stabilized against sintering by strong interaction with the titania support, seems to be the key to achieve satisfactory catalytic performance. In order to achieve these results, the synthesis conditions must be properly tuned.

## 4.4 Conclusions

In this chapter the catalytic activity of $TiO_2$-supported Ni catalysts in ESR was analyzed. The results highlighted that a high performance is strictly related to two parameters: nickel

reducibility and strong metal-support interactions. Nickel reducibility is an essential condition to obtain high performing catalysts, since it is related to the availability of metallic Ni, which is the active phase in ESR. For our samples, Ni incorporation (both in the anatase lattice of the support or in a scarcely reducible structure as Ni-freudenbergite) depressed the catalytic activity (*i.e.* low ethanol conversion and hydrogen productivity). The second condition is the stabilization of Ni particles through strong metal-support interactions. We found that Ni sintering led to fast coking and deactivation.

Nevertheless our results demonstrated that, in the case of $Ni/TiO_2$ catalysts, these two conditions can be reached only by properly tuning the synthesis conditions. Synthesis parameters such as the chemical nature of the support (*i.e.* titanium oxide or hydroxide) or the calcination temperature can dramatically change the properties of a catalyst and its performance.

# References


[1] S. Adhikari, S. D. Fernando, A. Haryanto, Renewable Energy. 33 (2008) 1097-1100.

[2] S.J. Tauster, S.C. Fung, R.L. Garden, J. Am. Chem. Soc. 100 (1978) 170-175.

[3] M.A. Vannice, R.L. Garten, J. Catal. 56 (1979) 236-248.

[4] T. Wu, Q. Yan, H. Wan, J. Mol. Catal. A: Chem. 226 (2005) 41-48.

[5] K. J. A. Raj, M. G. Prakash, R. Mahalakshmy, T. Elangovan, B. Viswanathan, Catal. Sci. Technol. 2 (2012) 1429-1436.

[6] Y. Men, M. Yang, Catal. Commun. 22 (2012) 68-73.

[7] A. Denis, W. Grzegorczyk, W. Gac, A. Machocki, Catal. Today. 137 (2008) 453-459.

[8] G. Wen, Y. Xu, H. Ma, Z. Xu, Z. Tian, Int. J. Hydrogen Energy. 33 (2008) 6657-6666.

[9] V. Nichele, M. Signoretto, F. Menegazzo, A. Gallo, V. Dal Santo, G. Cruciani, G. Cerrato, Appl. Catal. B: Environ. 111-112 (2012) 225-232.

[10] V. Trevisan, M. Signoretto, F. Pinna, G. Cruciani, G. Cerrato, Chem. Today. 30 (2012) 25-28.

[11] S. Brunauer, P.H. Emmett, E. Teller, J. Am. Chem. Soc. 60 (1938) 309-319.

[12] E.P. Barrett, L.G. Joyner, P.P. Halenda, J. Am. Chem. Soc. 73 (1951) 373-380.

[13] T. Allen, Particle size measurement – Surface area and pore size determination, Chapman & Hall, vol. 2, 5th ed, pag. 51 (1997).

[14] M. Benito, R. Padilla, A. Serrano-Lotina, L. Rodríguez, J.J. Brey, L. Daza, J. Power Sources. 192 (2009) 158-164.

[15] A. Carrero, J.A. Calles, A.J. Vizcaíno, Appl. Catal. A: General. 327 (2007) 82-94.

[16] M. Lindo, A.J. Vizcaíno, J.A. Calles, A. Carrero, Int. J. Hydrogen Energy. 35 (2010) 5895-5901.

[17] S.D. Sharma, D. Singh, K.K. Saini, C. Kant, V. Sharma, S.C. Jain, C.P. Sharma, Appl. Catal. A: General. 314 (2006) 40-46.

[18] J. Chen, G-H. Lu, H. Cao, T. Wang, Y. Xu, Appl. Phys. Lett. 93 (2008) 172504-172506.

[19] M.J. Lazaro, Y. Echegoyen, C. Alegre, I. Suelvea, R. Moliner, J.M. Palacios, Int. J. Hydrogen Energy. 33 (2008) 3320-3329.

[20] I. Rossetti, C. Biffi, C.L. Bianchi, V. Nichele, M. Signoretto, F. Menegazzo, E. Finocchio, G. Ramis, A. Di Michele, Appl. Catal. B: Environ. 117-118 (2012) 384-396.

[21] I. Rossetti, A. Gallo, V. Dal Santo, C.L. Bianchi, V. Nichele, M. Signoretto, E. Finocchio, G. Ramis, A. Di Michele, ChemCatChem. 5 (2013) 294-306.

[22] G. Centi, S. Perathoner, Catal. Today. 148 (2009) 191-205.

[23] V.M. Gonzalez-DelaCruz, J.P. Holgado, R. Pereníguez, A. Caballero, J. Catal. 257 (2008) 307-314.

[24] K.O. Christensen, D. Chen, R. Lødeng, A. Holmen, Appl. Catal. A: General. 314 (2006) 9-22.

[25] D. Chen, K.O. Christensen, E. Ochoa-Fernandez, Z. Yu, B. Tøtdal, N. Latorre, A.Monzòn, A. Holmen, J. Catal. 229 (2005) 82-96.

[26] P.K. de Bokx, R.L.C. Bonne, J.W. Geus, Appl. Catal. 30 (1987) 33-46.

[27] J. Chen, N. Yao, R. Wang, J. Zhang, Chem. Eng. J. 148 (2009) 164-172.

[28] Y. Zhang, Z. Li, X. Wen, Y. Liu, Chem. Engin. J. 121 (2006) 115-123.

[29] J.L. Ye, Y.Q. Wang, Y. Liu, H. Wang, Int. J. Hydrogen Energy. 33 (2008) 6602-6611.

[30] D.B. Goldman, J. Am. Ceram. Soc. 66 (1983) 811-814.

# Chapter 5. Inhibition of coke formation in ethanol steam reforming by CaO-doping of $Ni/ZrO_2$ catalysts*

## 5.1 Introduction

According to the results reported in Chapter 3, $Ni/ZrO_2$ seemed to be the best performing among the tested catalysts, in terms of both catalytic activity and hydrogen yield. The key role of several properties of the zirconia support on the catalytic performance was emphasized, such as its high surface area and stability in the reaction conditions. Moreover, strong metal-support interactions are essential to stabilize the active phase on the surface, thus preventing sintering phenomena, as it was ascertained also for $Ni/TiO_2$ catalysts in Chapter 4[1]. Zirconia is an optimal support in steam reforming reactions also because of its ability to first adsorb and then dissociate water, thus enhancing the adsorption of steam on its surface and activating the gasification of hydrocarbons[2] and the water-gas shift[3]. Nevertheless, a certain deactivation of the catalyst due to coke formation was detected.

Coke deposition can be controlled by properly tuning the operating conditions (*i.e.* steam-to-ethanol ratio, reaction temperature)[4], but the formulation of the catalyst plays a key role as well[5]. Coking is particularly significant at low temperature (*i.e.* 500 °C), since coke forms but is not effectively gasified by steam. However, in this work we decided to operate at 500 °C because, as reported also in Chapter 4, it would be very advantageous being able to operate around this temperature, in order to limit the energy input to the process with respect to common reaction conditions (T > 650°C). Therefore, improving catalyst resistance to coking represents a milestone for the development of low temperature ESR. The acidity of the support in particular should be properly tuned, since the side reactions leading to the formation of coke occur mainly on the acid sites of the support[6-8]. Zirconia is known to be a solid acid: both acidic OH groups and Lewis acid sites (coordinatively

* The results reported in this chapter are published as: "*$Ni/ZrO_2$ catalysts in ethanol steam reforming: Inhibition of coke formation by CaO-doping*", V. Nichele, M. Signoretto, F. Pinna, F. Menegazzo, I. Rossetti, G. Cruciani, G. Cerrato, A. Di Michele, Appl. Catal. B: Environ. 150-151 (2014) 12-20. 

unsaturated, *cus*, $Zr^{4+}$ ions) can be detected on the surface, depending on the synthesis conditions[9-11]. The addition of oxides of alkaline earth metals, such as CaO, which are strong Lewis bases, can decrease the acidity of the support[12-14], thus inhibiting the side reactions responsible for coke deposition. It should be considered that doping can modify also other properties, of both the support (oxygen transport, redox properties)[15,16] and the catalyst (dispersion of the active phase, interactions between metal and support)[17,18].

In this chapter, $Ni/ZrO_2$ catalysts doped with various amounts of CaO are synthesized and characterized, with the aim to improve the catalytic performance of the catalyst in the low temperature ESR, in particular with regard to inhibition of coke formation. The effect of CaO-doping of the zirconia support on both the physico-chemical properties of the materials and the catalytic performance of the samples is evaluated.

## 5.2 Experimental Section

### 5.2.1 Catalysts preparation

$Zr(OH)_4$ was prepared by a precipitation method[19,20], as reported in Chapter 3. $Zr(OH)_4$ was impregnated with an aqueous solution containing both the metal ($Ni(NO_3)_2*6H_2O$, *Sigma-Aldrich, purity ≥ 98.5%*) and the dopant ($Ca(NO_3)_2*4H_2O$, *Fluka, purity ≥ 99%*) precursors. The active phase (Ni) and the dopant (CaO) were added to $Zr(OH)_4$ simultaneously by means of the incipient wetness impregnation technique. Ni was kept constant in all the samples (10 wt%), whereas CaO varied (0, 3, 6, 9 wt%). It was chosen to add CaO by incipient wetness impregnation in order to optimize the synthesis procedure by adding both the metal and the dopant in one single step. The samples were dried overnight at 110 °C and finally heated (2 °C/min) up to 500 °C in flowing air (30 mL/min STP) and kept at this temperature for 4 hours.

The reference sample, $Ni/ZrO_2$, is labelled as ZNi (synthesized as reported in Chapter 3), whereas doped samples are labelled as $ZCa_xNi$, where $Ca_x$ denotes the CaO amount.

### 5.2.2 Catalysts characterization

Specific surface area and pores size distribution were evaluated through $N_2$ adsorption-desorption isotherms at -196 °C (MICROMERITICS, ASAP 2000 Analyser). Surface area was calculated on the basis of the BET equation[21]. Prior to the analyses the samples were reduced in $H_2$ flow for 1 h at 500 °C, dried overnight at 110 °C and then outgassed in vacuum at 300 °C for 2 hours.

X-ray powder diffraction (XRD) analyses were carried out in the lab of Prof. Giuseppe Cruciani in the University of Ferrara. XRD patterns were measured by a Bruker D8 Advance diffractometer equipped with a Si(Li) solid state detector (SOL-X) and a sealed tube providing Cu Kα radiation. The Rietveld refinement method as implemented in the Bruker TOPAS program was used to obtain the refined unit cell parameters, crystal size, and the quantitative phase analysis for the $ZrO_2$ support and metal phases in the samples. The crystal size determination is achieved by the integral breadth based calculation of volume weighted mean crystallize sizes assuming intermediate crystallite size broadening modelled by a Voigt function. The samples were reduced in $H_2$ flow for 1 h at 500 °C before the analysis.

Temperature programmed reduction (TPR) measurements were carried out by placing the catalyst in a quartz reactor and heating in a 5% $H_2$/Ar mixed gas stream flowing at 40 mL/min at a heating rate of 10 °C/min from 25 to 700 °C. $H_2$ consumption was monitored by a TCD detector.

Temperature programmed oxidation (TPO) of the spent catalysts was carried out by feeding 40 mL/min of a 10 vol% $O_2$/He gas mixture while heating by 10°C/min from 25 to 650°C.

$O_2$ pulse chemisorption measurements were performed at 25 °C by means of a lab-made equipment. Before chemisorption the sample (100 mg) was reduced in $H_2$ flow (40 mL/min) at 500 °C for 1 hour and then evacuated under helium gas at 500°C for 2 hours to remove all physisorbed hydrogen. A Ni/$O_2$ chemisorption stoichiometry = 2 was used[22].

Fourier transform infrared spectroscopy (FTIR) and (High-Resolution) Transmission electron microscopy (HR-TEM) analyses were carried out in the lab of Dr. Giuseppina Cerrato in the University of Turin.

In situ FTIR spectra were obtained on a Perkin Elmer 2000 spectrophotometer (4 $cm^{-1}$ resolution, MCT detector). Reduced samples were inspected in the form of self-supporting

tablets (~25 mg $cm^{-2}$). Quartz cells (equipped with KBr windows) connected to a gas vacuum line equipped with rotary and turbomolecular pumps (residual pressure $p < 10^{-5}$ Torr) were used. The samples were activated in oxygen at 300 °C. FTIR spectra of probe molecules (CO) adsorbed thereon were also run, in order to obtain information on surface acidity.

HR-TEM images were obtained by using a JEOL JEM 3010UHR (300 kV) TEM fitted with a single crystal $LaB_6$ filament and an Oxford INCA Energy TEM 200 energy dispersive X-ray (EDX) detector. All samples were dry deposited, after their reduction, on Cu "holey" carbon grids (200 mesh).

Scanning electron microscopy (SEM), HR-TEM and Micro-Raman analyses of the spent samples were carried out by Dr. Alessandro Di Michele in the University of Perugia.

SEM images have been obtained using a Field Emission Gun Electron Scanning Microscopy LEO 1525, after metallization with Cr. Elemental composition was determined using Bruker Quantax EDS.

HR-TEM images of spent samples have been obtained using a Philips 208 Transmission Electron Microscope. The samples were prepared by putting one drop of an ethanol dispersion of the catalysts on a copper grid pre-coated with a Formvar film and dried in air.

Micro-Raman sampling was made by an OLYMPUS microscope (model BX40) connected to an ISA Jobin–Yvon model TRIAX320 single monochromator, with a resolution of 1 $cm^{-1}$. The source of excitation was a Melles Griot 25LHP925 He-Ne laser that was used in single line excitation mode at l=632.8 nm. The power focused on the samples was always less than 2 mW. The scattered Raman photons were detected by a liquid-nitrogen cooled charge coupled device (CCD, Jobin Yvon mod. Spectrum One).

### 5.2.3 Catalytic tests

The ESR catalytic tests were carried out in the lab of Dr. Ilenia Rossetti in the University of Milan, in the conditions reported in Section 4.2.3. The catalysts were activated in 50 $cm^3$/min of a 20 vol% $H_2/N_2$ gas mixture, while heating by 10 °C/min up to 500 °C, then kept for 1 h. The activity tests were carried out at atmospheric pressure, GHSV = 2500 $h^{-1}$ (referred to the ethanol + water gaseous mixture) at 500 °C. Additional activity tests at 400 and 300°C as well as a long term run (ca. 100 h-on stream) were also carried out on the

most promising sample. Some samples were also tested at GHSV = 7755 $h^{-1}$ to better highlight their catalytic performance.

## 5.3 Results and discussion

The catalysts were characterized by means of $N_2$ physisorption, in order to evaluate the effect of CaO-doping on the textural properties of the support. According to IUPAC classification[23], the non-modified sample ZNi exhibits a IV-type isotherm containing a H3-type hysteresis, typical of materials that don't possess a well-defined mesoporous structure, with a surface area of approximately 140 $m^2/g$ (see Table 5.1). The isotherms of the doped samples present the same features, thus indicating that the CaO-doping neither affected the structure nor the morphology of the support.

| | **ZNi** | **$ZCa_3Ni$** | **$ZCa_6Ni$** | **$ZCa_9Ni$** |
|---|---|---|---|---|
| *Specific surface area / $m^2\ g^{-1}$* | 141 | 150 | 142 | 135 |
| *$c.s._{ZrO2}$ Rietveld / nm* | 7.3 | 8.1 | 9.3 | 13.4 |
| *$c.s._{Ni}$ Rietveld / nm* | 3.2 | 2.8 | 3.4 | 4.5 |
| *$d_{Ni}$ $O_2$ chemisorption / nm* | 4.5 | 3.8 | 4.6 | 5.4 |

Tab. 5.1: Specific surface area and crystal size (*c.s.*) of catalysts as determined by $O_2$ chemisorption and Rietveld refinement.

TPR measurements (Fig. 5.1) were carried out, in order to identify the different NiO species on the surface of the supports and their reduction temperature.

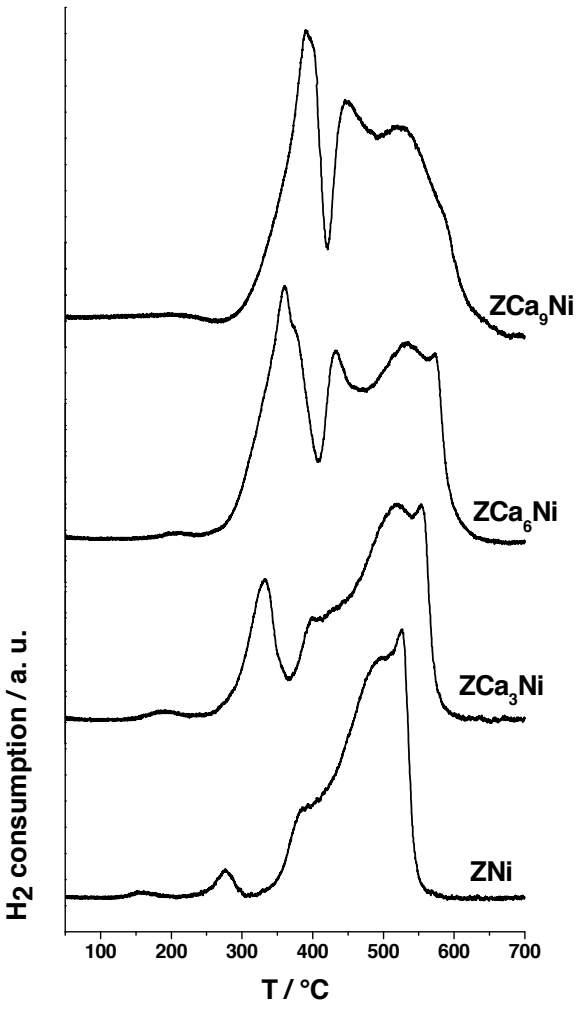


Fig. 5.1: TPR profiles of the catalysts with various CaO loadings.

As also detailed in Section 3.3, several reduction peaks, in a broad region between 250 and 550 °C, can be noticed in the TPR profile of ZNi. Since it is known that $Ni^{2+}$ is reduced to $Ni^0$ without any intermediate oxide[24], the presence of several peaks suggests the existence of NiO species differently interacting with the support[15,19]. The first peak can be assigned to non-interacting NiO, which is more easily reducible, since unsupported NiO reduces at about 280 °C[25,26]. The peak at about 380 °C can be ascribed to NiO weakly interacting with the support, while the higher temperature peaks (between 480 and 520 °C) indicates NiO species interacting stronger and stronger with zirconia[27,28].

When analyzing the TPR profiles of the doped samples, a progressive increase of the intensity of the first peak, roughly proportional to the rise in CaO content, can be evidenced. Therefore it seems that CaO-doping increases the NiO fraction reducible at lower temperatures. In previous papers this phenomenon was correlated to a significant decrease of metal dispersion[29,30], which negatively affected resistance to coking. Indeed, as previously reminded, smaller Ni particles are less prone to form carbon filaments. However, by looking at the crystal size variation reported in Table 5.1, just a small increase of Ni particle size can be observed. Therefore, according to the literature[15,16], an increased Ni reducibility in doped samples can be ascribed to the formation of oxygen vacancies, which favor NiO reduction by weakening the Ni-O bond. These oxygen vacancies arise from the replacement of the $Zr^{4+}$ cation with one with a lower positive charge (*i.e.* $Ca^{2+}$). The higher the CaO loading, the higher the concentration of oxygen vacancies and, then, of NiO species reduced at lower temperature.

XRD measurements and Rietveld refinements (Fig. 5.2) were carried out to determine the zirconia polymorph and ascertain if $Ca^{2+}$ actually replaced $Zr^{4+}$ in the lattice.

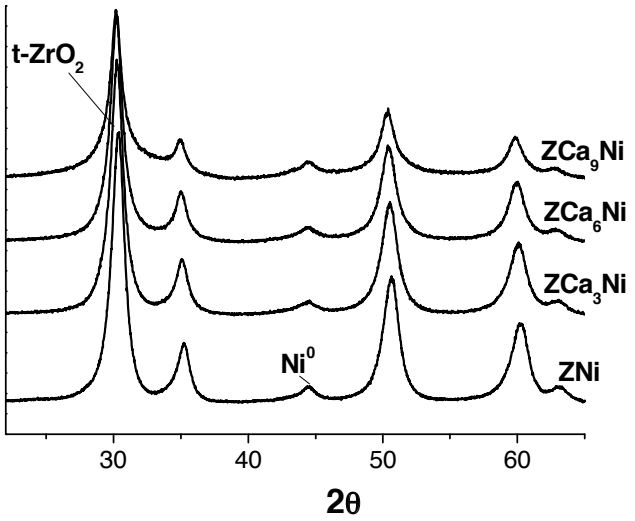


Fig. 5.2: XRD powder patterns of the reduced catalysts at increasing Ca content (from bottom to top).

As for the support, zirconia is present only in the tetragonal phase (*i.e.* the most intense peak at $2\theta \approx 30°$), irrespective of the CaO content. Thus it may be concluded that CaO-doping did not affect the nature of the $ZrO_2$ polymorph of the support. Nevertheless, a regular and incremental variation of the Rietveld-refined lattice parameters as the CaO

loading increased was observed (Fig. 5.3). The increase of the cell volume can be taken as an evidence of $Zr^{4+}$ (ionic radii 84 pm) substitution by $Ca^{2+}$ (ionic radii 99 pm) and supports the interpretation of the TPR results.

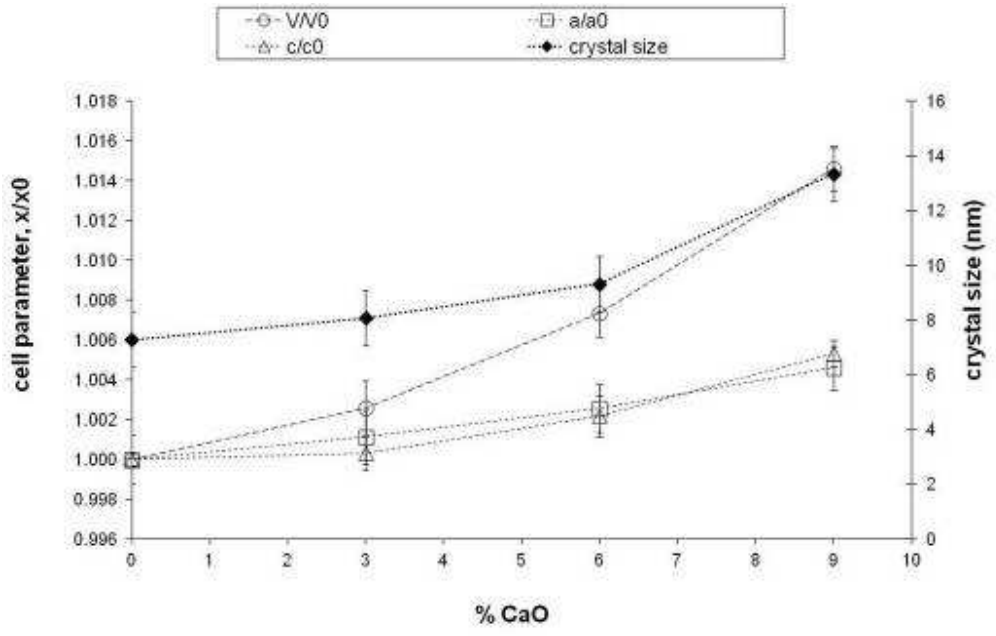


Fig. 5.3: Relative variation of the lattice parameters (ratios of unit-cell constants, $a/a_0$ and $c/c_0$, and volume, $V/V_0$, where $a_0$, $c_0$, and $V_0$ are the parameters of *t*-$ZrO_2$ without Ca) and crystal size of the zirconia phase as a function of the CaO loading.

The crystal size of *t*-$ZrO_2$ also shows a regular and non-linear increase (Table 5.1 and Fig. 5.3) while the direct comparison of powder patterns and Rietveld quantitative phase analysis shows that the fraction of crystalline zirconia decreases as a function of increasing CaO content. The addition of CaO to the synthesis batch appears to hinder the nucleation of *t*-$ZrO_2$ thus favoring its crystal growth.

In all the samples nickel appears only in the metallic form (peak at $2\theta = 44.5°$), suggesting that the reduction treatment at 500 °C substantially reduced all $Ni^{2+}$ to $Ni^0$.

Rietveld refinements of XRD patterns also provided a size estimate of Ni nanocrystals reported in Table 5.1. The size of Ni crystallites slightly increases with increasing CaO percentage. These data are in perfect agreement with the $O_2$ chemisorption results also given in Table 5.1.

FTIR spectroscopy of CO adsorption at RT (Room Temperature) is a well known procedure which can be resorted to, in order to evaluate the fraction of strong Lewis acidity

present at the surface of oxidic materials[31]. In the present case (see Fig. 5.4), the admittance of 100 Torr CO onto the activated samples evidences the formation of a unique spectral envelope either in the presence or in the absence of CaO: in particular, the band that forms in all cases is located in the 2170-2180 $cm^{-1}$. On the basis of both spectral position and literature data[32], this band can be attributed to the $\nu_{CO}$ stretching mode of a carbonyl-like species formed between CO and coordinatively unsaturated $Zr^{4+}$ cations located at the surface of all systems here under investigation (and set free by outgassing). However, the intensity of the band is decreasing as a consequence of the CaO loading, which might indicate that CaO is likely to bring about a sort of external coating on top of the $ZrO_2$ species. Moreover, the shift of the CO band (from ~2178 to ~2172 $cm^{-1}$) indicates that the "shielding" effect induced by the CaO species is more efficient towards the high-$\nu$ component of the CO band envelope: this, in turn, means that the highly uncoordinated $Zr^{4+}$ cations located in the most defective crystallographic positions (like high-index side terminations of the coin-like crystallites of $ZrO_2$)[10] are "shielded" by the dopant. It may be then preliminary concluded that the general acidity features of the catalysts are not totally changed by the presence of CaO, rather they are partially suppressed.

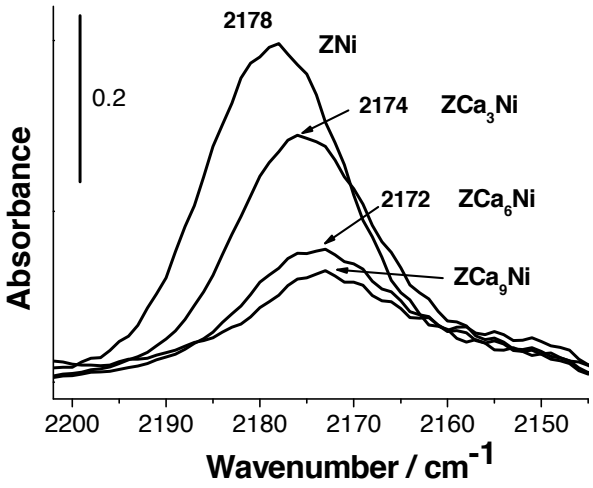


Fig. 5.4: FTIR spectra of adsorbed CO at RT on the reduced catalysts.

The morphological features of the catalysts have been investigated by means of HR-TEM. As it can be observed, all the systems exhibit $ZrO_2$ particles with good crystallinity. They are highly ordered but highly packed each other as well, and with average particle size of 5-8 nm (see both images reported in Fig. 5.5). As far as the amount of CaO increases, a

general lowering of the order is observed (see section b in Fig. 5.5), with the parallel evidence of an external partially amorphous habit. This amorphous overlayer is rather thin and transparent, still permitting the observation of the particles' contours.

These features are well consistent with the spectroscopic data reported in the previous section, as the decreasing intensity of the CO band is in good agreement with the partial amorphisation of the external habit of the catalysts due to the CaO dopant species. A decreased fraction of the crystalline zirconia phase, implying a larger content of the amorphous phase at high CaO loadings was also found by XRD.

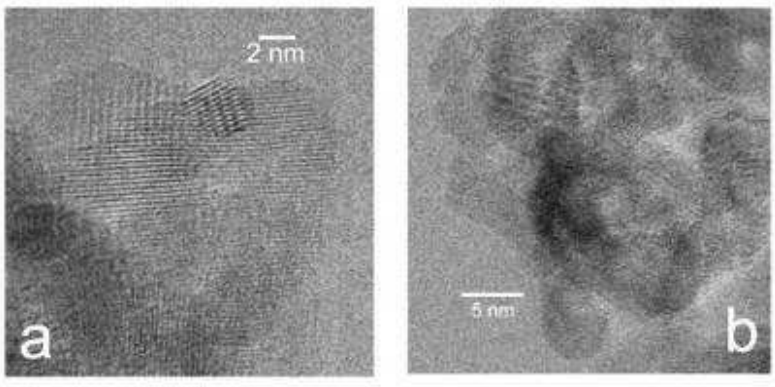


Fig. 5.5: TEM images of: a) ZNi; b) $ZCa_9Ni$.

It may be concluded that the specific surface area of the support did not change too much with the increased amount of CaO and therefore the Ni dispersion behaved similarly. It means that all samples are made by small and dispersed Ni nanoparticles which are essential in order to minimize coke formation.

By contrast, CaO addition to zirconia effectively reduced the Lewis acidity of the support, involved in coke deposition, and produced oxygen vacancies, which seem to affect Ni reducibility.

In order to check whether these modifications positively influenced the catalytic performance of the catalyst for the ESR reaction, activity tests were carried out. Table 5.2 shows the results of the activity tests at 500°C for every catalyst. Data reported are averaged out 4-8 h-on-stream. As already pointed out, this temperature is sufficiently high to achieve interesting catalytic performance, but it is critical as for coking and possible catalyst deactivation by this phenomenon.

| | Blank test | ZNi | $ZCa_3Ni$ | $ZCa_6Ni$ | $ZCa_9Ni$ |
|---|---|---|---|---|---|
| *EtOH conversion / %* | 13 ± 5 | 100 ± 0 | 100 ± 0 | 100 ± 0 | 100 ± 0 |
| *C balance / %* | 91 ± 2 | 88 ± 4 | 89 ± 4 | 89 ± 3 | 95 ± 3 |
| *$H_2$ productivity / mol/min $kg_{cat}$* | - | 0.96 ± 0.05 | 0.9 ± 0.1 | 0.96 ± 0.08 | 0.86 ± 0.05 |
| *$CH_4$ selectivity / %* | - | 17.3 ± 0.4 | 3.4 ± 1.0 | 7.2 ± 1.2 | 13 ± 1 |

Tab. 5.2: Results of the activity tests for ethanol steam reforming at 500 °C. Time-on-stream: 8 hours, data averaged out 4-8 h-on-stream, GHSV = 2500$h^{-1}$.

All the catalysts fully converted ethanol at 500°C when tested at GHSV = 2500 $h^{-1}$, with interesting $H_2$ productivity. These conditions were chosen as practically relevant for a possible catalyst implementation. Methane was observed as the only by-product at this reaction temperature (Table 5.2), without acetaldehyde nor ethylene. Some selectivity towards methane formation is indeed expected at this relatively low temperature, since its formation is due to ethanol decomposition into $CH_4 + CO + H_2$, but its reforming is limited because higher reaction temperature is needed for its complete conversion. Selectivity to methane seems roughly correlated to Ni crystal size: the lowest the size, the lowest the $CH_4$ fraction still unreformed at 500°C, thus indicating higher activity towards SR of $CH_4$ for higher Ni dispersion. Furthermore, methane concentration seems roughly constant with time-on-stream and it is not correlated to possible catalyst deactivation, as is sometimes the case of ethylene and acetaldehyde.

One of the most interesting parameters to keep under control is carbon balance. Although it may be correlated to many factors, *e.g.* the formation of different species, it can be conveniently taken as index of possible catalyst coking. The C balance obtained during the blank test was 91%, with a conversion of 13%. This was attributed to some ethanol dehydration/decomposition over the quartz material filling the reactor. Additional blank test with void reactor did not evidence any ethanol conversion (< 5%) and a substantially full C balance was obtained. We already observed very limited coking activity over $Ni/ZrO_2$ due to very high metal dispersion (confirmed for this samples series), which limits the accumulation of carbon filaments on the active phase with its consequent possible

deactivation[29]. It should be underlined that the active phase might still remain active due to simple displacement from the support also in case of extensive filaments formation. Indeed, due to accumulation of carbide species at the interface between the metal and the support, filaments growth may provoke the detachment of the metal particle from the support surface. This may not induce to complete deactivation of the particle, since Ni remains exposed to the reactants and may still exploit it activity. However, some differences in selectivity may become evident, since for instance the support may play a role in the activation of water, providing activated oxygen or oxydril species. If the metal site is no more in contact with the support these species may not reach the $CH_x$ species adsorbed on the metal provoking the formation of by-products. In any case, this means major modification of the sample and possible reactor failure.

The formation of carbon filaments is usually correlated with metal dispersion, *i.e.* smaller Ni particles are expected to form less filaments. We indeed observed such a correlation in other sets of catalysts in which a significant variation of Ni crystal size was present. In the present case, a substantially similar Ni dispersion should result in similar coking activity, or at least we would expect a trend of C balance opposite to Ni crystal size. By contrast, C balance was found also correlated to CaO loading.

Some coking might also occur due to ethylene polimerisation over acidic sites of the support. Therefore, acidity tuning achieved by this samples set may help limiting this additional coking feature.

Carbon balance slightly increased upon doping with CaO, reaching its maximum at the highest loading. In particular, it can be noted (Fig. 5.6) that carbon balance decreased significantly within 8 h-on-stream for sample ZNi, whereas it was stable and almost complete for $ZCa_9Ni$.

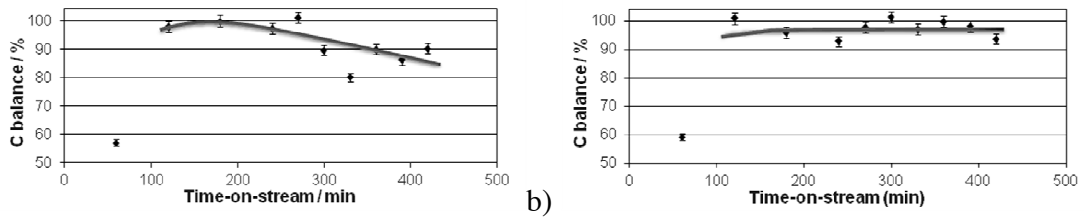


Fig. 5.6: Trend of C balance with time-on-stream for: a) ZNi; b) $ZCa_9Ni$.

Since $H_2$ productivity and ethanol conversion did not change significantly, we may conclude that acidity limitations brought about by the addition of CaO may be beneficial in depressing coking activity due to surface acidity.
Additional tests have been carried out at higher space velocity (7755 $h^{-1}$) for samples ZNi and $ZCa_9Ni$ in order to better highlight their differences at lower conversion (Table 3).

| | **ZNi** | **$ZCa_9Ni$** |
|---|---|---|
| *EtOH conversion / %* | 35 ± 7 | 53 ± 8 |
| *C balance / %* | 93 ± 6 | 100 ± 4 |
| *$H_2$ productivity / mol/min $kg_{cat}$* | n.d. | 1.94 ± 0.10 |
| *Sel. $CH_4$ (%)* | 0 | 6.4 ± 1.0 |
| *Sel. $CH_3CHO$ (%)* | 55 ± 11 | 35 ± 5 |
| *Sel. $CH_2CH_2$ (%)* | 0 | 4.9 ± 0.7 |

Tab. 5.3: Results of the activity tests for ethanol steam reforming at 500 °C. Time-on-stream: 8 hours, data averaged out 4-8 h-on-stream, GHSV = 7755 $h^{-1}$.

The catalytic activity on sample ZNi was in general worse than that of the Ca-doped one. Indeed, the steady state conversion was lower and the sample was mainly selective to acetaldehyde. By contrast, the activity of sample $ZCa_9Ni$ was stable with time-on-stream and allowed to reach significant $H_2$ productivity in spite of the presence of unreformed by-products, whose selectivity remained as well constant for the whole duration of the test.
The presence of unreformed ethylene is also interesting for $ZCa_9Ni$. Indeed, its concentration remained stable for the whole duration of the test, indicating its incomplete reforming under these conditions, but contemporarily negligible coke formation by its polimerisation over the catalyst surface. By contrast, some unreformed ethylene (15% selectivity) was evidenced during the first 2 h-on-stream for ZNi, accompanied by higher ethanol conversion. Then ethylene disappeared from the reaction products, likely accumulating over the acidic sites of the support, and this was accompanied by a decrease

of ethanol conversion, then stabilized to 35%. The difference of carbon balance was lower in this case. Indeed, the main contribution of C accumulation by filaments formation over Ni particles is limited by the very low ethanol decomposition activity. Indeed, if less carbide precursor species are present over the metal their accumulation in the form of nanotubes is unlikely.

Focusing our attention on sample $ZCa_9Ni$, particularly promising as for resistance to coking, we additionally performed activity tests at lower temperature at GHSV = 2500 $h^{-1}$ (Table 5.4).

| | **500°C** | **400°C** | **500°C_d1** | **500°C_d2** | **500°C_d3** | **500°C_d4** | **500°C_d5** |
|---|---|---|---|---|---|---|---|
| *EtOH conversion / %* | 100 ± 0 | 62 ± 9 (decreasing with t-o-s) | 100 ± 0 | 100 ± 0 | 100 ± 0 | 100 ± 0 | 100 ± 0 |
| *C balance / %* | 95 ± 3 | 74 ± 11 | 91 ± 4 | 92 ± 6 | 91 ± 7 | 94 ± 2 | 89 ± 4 |
| *$H_2$ productivity / mol/min $kg_{cat}$* | 0.86 ± 0.05 | 0.3 ± 0.4 | 0.84 ± 0.05 | 0.85 ± 0.03 | 0.82 ± 0.06 | 0.84 ± 0.05 | 0.80 ± 0.03 |
| *Sel. $CH_4$ (%)* | 13 ± 1 | 2.1 ± 0.5 | 12 ± 2 | 14 ± 2 | 13 ± 4 | 13 ± 1 | 12 ± 2 |
| *Sel. $CH_3CHO$ (%)* | 0 | 7 ± 2 | 0 | 0 | 1.1 ± 1.0 | 2.5 ± 0.4 | 1.7 ± 1.0 |
| *Sel. $CH_2CH_2$ (%)* | 0 | 20 ± 5 (increasing with t-o-s) | 0 | 0 | 0 | 0 | 0 |

Table 5.4: Results of the activity tests for ESR of sample $ZCa_9Ni$ at different temperature and durability test at 500°C for 5 days. T-o-s: time-on-stream; d1-d5: days 1 to 5; GHSV = 2500 $h^{-1}$.

Ethanol conversion unacceptably decreased when cooling the reactor down to 400°C and it was even lower at 300°C (*ca*. 0.05). Furthermore, at 400°C the major byproduct was ethylene, with selectivity increasing with time-on-stream, though acetaldehyde also formed. The carbon balance at such temperature became unacceptably low and decreasing with time-on-stream. This may suggest that carbon accumulation occurred at 400°C over the catalyst surface, likely in the form of polymers partially and progressively covering the

active phase, which indeed decreased its activity with time-on-stream. Thus 500°C was considered the lowest temperature to achieve satisfactory activity testing for this application.

At the end of activity tests at lower temperature, the reactor was heated up again at 500°C and a prolonged run was carried out for 5 days on the same $ZCa_9Ni$ sample. At first one may notice that test d1 in Table 5.3 recovered roughly the same results of the test on the freshly activated sample, ruling out the hypothesis of irreversible deactivation due to severe coking of the active phase at 400 and 300°C. Likely, coke gasification occurred when increasing temperature at 500°C allowing to recover the full activity of the active phase. Catalyst performance remained stable for *ca*. 100 h-on-stream, without any decrease of ethanol conversion. Some acetaldehyde started forming after ca. 50 h-on-stream, whereas ethylene was never observed at reactor outlet.

The addition of a basic promoter showed beneficial in improving catalyst resistance towards coking.

These results can be ascribed to the progressive decrease of the Lewis acidity of the support, which contributes to the side reactions leading to coke deposition. In average, a higher C balance, *i.e*. lower coking, was achieved with sample $ZCa_9Ni$.

CaO doping also induces the formation of oxygen vacancies, proportionally to its concentration. Oxygen vacancies may activate $CO_2$ and $H_2O$, thus favouring the gasification of coke[15,33,34]. This, coupled with the very small Ni particle size and to titration of the strongest acid sites helps in keeping under control coke deposition under critical reaction conditions.

In order to better characterise the coking phenomenon, the spent catalysts were characterised by means of Micro-Raman, TEM and FE-SEM.

Micro-Raman analysis (Fig. 5.7) evidenced the presence of both the D and G bands of graphite that were attributed to the presence of multiwalled carbon nanotubes (MWCNTs) and to encapsulating coke due to polymerization[35,36]. Some C was observed over the surface of sample $ZCa_9Ni$, e.g. graphite layers visible in Fig. 8. This has been likely loaded on the catalyst during low temperature testing and it is likely localised over the support surface, leaving substantially unaltered the active phase. On the contrary, catalyst ZNi was predominantly characterised by the contribution of ordered carbon. The latter was constituted by MWCNTs, 33-37 nm in diameter, as depicted in Fig. 5.8 and 5.9, which were completely absent in sample $ZCa_9Ni$.

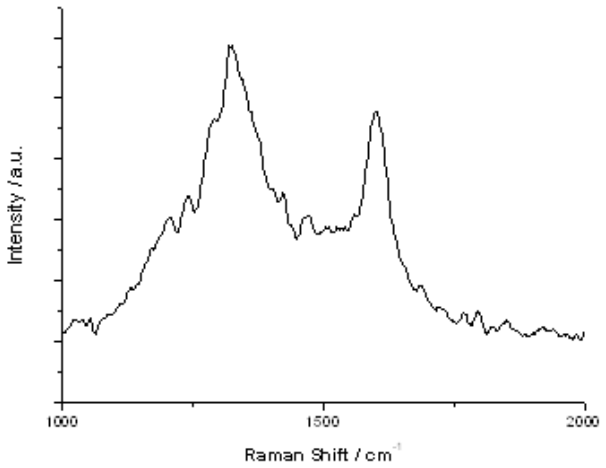


Fig. 5.7: Microraman spectra of the spent sample ZNi.

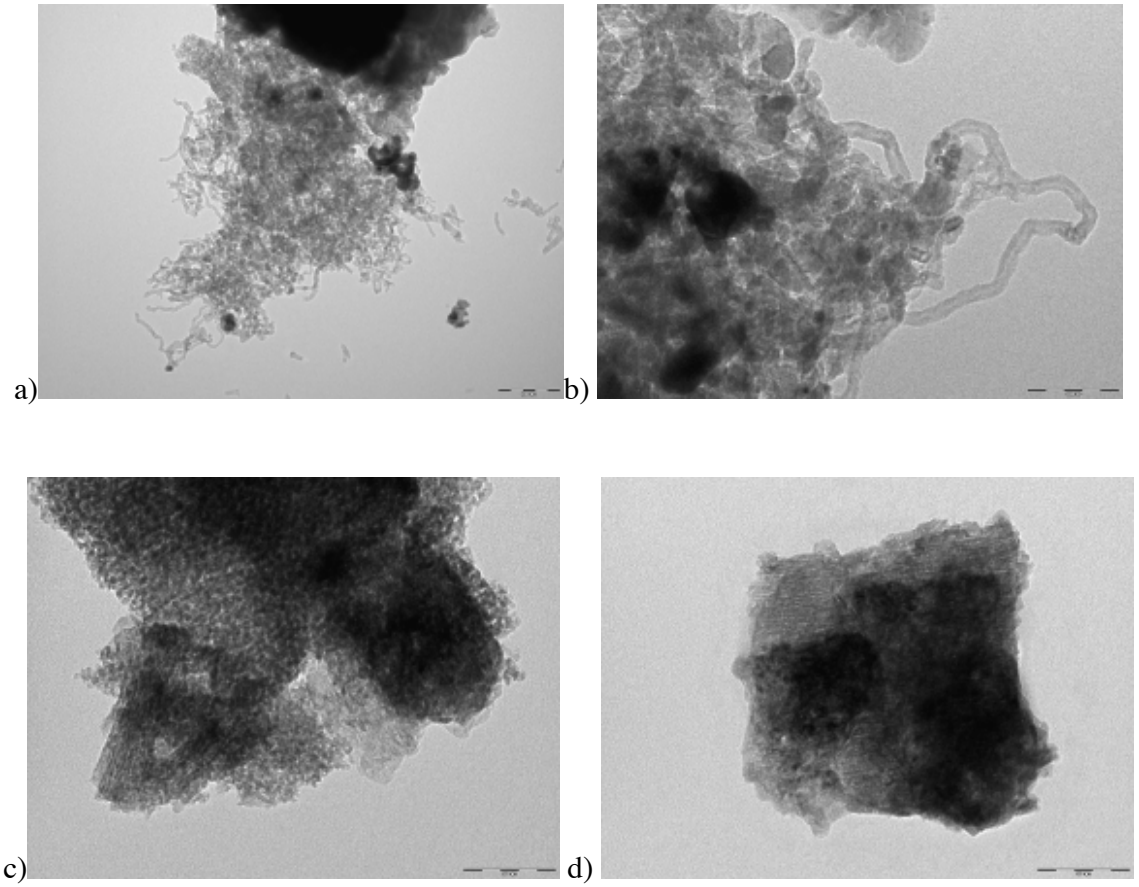


Fig. 5.8: TEM micrographs of spent samples ZNi (a, b) and $ZCa_9Ni$ (c, d).

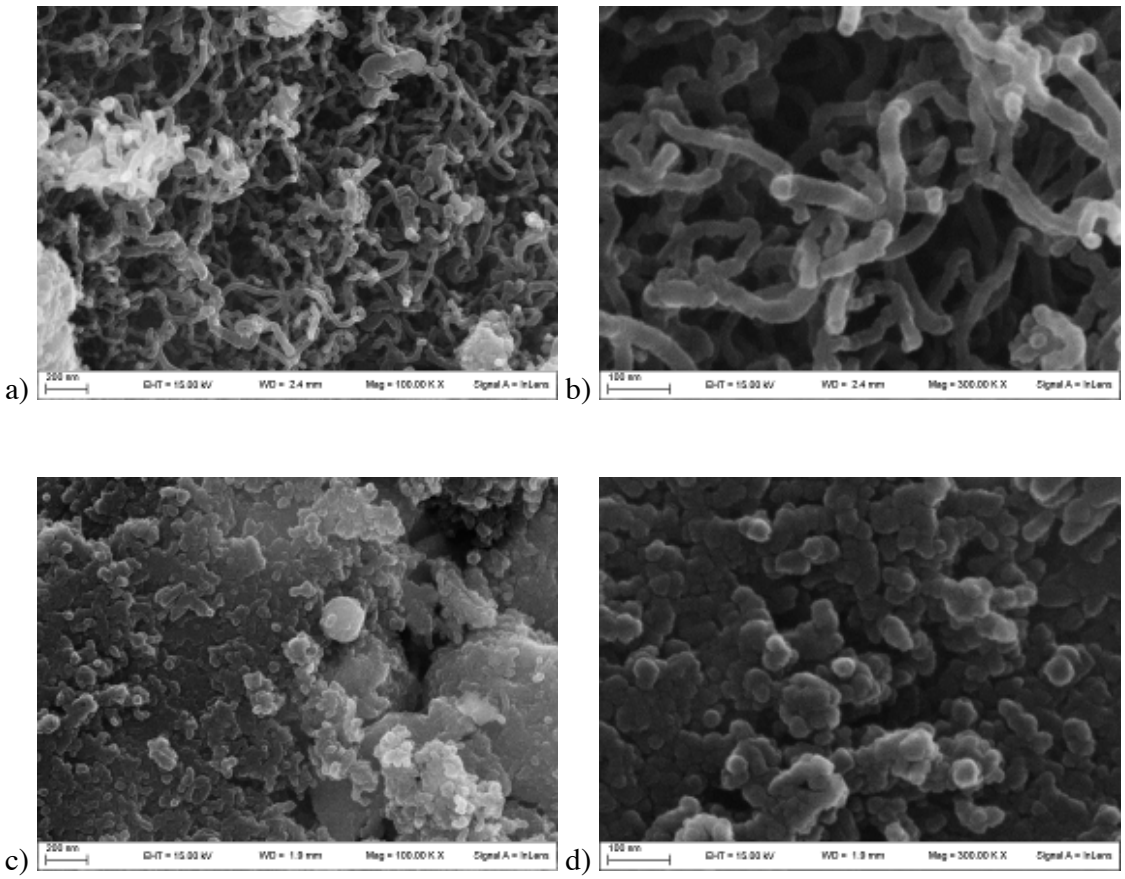

Fig. 5.9: FE-SEM images of spent samples ZNi (a, b) and $ZCa_9Ni$ (c, d).

The spent catalysts have been characterized also by TPO analysis. The sample ZNi used for the standard activity testing (8 h-on-stream at 500°C) returned a carbon deposition rate of 10.1 mg $C/g_{cat}$ h. Sample $ZCa_9Ni$, tested after the durability test (5 days-on-stream) evidenced a much more limited C accumulation, corresponding to a rate of 0.75 mg $C/g_{cat}$ h. These data were also semiquantitatively confirmed by EDX analysis.

Therefore, we can conclude that some accumulation of coke may be due to ethanol dehydration to ethylene, which may polymerise at relatively low temperature if it is not efficiently gasified. The titration of the strongest acidic sites with CaO may limit this phenomenon and additionally it can provide oxygen vacancies acting as activation sites for water and carbon dioxide, which helps cleaning the surface of the active phase.

MWCNTs may also form, promoted by Ni itself, especially when poorly dispersed or not sufficiently stabilised by the support. Therefore, in spite of the high Ni dispersion, similar for samples ZNi and $ZCa_9Ni$, CNTs were evident in the spent ZNi sample. Hence, we may additionally conclude that doping with CaO, and the consequent oxygen vacancies formation, helps in cleaning up the surface by providing activated OH or O radicals, which

are also able to stop the subsurface accumulation of carbon at the interface between Ni and the support. This effectively inhibits the growth of CNTs.

## 5.4 Conclusions

In this chapter it was demonstrated that the presence of Lewis acid sites on the surface of the zirconia support, due to coordinatively unsaturated $Zr^{4+}$ ions, was related to coke formation. The addition of CaO to the support was effective in reducing the Lewis acidity of zirconia and inhibiting coke formation. Moreover, CaO addition was responsible for the formation of oxygen vacancies, that can activate $CO_2$ and $H_2O$, thus favouring the gasification of coke. The latter also inhibited the growth of multiwalled carbon nanotubes. On the contrary, CaO-doping did not affect Ni dispersion, so Ni nanoparticles were small and dispersed in all samples, which is essential in order to minimize coke formation. The best performing sample was the one doped with the highest amount of CaO ($ZCa_9Ni$): its performance remained stable for *ca*. 100 h-on-stream, without any decrease of ethanol conversion, and a minimal carbon accumulation.

# References


[1] V. Nichele, M. Signoretto, F. Menegazzo, I. Rossetti, G. Cruciani, Int. J. Hydrogen Energy. 39 (2014) 4252-4258.

[2] M.H. Youn, J.G. Seo, H. Lee, Y. Bang, J.S. Chung, I.K. Song, Appl. Catal. B: Environ. 98 (2010) 57-64.

[3] K.G. Azzam, I.V. Babich, K. Seshan, L. Lefferts, J. Catal. 251 (2007) 153-162.

[4] A.N. Fatsikostas, X.E. Verykios, J. Catal. 225 (2004) 439-452.

[5] D.L. Trimm, Catal. Today. 37 (1997) 233-238.

[6] A. Le Valant, F. Can, N. Bion, D. Duprez, F. Epron, Int. J. Hydrogen Energy. 35 (2010) 5015-5020.

[7] A.J. Vizcaíno, A. Carrero, J.A. Calles, Int. J. Hydrogen Energy. 32 (2007) 1450-1461.

[8] S. Cavallaro, N. Mondello, S. Freni, J. Power Sources. 102 (2001) 198-204.

[9] C. Morterra, G. Cerrato, M. Signoretto, Catal. Lett. 41 (1996) 101-109.

[10] C. Morterra, G. Cerrato, V. Bolis, S. Di Ciero, M. Signoretto, J. Chem. Soc., Faraday Trans. 93(6) (1997) 1179-1184.

[11] C. Morterra, G. Cerrato, S. Di Ciero, Appl. Surf. Sci. 126 (1998) 107-128.

[12] J.A. Calles, A. Carrero, A.J. Vizcaíno, Micropor. Mesopor. Mater. 119 (2009) 200.207.

[13] Z. Hou, O. Yokota, T. Tanaka, T. Yashima, Appl. Catal. A: General. 253 (2003) 381-387.

[14] J. da S. Lisboa, D.C.R.M. Santos, F.B. Passos, F.B. Noronha, Catal. Today. 101 (2005) 15-21.

[15] J.D.A. Bellido, E.M. Assaf, J. Power Sources. 177 (2008) 24-32.

[16] J.D.A. Bellido, J.E. De Souza, J.C. M'Peko, E.M. Assaf, Appl. Catal. A: General. 358 (2009) 215-223.

[17] S. Liu, L. Guan, J. Li, N. Zhao, W. Wei, Y. Sun, Fuel. 87 (2008) 2477-2481.

[18] M.S. Fan, A.Z. Abdullah, S. Bhatia, Appl. Catal. B: Environ. 100 (2010) 365-377.

[19] V. Nichele, M. Signoretto, F. Menegazzo, A. Gallo, V. Dal Santo, G. Cruciani, G. Cerrato, Appl. Catal. B: Environ. 111-112 (2012) 225-232.

[20] F. Zane, S. Melada , M. Signoretto, F. Pinna, Appl. Catal. A: General. 299 (2006) 137-144.

[21] S. Brunauer, P.H. Emmett, E. Teller, J. Am. Chem. Soc. 60 (1938) 309-319.

[22] J.S. Smith, P.A. Thrower, M.A. Vannice, J. Catal. 68 (1981) 270-285.

[23] IUPAC Recommendations, Pure Appl. Chem. 57 (1985) 603-619.

[24] Y.J.O. Asencios, E.M. Assaf, Fuel Process. Technol. 106 (2013) 247-252.

[25] L. Zhang, J. Lin, Y. Chen, J. Chem. Soc. Faraday Trans. 88 (14) (1992) 2075-2078.

[26] Q.G. Yan, W.Z. Weng, H.L. Wan, H. Toghiani, R.K. Toghiani, C.U. Pittman, Jr, Appl. Catal. A: General. 239 (2003) 43-58.

[27] Y.Q. Song, D.H. He, B.Q. Xu, Appl.Catal. A: General. 337 (2008) 19-28.

[28] V. García, J.J. Fernández, W. Ruíz, F. Mondragón, A. Moreno, Catal. Commun. 11 (2009) 240-246.

[29] I. Rossetti, C. Biffi, C.L. Bianchi, V. Nichele, M.Signoretto, F. Menegazzo, E. Finocchio, G. Ramis, A. Di Michele, Appl. Catal. B: Environ. 117-118 (2012) 384-396.

[30] I. Rossetti, A. Gallo, V. Dal Santo, C.L. Bianchi, V. Nichele, M. Signoretto, E. Finocchio, G. Ramis, A. Di Michele, ChemCatChem. 5 (2013) 294-306.

[31] G. Herzberg, Molecular Spectra and Molecular Structure. II. Infrared and Raman Spectra of Polyatomic Molecules, Van Nostrand Co., New York, 1947, p. 274.

[32] G. Cerrato, S. Bordiga, S. Barbera, C. Morterra, Surf. Sci. 50 (1997) 377-379.

[33] Y.J.O. Asencios, J.D.A. Bellido, E.M. Assaf, Appl. Catal. A: General. 397 (2011) 138-144.

[34] T. Horiuchi, K. Sakuma, T. Fukui, Y. Kubo, T. Osaki, T. Mori, Appl. Catal. A: General. 144 (1996) 111-120.

[35] C. Gao, Y. Z. Jin, H. Kong, R.L.D. Whitby, S.F. A. Acquah, G.Y. Chen, H. Qian, A. Hartschuh, S.R.P. Silva, S. Henley, P. Fearon, H.W. Kroto, D.R.M. Walton, J. Phys. Chem. B. 109 (2005) 11925-11932.

[36] P. Delhaes, M. Couzi, M. Trinquecoste, J. Dentzer, H. Hamidou, C. Vix-Guterl, Carbon. 44 (2006) 3005-3013.

# Chapter 6. Effect of copper addition on the activity of a Ni/CaO-$ZrO_2$ catalyst in ethanol steam reforming*

## 6.1 Introduction

In Chapter 5 it was shown that CaO-doping of a Ni/$ZrO_2$ catalyst ($ZCa_9Ni$) can effectively inhibit coke formation even at low reaction temperature (500 °C), thus increasing the catalyst stability and durability[1]. In order to improve even further the performance of this catalyst, in particular in terms of hydrogen productivity we decided to modify once again the formulation of the catalyst, in particular adding a second metal. Since the main drawbacks of Ni-based catalysts are related to sintering and coking, we chose a metal that can be useful in controlling these phenomena, *i.e.* copper. Copper addition to a Ni-based catalyst can be effective in order to limit nickel sintering[2]. Copper alone is not so efficient for the promotion of ethanol steam reforming because of its low activity in C-C bonds cleavage[3]. Nevertheless, it was reported that copper can segregate the active Ni particles through the formation of Ni-Cu alloys, thus inhibiting both Ni sintering and coking phenomena[2,4]. Remón et al.[5] reported that the major carbon preventing effect of copper is to block the step sites on nickel particles, preventing the creation of nucleation sites responsible for graphite formation. Moreover, copper addition to nickel enhances the selectivity to hydrogen thanks to the ability of copper to change the affinity for carbon of nickel particles, which inhibits coke formation and improves stability[6,7]. Copper is considered to increase the selectivity to hydrogen also because of its high activity for water-gas shift reaction[8]. In this chapter the effect of copper addition on the performance of a Ni/$ZrO_2$ catalyst is evaluated. In particular, the effects of both the order of metals addition and the calcination temperature are considered.

---

* The results reported in this chapter are published as: "*Bimetallic Ni-Cu catalysts for the low-temperature ethanol steam reforming: importance of metal-support interactions*", V. Nichele, M. Signoretto, F. Pinna, E. Ghedini, M. Compagnoni, I. Rossetti, G. Cruciani, A. Di Michele, Catal. Letters. DOI: 10.1007/s10562-014-1414-2. 

## 6.2 Experimental Section

### 6.2.1 Catalysts preparation

$Zr(OH)_4$ was prepared by a precipitation method[1,9,10], as reported in Chapters 3 and 4.

Ni, Cu and CaO were added to $Zr(OH)_4$ by means of the incipient wetness impregnation technique using $Ni(NO_3)_2*6H_2O$ (*Sigma-Aldrich, purity ≥ 98.5%*), $Cu(NO_3)_2*3H_2O$ (*Sigma-Aldrich, puriss. p.a.*) and $Ca(NO_3)_2*4H_2O$ (*Fluka, purity ≥ 99%*) as precursors. Ni, Cu and CaO amounts were kept constant (Ni: 10 wt%; Cu: 2 wt%; CaO: 9 wt%).

The reference sample was prepared as reported in Chapter 4 by adding Ni- and CaO-precursors to $Zr(OH)_4$ simultaneously and calcining at 500 °C for 4 hours in flowing air (50 mL/min STP). This sample is labelled ZCaNi (the subscript "9" indicating the amount of CaO is now omitted for the sake of brevity, since all samples were prepared with the same amount of dopant).

In order to study the effect of copper addition, Ni-, CaO- and Cu-precursors were simultaneously impregnated on $Zr(OH)_4$. As already explained with regard to the nickel phase, also for copper it was chosen to use the incipient wetness impregnation technique to achieve a high dispersion and because this synthesis method is highly reproducible, easy and cheap. Part of the sample was calcined at 500 °C for 4 hours (ZCaNiCu), while the rest was calcined at 800 °C for 4 hours (ZCaNiCu800) to verify the effect of calcination temperature.

Two other samples were prepared by adding Ni and Cu in two separate and sequential steps. In $ZCaNi_1Cu_2$ Ni- and CaO-precursors were added simultaneously to $Zr(OH)_4$, the sample was calcined at 500 °C for 4 hours, then Cu-precursor was added and the catalyst was calcined again at 500 °C for 4 hours. In $ZCaCu_1Ni_2$ the order of addition of Ni and Cu was the opposite.

### 6.2.2 Catalysts characterization

Temperature programmed reduction (TPR) measurements were carried out by placing the catalyst in a quartz reactor and heating in a 5% $H_2$/Ar mixed gas stream flowing at 40

mL/min at a heating rate of 10 °C/min from 25 to 800 °C. $H_2$ consumption was monitored by a TCD detector.

X-ray powder diffraction (XRD) analyses were carried out in the lab of Prof. Giuseppe Cruciani in the University of Ferrara. XRD patterns were measured by a Bruker D8 Advance diffractometer equipped with a Si(Li) solid state detector (SOL-X) and a sealed tube providing Cu Kα radiation. The Rietveld refinement method as implemented in the Bruker TOPAS program was used to obtain the refined unit cell parameters, crystal size, and the quantitative phase analysis for the $ZrO_2$ support and metal phases in the samples. The crystal size determination is achieved by the integral breadth based calculation of volume weighted mean crystallize sizes assuming intermediate crystallite size broadening modelled by a Voigt function. The samples were reduced in $H_2$ flow for 1 h at 500 °C (750 °C for ZCaNiCu800) before the analysis.

TEM and Micro-Raman analyses were carried out by Dr. Alessandro Di Michele in the University of Perugia. TEM images have been obtained using a Philips 208 Transmission Electron Microscope. The samples were prepared by putting one drop of an ethanol dispersion of the catalysts on a copper grid pre-coated with a Formvar film and dried in air. Micro-Raman sampling was made by an OLYMPUS microscope (model BX40) connected to an ISA Jobin–Yvon model TRIAX320 single monochromator, with a resolution of 1 $cm^{-1}$. The source of excitation was a Melles Griot 25LHP925 He-Ne laser that was used in single line excitation mode at l=632.8 nm. The power focused on the samples was always less than 2 mW. The scattered Raman photons were detected by a liquid-nitrogen cooled charge coupled device (CCD, Jobin Yvon mod. Spectrum One).

Temperature programmed oxidation (TPO) of the spent catalysts was carried out by feeding 40 mL/min of a 10 vol% $O_2$/He gas mixture while heating by 10°C/min from 25 to 650°C.

### 6.2.3 Catalytic tests

The ESR catalytic tests were carried out in the lab of Dr. Ilenia Rossetti in the University of Milan, in the conditions reported in Section 4.2.3. The catalysts were activated in 50 $cm^3$/min of a 20 vol% $H_2/N_2$ gas mixture, while heating by 10 °C/min up to 500 °C (750 °C for ZCaNiCu800), then kept for 1 h. During activity testing 0.017 $cm^3$/min of a 3:1

(mol/mol) $H_2O$:$CH_3CH_2OH$ liquid mixture were fed to the reactor by means of a Hitachi, mod. L7100, HPLC pump. 56 $cm^3$/min of $N_2$, used as internal standard, and 174 $cm^3$/min of He were also added. Such dilution of the feed stream was calibrated so to keep the reactants mixture in the vapour phase even at zero conversion at the reactor outlet. The activity tests were carried out at atmospheric pressure, GHSV = 2500 $h^{-1}$ (referred to the ethanol + water gaseous mixture) at 500 °C for the samples calcined at 500 °C, at 750 and 500 °C for the sample calcined at 800 °C.

## 6.3 Results and discussion

### 6.3.1 Effect of copper addition

In Table 6.1 the results of ESR tests are reported. Data reported are averaged out 4-8 h-on-stream.

| | **Blank test** | **ZCaNi** | **ZCaNiCu** | **$ZCaNi_1Cu_2$** | **$ZCaCu_1Ni_2$** | **ZCaNiCu800** | **ZCaNiCu800 750 °C** |
|---|---|---|---|---|---|---|---|
| **EtOH conversion / %** | 13 ± 5 | 100 ± 0 | 72 ± 9 | 100 ± 0 | 100 ± 0 | 48 ± 11 | 100 ± 0 |
| **$H_2O$ conversion / %** | | 63 ± 5 | 47 ± 2 | 68 ± 2 | 52 ± 6 | 47 ± 6 | 60 ± 2 |
| **$H_2$ productivity / mol / min $kg_{cat}$** | - | 0.86 ± 0.05 | 0.45 ± 0.10 | 1.04 ± 0.04 | 0.65 ± 0.08 | - | 1.13 ± 0.02 |
| **$CH_4$ selectivity / %** | - | 13 ± 1 | 5 ± 1 | 12 ± 2 | 4 ± 1 | 11 ± 2 | - |
| **$CH_3CHO$ selectivity / %** | - | - | 36 ± 4 | - | 7 ± 3 | 38 ± 9 | - |
| **$C_2H_4$ selectivity / %** | - | - | 19 ± 5 | 2 ± 2 | 14 ± 3 | 19 ± 2 | - |

Tab. 6.1: Results of the activity tests for ethanol steam reforming at 500 °C (in the last column, at 750 °C for ZCaNiCu800). Activation at 500 °C for 1 h for every sample except ZCaNiCu800, activated at 750 °C for 1 h. Time-on-stream: 8 h, data averaged out 4-8 h-on-stream.

By analyzing the results related to ZCaNiCu it is possible to evaluate the effect of copper addition, with respect to the activity of the reference sample ZCaNi. Contrary to what expected, Cu doping has made the catalytic performance worse. Ethanol conversion is much lower with ZCaNiCu than with ZCaNi. In particular, ethanol conversion is complete and stable with ZCaNi (Fig. 6.1(a)), while in the case of ZCaNiCu it decreases sharply after about 3 h-on-stream, in correspondence to an increase of the carbon balance (Fig. 6.1(b)).

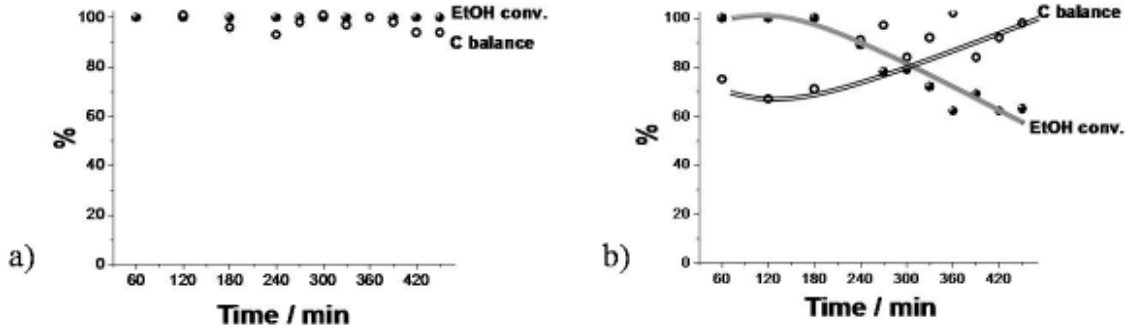


Fig. 6.1: Ethanol conversion (●) and C balance (**o**) trends for: a) ZCaNi; b) ZCaNiCu.

Contemporarily, the selectivity to acetaldehyde and ethylene, initially nil, started increasing after *ca*. 3 h-on-stream, reaching the steady state value reported in Table 6.1. Although it may be correlated to many factors, *i*. *e*. the formation of different species, the carbon balance can be conveniently taken as index of possible catalyst coking. In particular, low values of C balance can denote coke formation. In the case of ZCaNiCu, the low C balance (average value: 69%) in the first three hours of the test seems to suggest that a certain accumulation of coke took place (*vide infra*), leading to deactivation of the catalyst and a fast decrease of ethanol conversion and increase in the selectivity of by-products.

This result can be related to the fact that ZCaNiCu shows a certain selectivity to C2 by-products, that were absent with ZCaNi. The presence of these by-products can be ascribed to copper, which is not active in C-C bonds cleavage, as already reported in the Introduction. It seems that the presence of copper favoured mainly the secondary reactions leading to by-products, such as acetaldehyde and ethylene, which are precursors of coke. The formation of coke, suggested by the initial low C balance, led to the deactivation of the Ni active sites of the catalyst, indicated by the decrease of ethanol conversion. As a

consequence of the formation of significant amounts of by-products, a strong decrease of hydrogen productivity was also observed.

In conclusion, copper addition was not satisfactory for ESR. Several characterization measurements were carried out in order to explain these results.

The TPR profiles of ZCaNi and ZCaNiCu are reported in Fig. 6.2.

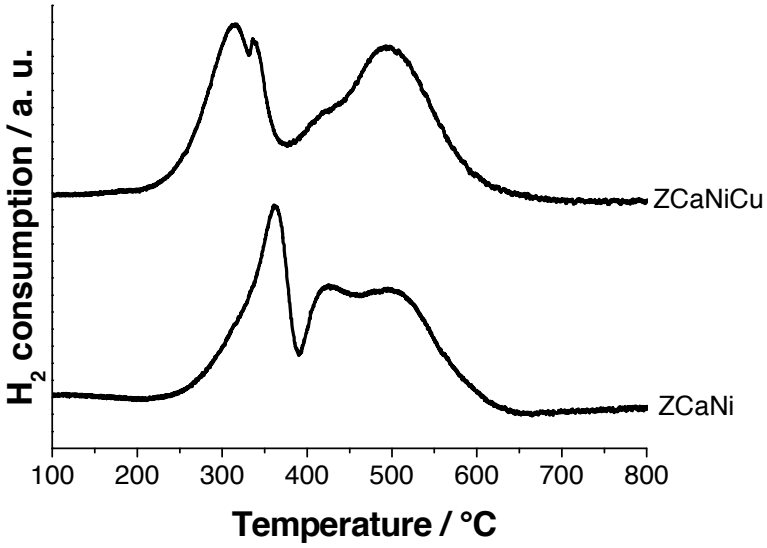


Fig. 6.2: TPR profiles of ZCaNi and ZCaNiCu.

For both samples several reduction peaks, in a broad region between 250 and 550 °C, can be detected. As for ZCaNi, since it is known that $Ni^{2+}$ is reduced to $Ni^0$ without any intermediate oxide[11], the presence of several peaks suggests the existence of NiO species differently interacting with the support[9,12]. The first peak at 360 °C can be assigned to poorly interacting NiO, which is more easily reducible, since unsupported NiO reduces at about 280 °C[13,14]. The second and third peaks, at about 420 °C and 510 °C, respectively, can be ascribed to NiO progressively more strongly interacting with the support[15,16]. No peak related to the reduction of $Ca^{2+}$ can be detected, but CaO modifies nickel reducibility. As we previously reported[1] and according to the literature[12,17], in ZCaNi $Ca^{2+}$ replaces $Zr^{4+}$ in the lattice, thus generating oxygen vacancies which weaken the Ni-O bond and increase nickel reducibility (*i. e.* the intensity of the first peak) with respect to the undoped sample.

With regard to ZCaNiCu, the same three peaks related to $Ni^{2+}$ reduction can be noticed, plus one peak at 280 °C ascribable to the reduction of CuO. A lower reduction temperature can be ascribed to lower metal-support interaction strength and/or to bigger particle size of NiO. Nevertheless, a substantial difference in the relative intensity of the three Ni peaks

must be underlined, that is the increase of the intensity of the third peak (the fraction of NiO with strong interactions with zirconia) at the expense of the first two (NiO weakly and non-interacting). Even if the TPR analysis is not used here as a quantitative technique, the intensity of a peak is roughly proportional to the amount of reduced species. We can conclude that copper addition seems to have increased the fraction of strongly interacting Ni species. In our previous works[9,18-20] we demonstrated that the interactions between the active phase and the support play a key role in determining the performance of a catalysts. However, it also appears a non negligible contribution of highly reducible Ni species. TEM characterization (Fig. 6.3) helps throwing light on the attribution of these reduction features. The fresh ZCaNi sample (Fig. 6.3(a)) is characterized by a uniform array of 5-10 nm Ni particles, whereas sample ZCaNiCu (Fig. 6.3(b)) is constituted by poorly uniform metal particles, where much bigger particles coexist with smaller ones. This confirms the attribution of the low temperature TPR peak to sintered Ni particles.

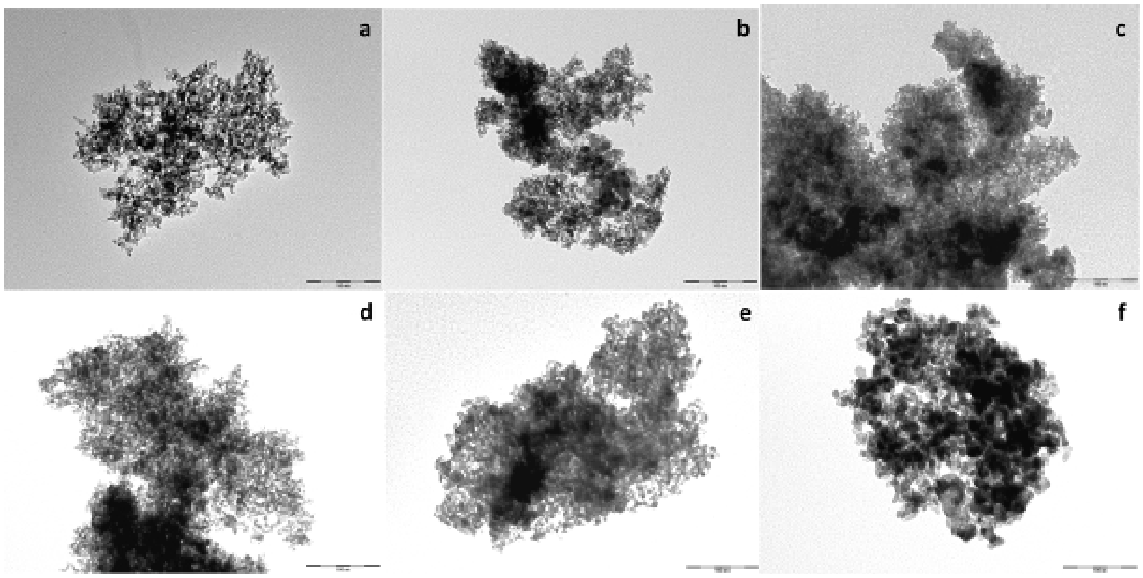


Fig. 6.3: TEM micrographs of fresh catalysts. a) ZCaNi; b-c) ZCaNiCu; d) $ZCaNi_1Cu_2$; e) $ZCaCu_1Ni_2$; f) ZCaNiCu800. Marker size 100 nm.

The results here reported seem to suggest that also the ratio between the different reducible species is important and correlated with metal particle size.

For a further understanding of the role of crystallographic nature of metal/support phases on the catalytic performances, XRD patterns of ZCaNi and ZCaNiCu were taken as reported in Fig. 6.4.

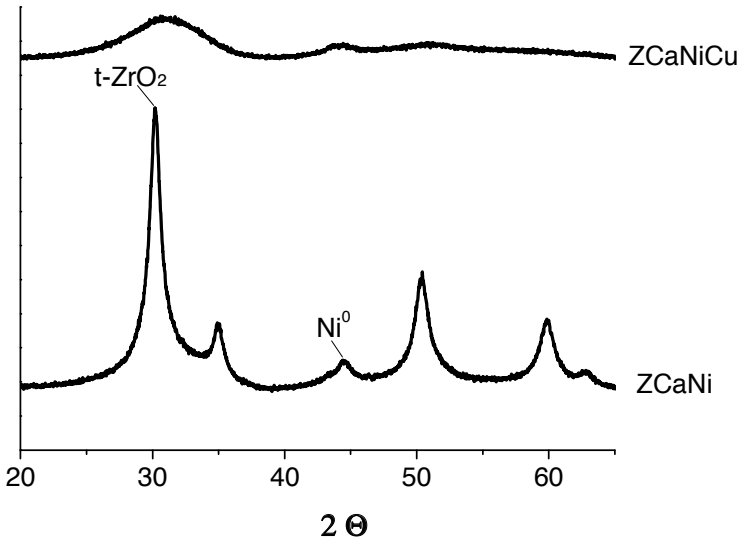


Fig. 6.4: XRD powder patterns of reduced ZCaNi and ZCaNiCu.

As for ZCaNi, zirconia is present only in the tetragonal phase (the most intense peak at 2θ ≈ 30°). In our previous study[1] we showed that $Zr^{4+}$ substitution by $Ca^{2+}$ takes place; this replacement does not affect the nature of the $ZrO_2$ polymorph of the support, but it modifies Ni reducibility, in accordance with the TPR results, because oxygen vacancies are generated. Nickel appears only in the metallic form (peak at 2θ = 44.5°), suggesting that the reduction treatment at 500 °C substantially reduced all $Ni^{2+}$ to $Ni^0$. With regard to ZCaNiCu, a substantial difference can be detected: this sample appears X-ray amorphous. This could be due to the synthetic approach we adopted, in which all metals have been added to the support simultaneously. It is known that dopant addition can modify the crystallization process[21,22].

In conclusion, besides the different ratio between the NiO species on the support, another important difference between ZCaNi and ZCaNiCu can be highlighted, that is the crystallographic nature of zirconia, which is crystalline in ZCaNi, while it is amorphous in ZCaNiCu.

Since the catalytic behaviour of the two samples is completely different, we decided to check the role of both the ratio between the various NiO species on the support and the crystallographic nature of zirconia. To do this, one possible way is to modify the synthesis procedure.

### 6.3.2 Effect of the order of metals addition

The results have shown that the contemporary addition of all the metals alters the crystallization process, so we decided to add Ni and Cu in two separate and sequential steps (samples $ZCaNi_1Cu_2$ and $ZCaCu_1Ni_2$ described in Section 6.2.1). The catalytic results reported in Table 6.1 show that the two samples have markedly different catalytic performance, also if compared to the reference catalyst ZCaNi, confirming that the synthesis procedure can strongly affect the catalytic behaviour.

In particular, we can observe that ethanol conversion is complete with both $ZCaNi_1Cu_2$ and $ZCaCu_1Ni_2$, but the products distribution is totally different once again.

With regard to $ZCaCu_1Ni_2$, the products distribution is quite similar to the ZCaNiCu one. A certain amount of C2 by-products and a low $H_2$ productivity can be achieved. As with ZCaNiCu, also in this case the presence of copper seems to negatively affect the conversion of by-products, acetaldehyde and ethylene, which are not completely converted over the active phase. However, the observed selectivity to acetaldehyde and ethylene is lower when Cu is added before Ni with respect to their contemporary addition. Accordingly, the selectivity to ethylene and acetaldehyde, initially nil, started increasing after 4 h-on-stream to the steady state value reported in Table 1. Thus we can conclude that the addition of Cu modifies the Ni active sites, partially limiting their activity in C-C bond cleavage, depending likely on its surface exposure.

On the contrary, the behavior of $ZCaNi_1Cu_2$ is in line with that of ZCaNi, but the ESR results are even better. In fact, all other results being equal, hydrogen productivity increased from 0.86 (reference ZCaNi) to 1.04 mol/min $kg_{cat}$. This result is accompanied by a higher water conversion with $ZCaNi_1Cu_2$ and the absence of C2 by-products (with the exception of a very little formation of ethylene towards the end of the test).

Some characterization measurements have been carried out to interpret these results.

The XRD patterns of $ZCaNi_1Cu_2$ and $ZCaCu_1Ni_2$ are reported in Fig. 6.5.

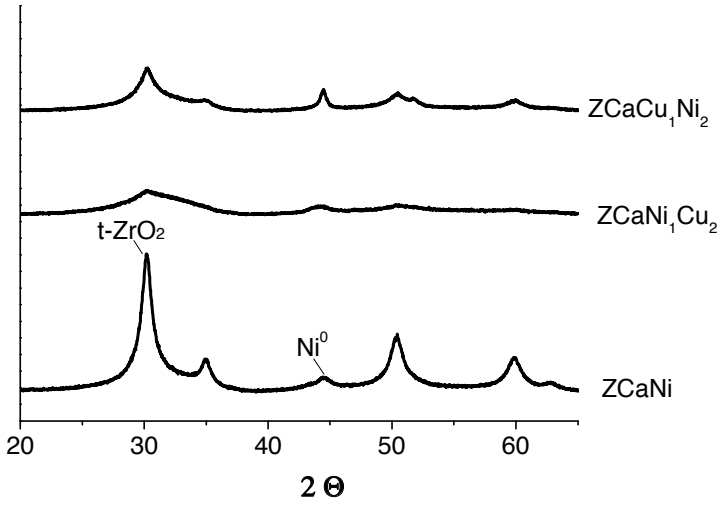


Fig. 6.5: XRD powder patterns of reduced ZCaNi, $ZCaNi_1Cu_2$ and $ZCaCu_1Ni_2$.

They show that the zirconia support is poorly crystalline (very little crystallite size), nearly X-ray amorphous in both samples. These results seem to confirm that the addition of both metals hampers the crystallization of the catalyst. On the other hand, the crystalline phase of the support does not affect the catalytic activity so deeply, since good catalytic performance was achieved with the almost amorphous $ZCaNi_1Cu_2$ sample. With regard to the second parameter we decided to investigate, namely the ratio between the different NiO species on the support, the TPR profiles of the samples are reported in Fig. 6.6.

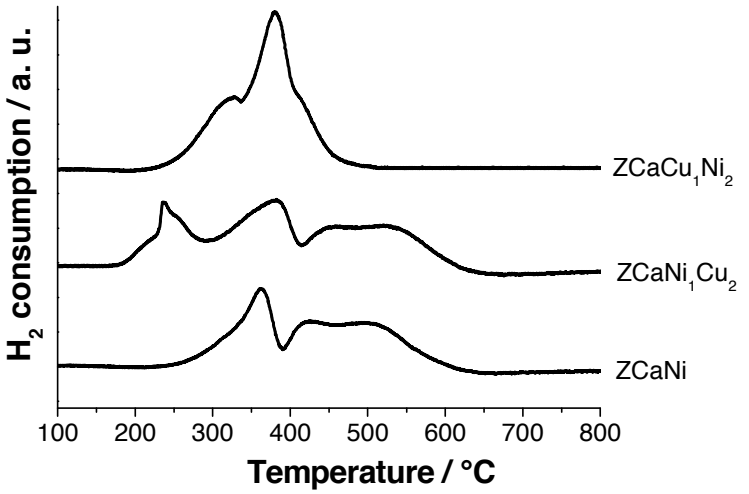


Fig. 6.6: TPR profiles of ZCaNi, $ZCaNi_1Cu_2$ and $ZCaCu_1Ni_2$.

Comparing the TPR pattern of $ZCaNi_1Cu_2$ with the ZCaNi one, it can be noticed that in $ZCaNi_1Cu_2$ a CuO species reduction peak is located between 180 and 290 °C. With regard to the region of $Ni^{2+}$ reduction, the two profiles are almost identical, in terms of both the position of the peaks and their relative intensities. On the contrary, the TPR profile of $ZCaCu_1Ni_2$ is completely different. The most evident differences lies in: i) the final reduction temperature of NiO, which was lower of about 200 °C (from 650 to 450 °C); ii) the relative distribution of the various $Ni^{2+}$ species. In the literature it is often reported that the presence of copper lowers the reduction temperature of nickel[7,23,24]. Pérez-Hernández et al.[25], for example, reported that Cu probably causes spillover of hydrogen on nickel, inducing a competitive reduction of both copper oxide and NiO. Our results show that this depends also on the synthesis approach. The sequential impregnation of Ni and Cu precursors ($ZCaNi_1Cu_2$ and $ZCaCu_1Ni_2$) leads to better results than the simultaneous one (ZCaNiCu). Nevertheless the order of metals impregnation is important as well, as reported also by other authors[26,27]. In our case, the catalytic results showed that $ZCaNi_1Cu_2$ is more active than $ZCaCu_1Ni_2$. Maybe this can be ascribed to the fact that in this sample the proper ratio between NiO species with medium and strong interactions with the support has been preserved, as in the reference sample ZCaNi. On the contrary, in $ZCaCu_1Ni_2$ NiO with low interaction seems to be present.

TEM analysis is reported in Fig. 6.3 also for these samples. Substantially uniform, ca. 5 nm, metal nanoparticles may be observed for sample $ZCaNi_1Cu_2$, whereas a broader particle size distribution was evident for sample $ZCaCu_1Ni_2$.

By considering all these results we may conclude that the composition and synthesis conditions which allow the formation of stable and uniform small Ni particles, as in the case of samples ZCaNi and $ZCaNi_1Cu_2$, lead to high activity and stability of the catalyst with time-on-stream. The absence or limited formation of coke deposits ensures the absence of C2 by-products. The latter are usually found when Ni becomes more and more covered by coke, which effectively limits the C-C bond breaking ability of the active site. Therefore, when big Ni particle size is present and/or Ni species poorly interacting with the support which easily sinter during use, a low initial C balance is usually observed at the beginning of the test, increasing with time-on-stream accompanied by a decrease in ethanol conversion and increasing selectivity towards ethylene and acetaldehyde.

### 6.3.3 Effect of the calcination temperature

Calcination temperature is another important parameter that can affect both the interactions between metal and support and the crystallographic phase of the support. We showed that the calcination temperature affects the speciation of Ni when supported over oxides which establish a strong metal support interaction[28,29]. For instance, when $Ni/TiO_2$ is calcined at 500 °C it is completely inactive, whereas when calcined at 800 °C it exhibits satisfactory catalytic performance. In the present case a different calcination temperature may also affect the mutual interaction between the two metals. Therefore, a sample for comparison has been prepared by contemporarily adding Ni and Cu precursors and calcining at 800 °C (sample ZCaNiCu800). This sample was tested at 500 °C after activation at 750 °C under reducing conditions (Tab.1). A further test at 750 °C was also added.

The catalytic performance of sample ZCaNiCu800 at 500 °C was even worse than that achieved after calcination at 500 °C, with negligible $H_2$ productivity and lower activity for both ethanol and methane reforming. Selectivity to C2 by-products and the decrease of ethanol conversion became evident after the first hour-on stream. It has been also observed that C balance was rather low at the beginning of the test (ca. 86%) and increased with time-on-stream to reach ca. 100%. This behavior may be related to some sintering of the active phase with respect to the sample calcined at 500 °C, inducing broader formation of carbon filaments which induce a faster catalyst deactivation. By contrast, operation at 750 °C gave rise to satisfactory and stable results, with full ethanol conversion and good carbon balance, no C2 by-products and no methane. This means that at high temperature coke gasification occurs and avoids the encapsulation of the active phase which leads to the deactivation observed at 500 °C.

Upon calcination of ZCaNiCu catalyst at 800 °C a clear shift to lower 2-theta angle (larger *d*-spacing) is observed for the diffraction line of metal (see XRD patterns in Fig. 6.7). The Rietveld refined unit cell parameter is intermediate between that of pure Ni and pure Cu, suggesting that a Ni-Cu alloy was formed.

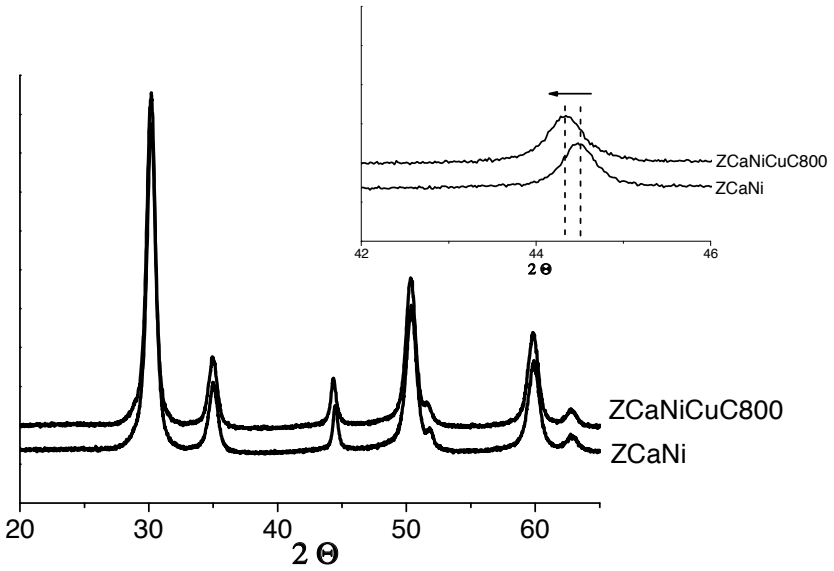


Fig. 6.7: XRD patterns of ZCaNi and ZCaNiCu800.

Furthermore, the TPR analysis (not reported for the sake of brevity) evidenced a much higher reducibility of Ni in sample ZCaNiCu800 with respect to sample ZCaNi. In particular, only highly reducible Ni species survived and the more disperse ones, strongly interacting with the support, completely disappeared. This confirms the tendency to sinter of Ni, according to our previous results[18,19,28], and helps elucidating why at 500 °C, where coke gasification is not useful to clean up metal surface, progressive and fast deactivation takes place.

Therefore, preparation conditions which favor the instauration of a stronger metal support interaction allow to keep dispersed the active phase and limit the formation of coke filaments during low temperature operation. The relative amount of these species may be correlated with catalyst life during testing at 500 °C. Indeed the sample for which only very reducible species were present was the least stable. By contrast, samples characterized by a significant concentration of less reducible Ni species (higher dispersion and stronger metal-support interaction) demonstrated higher activity for ethanol (and methane) reforming and above all higher stability with time-on-stream. This is ultimately due to a higher resistance towards coking.

### 6.3.4 Spent samples

Finally, the spent samples have been characterized by TEM (Fig. 6.8) and Raman spectroscopy (Fig. 6.9).

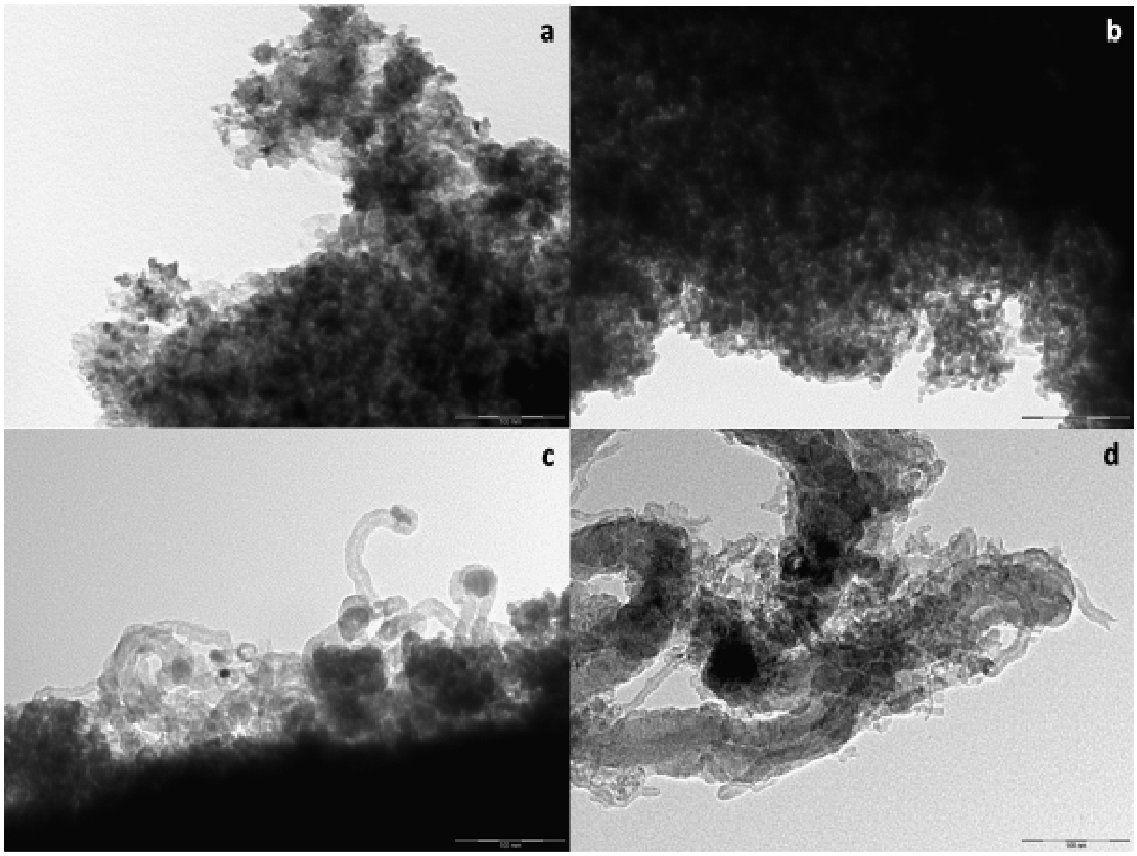


Fig. 6.8: TEM images of spent samples. a) $ZCaNi_1Cu_2$; b-c) ZCaNiCu; d) ZCaNiCu800. Marker size 100 nm.

TEM confirms limited sintering after use of samples ZCaNiCu and $ZCaNi_1Cu_2$. This confirms that the presence of poorly reducible species, *i. e.* strongly interacting with the support, helps in keeping Ni dispersed during use. Some formation of carbon nanotubes is observed for ZCaNiCu and substantially due to bigger metal particles, which are well known to be more prone to C accumulation (Fig. 6.8(c)). According to the much bigger Ni particle size, extensive nanotubes formation was achieved with sample ZCaNiCu800 (Fig. 6.8(d)).

Some graphitic C deposition may also be present due to the presence of some residual Lewis acid sites on the $ZrO_2$ support, as evidenced by micro-Raman analysis (Fig. 6.9).

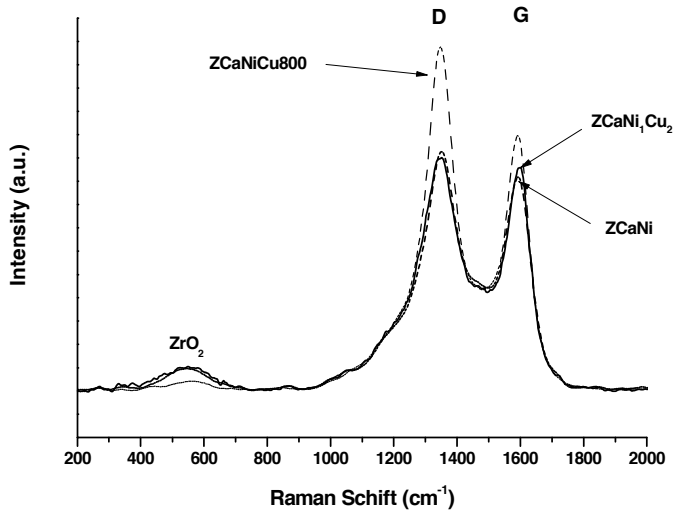


Fig. 6.9: MicroRaman spectra of spent samples.

The latter spectroscopy allows to identify two typical bands ascribable to coke, the D and G contributions. The latter is usually attributed to ordered graphite layers, whereas the former is mostly attributed to much disordered carbon species with respect to graphite layers (amorphous carbon and nanotubes) and is predominant for sample ZCaNiCu800.

TPO analyses were also carried out on the spent samples. They may further help elucidating the nature of carbon species deposed on the samples, since lower oxidation temperature ($T_{ox}$) may be attributed to amorphous carbon, whereas more ordered forms such as nanotubes and graphitic layers are expected to oxidise at higher temperature.

According to this qualitative scale, the coke deposed over sample ZCaNiCu, with $T_{ox}$ <450 °C, was predominantly amorphous. $T_{ox}$ progressively increased with $ZCaNi_1Cu_2$ and $ZCaCu_1Ni_2$ and finally a very intense peak with maximum at 589 °C characterised sample ZCaNiCu800, which was abundantly covered by carbon nanotubes.

## 6.4 Conclusions

In this chapter it was shown that big Ni particles and/or Ni species poorly interacting with the support, which easily sinter during use, cause a low initial C balance, accompanied by a decrease in ethanol conversion and an increase in selectivity towards C2 by-products.

High activity and stability of the catalyst were reached by properly tuning the synthesis conditions in order to obtain the formation of stable and uniform small Ni particles (*i. e.* favoring the instauration of a stronger metal support interaction). The separate and sequential addition of the metals, as well as the proper calcination temperature, are compulsory to achieve the best performance.

# References


[1] V. Nichele, M. Signoretto, F. Pinna, F. Menegazzo, I. Rossetti, G. Cruciani, G. Cerrato, A. Di Michele, Appl. Catal. B: Environ. 150-151 (2014) 12-20.

[2] F. Wang, Y. Li, W. Cai, E. Zhan, X. Mu, W. Shen, Catal. Today. 146 (2009) 31-36.

[3] R.R. Davda, J.W. Shabaker, G.W. Huber, R.D. Cortright, J.A. Dumesic, Appl. Catal. B: Environ. 56 (2005) 171-186.

[4] L. Qihai, L. Zili, Z. Xinhua, L. Cuijin, D. Jiao, J. Rare Earths. 29 (2011) 872-877.

[5] J. Remón, J.A. Medrano, F. Bimbela, L. García, J. Arauzo, Appl. Catal. B: Environ. 132-133 (2013) 433-444.

[6] V. Fierro, O. Akdim, C. Mirodatos, Green Chem. 5 (2003) 20-24.

[7] J.A. Calles, A. Carrero, A.J. Vizcaíno, Micropor. Mesopor. Mater. 119 (2009) 200-207.

[8] P.V. Tuza, R.L. Manfro, N.F.P. Ribeiro, M.M.V.M. Souza, Renewable Energy. 50 (2013) 408-414.

[9] V. Nichele, M. Signoretto, F. Menegazzo, A. Gallo, V. Dal Santo, G. Cruciani, G. Cerrato, Appl. Catal. B: Environ. 111-112 (2012) 225-232.

[10] F. Zane, S. Melada , M. Signoretto, F. Pinna, Appl. Catal. A: General. 299 (2006) 137-144.

[11] Y.J.O. Asencios, E.M. Assaf, Fuel Process. Technol. 106 (2013) 247-252.

[12] J.D.A. Bellido, E.M. Assaf, J. Power Sources. 177 (2008) 24-32.

[13] L. Zhang, J. Lin, Y. Chen, J. Chem. Soc. Faraday Trans. 88 (14) (1992) 2075-2078.

[14] Q.G. Yan, W.Z. Weng, H.L. Wan, H. Toghiani, R.K. Toghiani, C.U. Pittman, Jr, Appl. Catal. A: General. 239 (2003) 43-58.

[15] Y.Q. Song, D.H. He, B.Q. Xu, Appl.Catal. A: General. 337 (2008) 19-28.

[16] V. García, J.J. Fernández, W. Ruíz, F. Mondragón, A. Moreno, Catal. Commun. 11 (2009) 240-246.

[17] J.D.A. Bellido, J.E. De Souza, J.C. M'Peko, E.M. Assaf, Appl. Catal. A: General. 358 (2009) 215-223.

[18] I. Rossetti, C. Biffi, C.L. Bianchi, V. Nichele, M.Signoretto, F. Menegazzo, E. Finocchio, G. Ramis, A. Di Michele, Appl. Catal. B: Environ. 117-118 (2012) 384-396.

[19] I. Rossetti, A. Gallo, V. Dal Santo, C.L. Bianchi, V. Nichele, M. Signoretto, E. Finocchio, G. Ramis, A. Di Michele, ChemCatChem. 5 (2013) 294-306.

[20] I. Rossetti, J. Lasso, V. Nichele, M. Signoretto, E. Finocchio, G. Ramis, A. Di Michele, Appl. Catal. B: Environ. 150-151 (2014) 257-267.

[21] J.D.A. Bellido, E.M. Assaf, Appl. Catal. A: General. 352 (2009) 179-187.

[22] S. Fabris, A.T. Paxton, M.W. Finnis, Acta Mater. 50 (2002) 5171-5178.

[23] A.J. Vizcaino, A. Carrero, J.A. Calles, Int. J. Hydrogen Energy. 32 (2007) 1450-1461.

[24] L. Zhang, J. Liu, W. Li, C. Guo, J. Zhang, J. Natural Gas Chem. 18 (2009) 55-65.

[25] R. Pérez-Hernández, G. Mondragón Galicia, D. Mendova Anaya, J. Palacios, C. Angeles-Chavez, J. Arenas-Alatorre, Int. J. Hydrogen Energy. 33 (2008) 4569-4576.

[26] T.A. Maia, J.D. A. Bellido, E.M. Assaf, J.M. Assaf, Quim. Nova. 30 (2007) 339-345.

[27] P. López, G. Mondragón-Galicia, M.E. Espinosa-Pesqueira, D. Mendoza-Anaya, M.E. Fernández, A. Gómez-Cortés, J. Bonifacio, G. Martínez-Barrera, R. Pérez-Hernández, Int. J. Hydrogen Energy. 37 (2012) 9018-9027.

[28] V. Nichele, M. Signoretto, F. Menegazzo, I. Rossetti, G. Cruciani, Int. J. Hydrogen Energy. 39 (2014) 4252-4258.

[29] I. Rossetti, J. Lasso, E. Finocchio, G. Ramis, V. Nichele, M. Signoretto, A. Di Michele, Appl. Catal. A: General. 477 (2014) 42-53.

# Chapter 7. Conclusions

In this thesis it was shown that Ni-based catalysts are suitable to be used in the steam reforming of biomass derivatives, due to Ni activity in breaking C–C bonds and also in promoting the water-gas shift reaction. Nevertheless, the support demonstrated to be anything but a simple spectator of the reaction. Fig. 7.1 summarizes the essential features that a Ni-supported catalyst for the steam reforming of oxygenated compounds must possess and the way we achieved them.

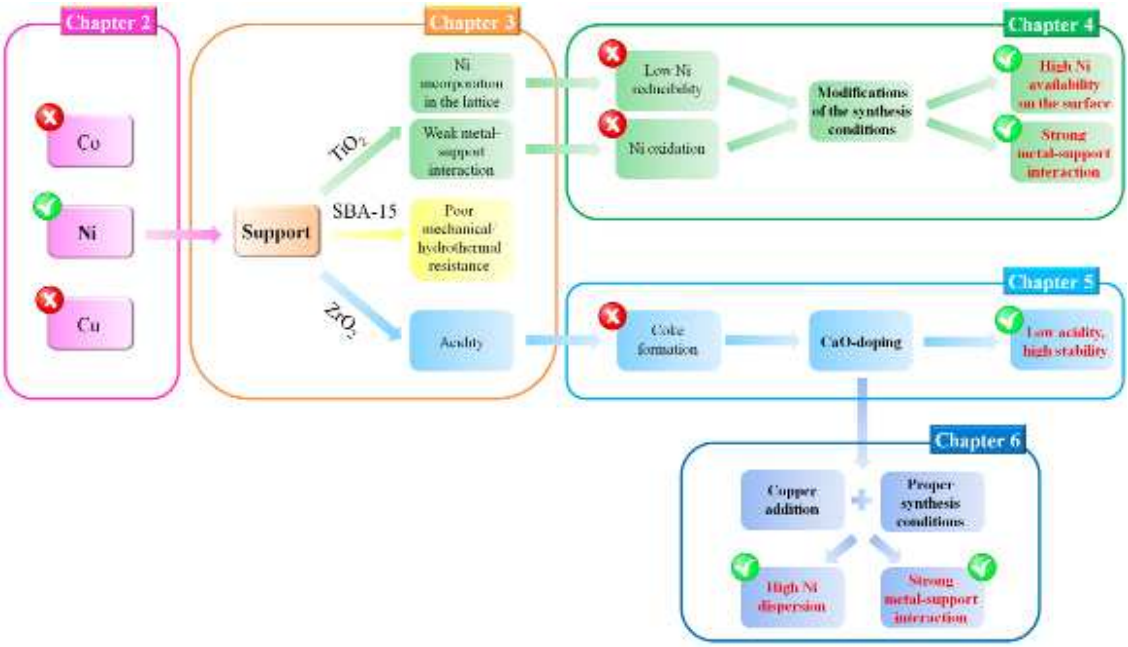


Fig. 7.1: Essential features for high performing Ni catalysts: final remarks.

In Chapter 3 it was shown that the mechanical and thermal stability of the support is an essential feature. Nevertheless, according to the support material, also other factors must be considered. In the case of the titania-based systems, it was highlighted that the activity and selectivity of the catalyst are strictly related to the ability of the support to make the active phase available for the reaction and the stabilization of the metal. In Chapter 4 it was shown that these features can be obtained by properly designing the synthesis conditions. Choosing the proper calcination temperature, as well as the modality of Ni introduction, allows to achieve a high Ni dispersion on the surface and strong metal-support interactions.

A high dispersion of metallic Ni is fundamental not only to increase the activity of the catalyst, but also to avoid coking phenomena.

Another important feature related to coke formation is the acidity of the support. The acidic features of zirconia were probably responsible for coking on the catalyst surface, thus causing a slight deactivation of the catalyst itself. In Chapter 5 it was reported that the Lewis acidity of the zirconia support was efficiently decreased by CaO-doping, thus inhibiting coke formation and increasing the stability with time-on-stream.

Finally, in Chapter 6 it was shown that copper addition to a $ZrO_2$-based system can be effective in improving the performance of the catalyst, provided that a high Ni dispersion and strong metal-support interactions are guaranteed. These results can be achieved only by choosing the proper synthesis conditions, *i.e.* the separate and sequential addition of the metals and the proper calcination temperature.

# Appendix Effect of the water-to-ethanol molar ratio on catalyst deactivation

## A.1 Introduction

A part of the work was devoted to the study of the influence of the reactant mixture composition, in particular the water-to-ethanol molar ratio (R), on the catalytic performance. This part was carried out during a research stay at the Consejo Superior de Investigaciones Científicas (CSIC) of Madrid in the lab of Dr. Vicente Cortes Corberan.

All the ESR tests reported in this thesis were carried out using a stoichiometric water/ethanol mixture, *i.e.* 3:1 mol/mol. It is well known that R is a crucial parameter in steam reforming reactions, affecting in particular the product distribution and the rate of coke formation[1-3]. Ratios lower than the stoichiometric value increase the production of intermediates[4] and the formation of coke, particularly at T < 600 °C[5,6]. On the contrary, increasing R can reduce the coke formation rate[7,8].

We decided to carry out a catalytic test at R = 6 in order to check the effect of this parameter on the deactivation rate of a catalyst due to coke formation. For this test, we used sample ZCaNiCu800 (prepared as described in Section 6.2.1). As reported in Chapter 6, this catalyst quickly deactivated because of a broad formation of carbon filaments. We wanted to verify if working at R = 6 could slow down the catalyst deactivation.

## A.2 Experimental Section

### A.2.1 Catalytic tests

The catalytic tests[9] were carried out in a Microactivity Reference unit (*PID Eng&Tech*), equipped with a fix-bed tubular reactor. The catalyst, sieved into 0.25 mm particles and diluted 1:3 (v/v) with SiC 0.42-0.59 mm, was located in the reactor within two layers of quartz wool. The reactor was filled with SiC (0.84 mm). The temperature inside the reactor was controlled by a thermocouple positioned in the catalytic bed. The reactor was located

inside an oven, which was in turn contained in a box heated at 130 °C. Catalyst activation was accomplished by feeding 30 mL/min of $H_2$, while heating by 5 °C /min up to 700 °C, then kept for 1 h. The reactor was purged with He (260 mL/min) for 30 minutes, then the reactant mixture was fed.

In the standard operating conditions of this plant, 0.05 mL/min of a liquid mixture of water and ethanol (6:1 mol/mol) were fed by means of a Gilson 307 HPLC pump to an evaporator operating at 165 °C, then diluted with 260 mL/min of He. 100 mg of catalysts were used. When the molar composition of the reagents mixture was changed from 6:1 to 3:1, some operating conditions were modified in order to maintain the same contact time (catalyst amount: 123 mg; flow of the pump: 0.04 mL/min; He flow: 338 mL/min).

The catalytic tests were carried out at atmospheric pressure at 500 °C. The analysis of the out-flowing gases was carried out by a gas chromatograph Varian 3400 equipped with two columns connected in series (Porapak Q and MS) with a TCD detector. The catalyst deactivation was evaluated in terms of ethanol conversion at different time-on-stream, calculated as the sum of the yields of the carbonaceous products.

## A.3 Results and discussion

The result of the test is reported in Fig. A.1.

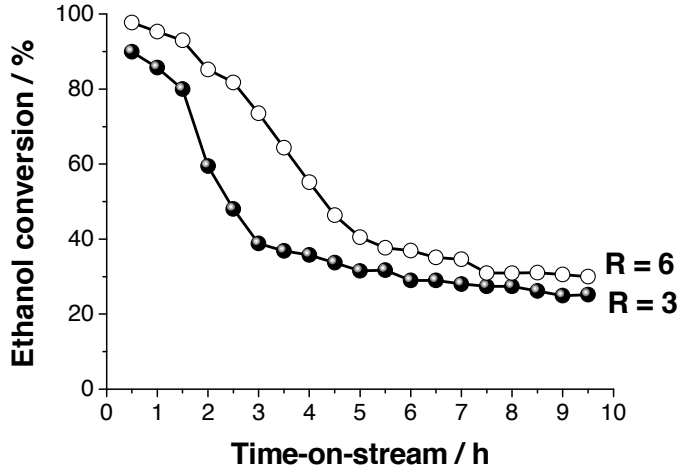


Fig. A.1: Ethanol conversion of ZCaNiCu800 at R = 3 (•) and R = 6 (o).

As we expected, there is a certain effect of the molar ratio of the reagents mixture. It can be noted that when R = 3 the catalyst deactivates quickly, reaching an ethanol conversion of 38% just after 3 h. At R = 6 the deactivation is more gradual, and the catalyst reaches the same value of ethanol conversion after 5 h and a half. This result can be ascribed to a higher gasification of coke when a higher amount of water is present in the reactant mixture (*i.e.* at higher R), in line with the results reported in the literature[10,11].

Our standard reaction conditions (low temperature, low water/ethanol ratio) are quite severe condition in terms of coke formation, but they were specifically selected. As previously discussed, a low reaction temperature was chosen to limit the heat input to the reactor. Analogously, lower R values improve the energetic efficiency of the process. Ioannides[12] carried out a thermodynamic study on the effect of R and showed that R values higher than stoichiometry results in reduced efficiency in hydrogen production because of the higher energy input necessary for water evaporation, which is disadvantageous also from the economical point of view[10]. Moreover, working is such stressing conditions as for coking, which is one of the most critical points for steam reforming reactions, allows to obtain useful data on the stability of the catalysts under practically relevant conditions.

# References


[1] M. Benito, R. Padilla, L. Rodríguez, J.L. Sanz, L. Daza, J. Power Sources. 169 (2007) 167-176.

[2] Daniel Montané, Evgeny Bolshak, Sònia Abelló, Chem. Eng. J. 175 (2011) 519-533.

[3] X. Deng, J. Sun, S. Yu, J. Xi, W. Zhu, X. Qiu, Int. J. Hydrogen Energy. 33 (2008) 1008-1013.

[4] F. Gallucci,A. Basile, S. Tosti, A. Iulianelli, E. Drioli, Int. J. Hydrogen Energy. 32 (2007) 1201-1210.

[5] V. Palma, F. Castaldo, P. Ciambelli, G. Iaquaniello, G. Capitani, Int. J. Hydrogen Energy. 38 (2013) 6633-6645.

[6] E.C. Wanat, K. Venkataraman, L.D. Schmidt, Appl. Catal. A: General. 276 (2004) 155-162.

[7] V. Mas, R. Kipreos, N. Amadeo,M. Laborde, Int. J. Hydrogen Energy. 31 (2006) 21-28.

[8] V. Palma, F. Castaldo, P. Ciambelli, G. Iaquaniello, Appl. Catal. B: Environ. 145 (2014) 73-84.

[9] R. Olivera Fraile, *Activity and stability of catalysts for hydrogen production by partial oxidation and reforming of ethanol*, PhD Thesis, UAM, Madrid, 2012 (in Spanish).

[10] R. Trane-Restrup, S. Dahl, A.D. Jensen, Int. J. Hydrogen Energy. 39 (2014) 7735-7746.

[11] A. Birot, F. Epron, C. Descorme, D. Duprez, Appl. Catal. B: Environ. 79 (2008) 17-25.

[12] T. Ioannides, J. Power Sources. 92 (2001) 17-25.

# Curriculum Vitae

Born in 1985, I graduated cum laude in Industrial Chemistry at University Ca' Foscari Venice in April 2010, with a thesis on β-galactosidase/silica systems for the treatment of lactose intolerance. In September 2010 I won the Prize of the Scuola GIC 2010 for my degree thesis.
Since May 2010 to September 2011 I worked at Dept. Molecular Sciences and Nanosystems, University Ca' Foscari Venice, as young scientist with research fellowship. Since September 2011 I am working as PhD student.
My research is focused in nanostructured materials for catalytic applications, in particular for the development of new catalysts for the valorization of biomasses through hydrogen production, but also for the development of new drug delivery systems. My research activity is documented by some papers published on peer-reviewed international journals and national and international congresses memories.

# List of publications and conference presentations based on this thesis

## Chapter 2

### Publications

"*Silica and zirconia supported catalysts for the low-temperature ethanol steam reforming*", I. Rossetti, J. Lasso, V. Nichele, M. Signoretto, E. Finocchio, G. Ramis, A. Di Michele, Appl. Catal. B: Environ. 150-151 (2014) 257-267.

"*$TiO_2$-supported catalysts for the steam reforming of ethanol*", I. Rossetti, J. Lasso, E. Finocchio, G. Ramis, V. Nichele, M. Signoretto, A. Di Michele, Appl. Catal. A: General. 477 (2014) 42-53.

**Conference presentation**

V. Nichele, M. Signoretto, F. Menegazzo, F. Pinna, A. Gallo, V. Dal Santo, G. Cruciani, G. Cerrato, "*SBA-15 based catalysts for glycerol steam reforming: effect of the active phase*", EFCATS Summer School 2012, Verbania – Pallanza, 11-15 Settembre 2012.

## Chapter 3

**Publications**

"*Glycerol steam reforming for hydrogen production: Design of Ni supported catalysts*", V. Nichele, M. Signoretto, F. Menegazzo, A. Gallo, V. Dal Santo, G. Cruciani, G. Cerrato, Appl. Catal. B: Environ. 111-112 (2012) 225-232.

"*Ni/$SiO_2$ and Ni/$ZrO_2$ catalysts for the steam reforming of ethanol*", I. Rossetti, C. Biffi, C. L. Bianchi, V. Nichele, M. Signoretto, F. Menegazzo, E. Finocchio, G. Ramis, A. Di Michele, Appl. Catal. B: Environ. 117-118 (2012) 384-396.

"*Nickel catalysts supported over $TiO_2$, $SiO_2$ and $ZrO_2$ for the steam reforming of glycerol*", I. Rossetti, A. Gallo, V. Dal Santo, C. L. Bianchi, V. Nichele, M. Signoretto, E. Finocchio, G. Ramis, A. Di Michele, ChemCatChem. 5 (2013) 294-306.

**Conference presentation**

V. Nichele, M. Signoretto, F. Menegazzo, F. Pinna, V. Dal Santo, G. Cruciani, G. Cerrato, "*Ni catalysts for hydrogen production through glycerol steam reforming*", IX PhD-Chem Day, Padova, April 12$^{th}$ 2012.

## Chapter 4

**Publication**

"*Hydrogen production by ethanol steam reforming: Effect of the synthesis parameters on the activity of Ni/$TiO_2$ catalysts*", V. Nichele, M. Signoretto, F. Menegazzo, I. Rossetti, G. Cruciani, Int. J. Hydrogen Energy. 39 (2014) 4252-4258.

**Conference presentations**

- V. Nichele, M. Signoretto, F. Menegazzo, F. Pinna, I. Rossetti, G. Cruciani, G. Cerrato, "*Effects of the synthesis parameters on Ni/$TiO_2$ catalysts for ethanol steam reforming*", XVIII Congresso Nazionale DCI-SCI, Firenze, June 11$^{th}$ -14$^{th}$ 2012.

V. Nichele, M. Signoretto, F. Menegazzo, F. Pinna, I. Rossetti, C. Biffi, G. Cruciani, G. Cerrato, "*Ni/$TiO_2$ for ethanol steam reforming: which is the best synthetic approach?*", 15$^{th}$ ICC 2012, Monaco, July 1$^{st}$ -6$^{th}$ 2012.

## Chapter 5

**Publication**

"*Ni/$ZrO_2$ catalysts in ethanol steam reforming: Inhibition of coke formation by CaO-doping*", V. Nichele, M. Signoretto, F. Pinna, F. Menegazzo, I. Rossetti, G. Cruciani, G. Cerrato, A. Di Michele, Appl. Catal. B: Environ. 150-151 (2014) 12-20.

**Conference presentations**

V. Nichele, A. Iwanska, M. Signoretto, F. Menegazzo, I. Rossetti, G. Cruciani, F. Vindigni, G. Cerrato, "*Ni/$ZrO_2$ catalysts for ethanol steam reforming: effect of Ca-doping*", EuropaCat XI, Lione, September 1$^{st}$ -6$^{th}$ 2013.

V. Nichele, A. Iwanska, M. Signoretto, F. Menegazzo, I. Rossetti, G. Cruciani, F. Vindigni, G. Cerrato, "*Effect of CaO-doping on coke resistance of Ni/$ZrO_2$ catalysts in ethanol steam reforming*", Congresso GIC-AIZ 2013, Riccione, September 15$^{th}$-18$^{th}$ 2013.

## Chapter 6

**Publication**

*"Bimetallic Ni-Cu catalysts for the low-temperature ethanol steam reforming: importance of metal-support interactions*", V. Nichele, M. Signoretto, F. Pinna, E. Ghedini, M. Compagnoni, I. Rossetti, G. Cruciani, A. Di Michele, Catal. Letters. DOI: 10.1007/s10562-014-1414-2.

## Other publications

"*One-step synthesis of silica gel used in the controlled release of drug*", M. Signoretto, V. Nichele, E. Ghedini, F. Pinna, G. Cerrato, Stud. Surf. Sci. & Catal., vol.174A, A. Gedeon, P. Massiani, F. Babonneau, Eds. Elsevier, Amsterdam (2008) 489-492.

"*Effect of textural properties on the drug delivery behaviour of nanoporous $TiO_2$ matrices*", M. Signoretto, E. Ghedini, V. Nichele, F. Pinna, V. Crocellà, G. Cerrato, Micropor. Mesopor. Mater. 139 (2011) 189-196.

"β-*galactosidase entrapment in silica gel matrices for a more effective treatment of lactose intolerance*", V. Nichele, M. Signoretto, E. Ghedini, J. Molec. Catal. B: Enzymatic, 71 (2011) 10-15.

"*Effect of the support on Ni catalytic performances in glycerol steam reforming*", V. Nichele, M. Signoretto, F. Menegazzo, F. Pinna, A. Gallo, V. Dal Santo, G. Cerrato, *Atti del XXIV Congresso Nazionale della Società Chimica Italiana*, pag. 619, eISBN 978-88-8305-085-5.

"*Structure-directing agents for the synthesis of $TiO_2$-based Drug-Delivery Systems*", E. Ghedini, V. Nichele, M. Signoretto, G. Cerrato, Chem. Eur. J. 18 (2012) 10653-10660.

**Estratto per riassunto della tesi di dottorato**

**Studente:** Valentina Nichele **Matricola:** 816875

**Dottorato:** Scienze Chimiche **Ciclo:** XXVII

**Titolo della tesi:** *Innovative and versatile heterogeneous catalysts for hydrogen production from renewable sources*

**Abstract:** The steam reforming of biomass derivatives such as ethanol and glycerol is an attractive process to produce hydrogen, the energy carrier of the future. The fulfillment of this process on industrial scale is strictly related to the design of a highly active and selective catalyst. This study focused on the effect of different parameters (the physico-chemical properties of the support; the metal-support interaction; the reducibility and the dispersion of the active phase) on the performance of Ni-based catalysts. It was demonstrated that Ni is an effective active phase in the steam reforming of oxygenated compounds and that the support is anything but a simple spectator of the reaction. Several features, such as low acidity and high stability of the support, high availability and dispersion of metallic Ni, strong metal-support interactions, must be guaranteed in order to obtain a high performing catalyst. A properly tuning of the synthesis procedure is essential to pursue these goals.

Lo *steam reforming* di derivati delle biomasse, come etanolo e glicerolo, è un processo efficiente per produrre idrogeno, il vettore energetico del futuro. La sua realizzazione su scala industriale è strettamente correlata alla messa a punto di un catalizzatore attivo e selettivo. Il presente studio si focalizza sull'effetto di vari parametri (le proprietà chimico-fisiche del supporto; le interazioni supporto-fase attiva; la riducibilità e la dispersione del metallo) sull'attività di catalizzatori a base di Ni. È stato dimostrato che il Ni è un metallo attivo nello *steam reforming* di composti ossigenati e che il supporto è tutt'altro che un semplice spettatore della reazione. Diverse condizioni (bassa acidità, alta stabilità del supporto, elevate disponibilità e dispersione della fase attiva, forti interazioni metallo-supporto) devono essere garantite. La scelta delle più opportune condizioni di sintesi si è rivelata essere un fattore essenziale per perseguire questi obiettivi.

Firma dello studente